

Karolina Krawczyk-Wołoszyn

**„Mikroskopia sił atomowych (AFM) jako innowacyjna metoda
obrazowania i diagnostyki chorób włosów.”**

**‘Atomic force microscopy (AFM) as an innovative imaging and diagnostic method
for hair diseases.’**

**Rozprawa na stopień doktora
w dziedzinie nauk medycznych i nauk o zdrowiu
w dyscyplinie nauki medyczne**

Promotor: prof. dr hab. n. med. Adam Reich

Zakład i Klinika Dermatologii, Wydział Medyczny, Collegium Medicum,
Uniwersytet Rzeszowski

Promotor pomocniczy: dr hab. n. med. Magdalena Żychowska, prof. UR

Zakład i Klinika Dermatologii, Wydział Medyczny, Collegium Medicum,
Uniwersytet Rzeszowski



Rzeszów 2025 r.

*Pragnę złożyć najserdeczniejsze podziękowania prof. dr hab. n. med. Adamowi Reichowi oraz dr hab. n. med. Magdalenie Żychowskiej za inspirację, motywację, a przede wszystkim za nieocenioną pomoc podczas tworzenia tej rozprawy.
To zaszczyt i przywilej mieć takich Promotorów.*

Szczególne podziękowania kieruję również do moich Najbliższych, którzy nieustannie mnie wspierają.

Spis treści

1. Curriculum Vitae	4
2. Wykaz skrótów	10
3. Wykaz publikacji stanowiących rozprawę doktorską	11
4. Wstęp	12
5. Cel pracy	14
6. Materiały i metody	15
7. Wyniki	17
8. Dyskusja	19
9. Publikacje stanowiące rozprawę doktorską	20
10. Wnioski	68
11. Piśmiennictwo	69
12. Streszczenie w języku polskim	71
13. Abstract (streszczenie w języku angielskim)	73
14. Oświadczenia współautorów	75
15. Załączniki	82

1. Curriculum Vitae

Doświadczenie zawodowe i wykształcenie

2020-2024	Uniwersytet Rzeszowski, Szkoła Doktorska doktorant (nauki medyczne)
2023-	Uniwersytecki Szpital Kliniczny im. Fryderyka Chopina w Rzeszowie, Klinika Dermatologii i Dermatologii Onkologicznej Stanowisko: lekarz rezydent w trakcie specjalizacji z dermatologii i wenerologii
2020-2022	Kliniczny Szpital Wojewódzki Nr 1 w Rzeszowie, Klinika Dermatologii Stanowisko: lekarz rezydent w trakcie specjalizacji z dermatologii i wenerologii
2018-2019	Uniwersytecki Szpital Kliniczny nr 1 im. Norberta Barlickiego w Łodzi, Stanowisko: lekarz stażysta
2012-2018	Uniwersytet Medyczny w Łodzi Kierunek: lekarski Ukończenie studiów z wyróżnieniem. Uzyskanie tytułu zawodowego lekarza z wynikiem bardzo dobrym.
2009-2012	I Liceum Ogólnokształcące im. gen. Władysława Sikorskiego we Włoszczowie Profil: biomedyczny Uzyskanie świadectwa maturalnego z wyróżnieniem.

Aktywność organizacyjna i naukowa

Publikacje (z wyłączeniem prac będących częścią rozprawy doktorskiej)

1. Krawczyk K, Kołt-Kamińska M, Reich A. Nerwiakowłóknikowatość typu I — obraz kliniczny i diagnostyka. *Forum Dermatologicum*. 2020; 6: 67-72. doi: 10.5603/FD.a2020.0011.
2. Kołt-Kamińska M, Krawczyk K, Reich A. Selumetynib — pierwszy lek skuteczny w terapii nerwiakowłókników spłotowatych w przebiegu neurofibromatozy typu 1. *Forum Dermatologicum*. 2020; 6: 50-54. doi: 10.5603/FD.a2020.0006.
3. Krawczyk K, Mazur E, Kargol J, Kijowski R, Reich A. The Case of a Patient with Limited Systemic Sclerosis and Interstitial Lung Disease Overlapping with Systemic Lupus Erythematosus. *Dermato*. 2021; 1(2):59-70. doi: 10.3390/dermato1020009
4. Krawczyk K, Mazur E, Reich A. Tick-borne lymphadenopathy – rickettsial skin infection with local lymphadenopathy and systemic symptoms following a tick bite. *Dermatology Review/Przegląd Dermatologiczny*. 2021;108(5):414-421. doi:10.5114/dr.2021.113159.
5. Krawczyk K, Reich A. Pieluszkowe zapalenie skóry z podrażnienia, w: red. Dobrzańska A, Obrycki Ł, Socha P, *Pediatrics w praktyce lekarza POZ*. Media-Press sp. z o.o. Warszawa 2022. s. 600-602
6. Krawczyk K, Reich A. Atopowe zapalenie skóry– punkt widzenia dermatologa, w: red. Dobrzańska A, Obrycki Ł, Socha P, *Pediatrics w praktyce lekarza POZ*. Media-Press sp. z o.o. Warszawa 2022. s. 603-608
7. Krawczyk K, Reich A. Ciemieniucha i łojotokowe zapalenie skóry, w: red. Dobrzańska A, Obrycki Ł, Socha P, *Pediatrics w praktyce lekarza POZ*. Media-Press sp. z o.o. Warszawa 2022. s. 609-611
8. Krawczyk K, Reich A. Mięczak zakaźny, w: red. Dobrzańska A, Obrycki Ł, Socha P, *Pediatrics w praktyce lekarza POZ*. Media-Press sp. z o.o. Warszawa 2022. s. 612-615
9. Krawczyk K, Reich A. Świerzb, w: red. Dobrzańska A, Obrycki Ł, Socha P, *Pediatrics w praktyce lekarza POZ*. Media-Press sp. z o.o. Warszawa 2022. s. 616-620

10. Krawczyk K, Reich A. Wszawica, w: red. Dobrzańska A, Obrycki Ł, Socha P, *Pediatric w praktyce lekarza POZ*. Media-Press sp. z o.o. Warszawa 2022. s. 621-624
11. Krawczyk K, Reich A. Liszajec zakaźny, w: red. Dobrzańska A, Obrycki Ł, Socha P, *Pediatric w praktyce lekarza POZ*. Media-Press sp. z o.o. Warszawa 2022. s. 625-629
12. Krawczyk K, Reich A. Łupież różowy Giberta, w: red. Dobrzańska A, Obrycki Ł, Socha P, *Pediatric w praktyce lekarza POZ*. Media-Press sp. z o.o. Warszawa 2022. s. 630-632
13. Krawczyk K, Reich A. Znamiona, w: red. Dobrzańska A, Obrycki Ł, Socha P, *Pediatric w praktyce lekarza POZ*. Media-Press sp. z o.o. Warszawa 2022. s. 633-638
14. Krawczyk K, Reich A. Świerzb - przegląd najnowszych kryteriów diagnostycznych i zaleceń terapeutycznych. *Forum Dermatologicum*. 2022; 8: 89-92. doi: 10.5603/FD.2022.0017
15. Kołcz K, Krawczyk-Wołoszyn K, Reich A, Żychowska M. Pruritus in Lichen Planopilaris and Frontal Fibrosing Alopecia-Clinical Characteristics and Dermoscopic Correlations. *J Clin Med*. 2024 Aug 19;13(16):4898. doi: 10.3390/jcm13164898.
16. Wojtowicz I, Krawczyk-Wołoszyn K, Ostańska E, Reich A, Żychowska M. Choose your biopsy site wisely - the utility of dermoscopy in the diagnosis of Bowen's disease of the face. *Forum Dermatologicum*. 2024; 10: 50-53. doi: 10.5603/fd.99280
17. Krawczyk-Wołoszyn K, Reich A. Zmiany skórne w przebiegu chorób układu pokarmowego, w: red. Krasowska D, Michalska-Jakubus M, *Dermatologia pediatryczna w teorii i przypadkach*. Tom 2. PZWL Wydawnictwo Lekarskie – *w trakcie procesu publikacji*
18. Krawczyk-Wołoszyn K, Wołoszyn M, Żychowska M. Correlation between reflectance confocal microscopy and high-magnification dermoscopy findings in lentigo maligna of the external ear. *Forum Dermatologicum*. 2024; 10(4): 146-150. doi: 10.5603/fd.102081
19. Krawczyk-Wołoszyn K, Reich A. Application of AFM technique in the study of human hair - a narrative review. *International Journal of Trichology* – *w trakcie procesu recenzji*

Doniesienia zjazdowe

1. Krawczyk-Wołoszyn K. Ocena struktury i morfologii powierzchni włosów pacjentów z liszajem płaskim mieszkowym (LPP) za pomocą mikroskopii sił atomowych (AFM). Zjazd Sekcji Forum Młodych Polskiego Towarzystwa Dermatologicznego. Łódź, 24–25 października 2024 r (II miejsce w kategorii Praca Eksperymentalna).
2. Krawczyk-Wołoszyn K. Lentigo maligna małżowiny usznej. Konferencja naukowa "Cyklówki dermatologiczne" pod egidą Oddziału Podkarpackiego Polskiego Towarzystwa Dermatologicznego. Rzeszów, 7 grudnia 2024 r.
3. Krawczyk-Wołoszyn K. Praktyczne aspekty zastosowania wideodermatoskopii w biopsji celowanej oraz kwalifikacji do wycięcia chirurgicznego nowotworowych zmian skórnych. Konferencja naukowa "Cyklówki dermatologiczne" pod egidą Oddziału Podkarpackiego Polskiego Towarzystwa Dermatologicznego. Rzeszów, 16 grudnia 2023 r.
4. Krawczyk K. Potocki A. Świerzbiczka guzkowa jako manifestacja zaburzeń psychicznych. Konferencja naukowo-szkoleniowa Oddziału Podkarpackiego Polskiego Towarzystwa Dermatologicznego. Rzeszów, 3 grudnia 2022 r.
5. Krawczyk K. Ocena występowania i nasilenia świądu oraz jego wpływu na jakość życia u pacjentów chorujących na łysienie czołowe bliznowaciejące (FFA) oraz liszaja płaskiego mieszkowego (LPP). Zjazd Sekcji Forum Młodych Polskiego Towarzystwa Dermatologicznego. Łódź, 20–21 października 2022 r.
6. Krawczyk K. Liszaj płaski przerostowy (Hypertrophic lichen planus) współistniejący z łysieniem czołowym bliznowaciejącym (Frontal fibrosing alopecia - FFA). IV Bieszczadzkie Spotkania z Dermatologią. Arłamów, 2 września 2022 r.
7. Krawczyk K. Zakażenie HIV w praktyce lekarza dermatologa. Konferencja naukowo-szkoleniowa PTD Oddziału Podkarpackiego. Rzeszów, 4 grudnia 2021 r.
8. Krawczyk K. Tick-born lymphadenopathy: riketsjozowa infekcja skóry z lokalną limfadenopatią i objawami ogólnymi po ugryzieniu przez kleszcza. Szkoła Mistrzów Dermatologii. Sulejów, 20 listopada 2021 r.

9. Krawczyk K. Trądzik piorunujący w przebiegu zespołu PAC (pyoderma, acne, colitis). III Bieszczadzkie Spotkania z Dermatologią. Arłamów, 3 września 2021 r.
10. Krawczyk K. Pistor G. Mnogi objaw pierwotny. Konferencja naukowo-szkoleniowa Oddziału Podkarpackiego Polskiego Towarzystwa Dermatologicznego. Rzeszów, 12 czerwca 2021 r.
11. Krawczyk K. Zespół PAC (pyoderma gangrenosum, acne, colitis ulcerosa). Konferencja naukowo-szkoleniowa Oddziału Podkarpackiego Polskiego Towarzystwa Dermatologicznego. Rzeszów, 17 kwietnia 2021 r.
12. Krawczyk K. Limfadenopatia odkleszczowa (TIBOLA). Konferencja naukowo-szkoleniowa Oddziału Podkarpackiego Polskiego Towarzystwa Dermatologicznego. Rzeszów, 12 grudnia 2020 r.
13. Krawczyk K. Piodermia zgorzelinowa u pacjentki z reumatoidalnym zapaleniem stawów leczonej adalimumabem. „Trendy i wyzwania w leczeniu łuszczycy”. Rzeszów, 8-10 października 2020 r.
14. Krawczyk K. Pyodermia chancriformis. „Trendy i wyzwania w leczeniu łuszczycy”. Rzeszów, 8-10 października 2020 r.
15. Krawczyk K. Chancriform Pyoderma – przypadek kliniczny. Konferencja naukowo-szkoleniowa Oddziału Podkarpackiego Polskiego Towarzystwa Dermatologicznego. Rzeszów, 19 września 2020 r.

Udział w projektach badawczych

1. A Randomized, Double-Blinded, Placebo-Controlled Trial to Investigate the Efficacy, Safety, and Tolerability of Efgartigimod PH20 SC in Adult Patients With Pemphigus (Vulgaris or Foliaceus), Protocol Number: ARGX-113-1904
2. An Open Label, Multicenter, Follow up Trial of ARGX-113-1904 to Evaluate the Safety, Tolerability, and Efficacy of Efgartigimod PH20 SC in Patients With Pemphigus, Protocol Number: ARGX-113-1905
3. Open label exploratory phase IIA trial to investigate the safety and efficacy of IFX-1 in treating subjects with Pyoderma Gangrenosum, Protocol Number: IFX-1-P2.7;
4. UCB BioPharma SRL, HS0004, A Phase 3, Randomized, Double-blind, Placebo-controlled, Multicenter Study Evaluating the Efficacy and Safety of

Bimekizumab in Study Participants with moderate to Severe Hidradenitis Suppurativa , 243509, 40293, Protocol Number: HS0004.

5. A Phase 2a, Randomized, Double Blind, Vehicle Controlled, Parallel Group Study To Assess The Efficacy, Safety, Tolerability And Pharmacokinetics Of Pf-07038124 Ointment For 6 Weeks In Participants With Mild To Moderate Atopic Dermatitis Or Plaque Psoriasis, Protocol Number: C3941002
6. A Phase 2, Randomized, Placebo-controlled, Double-blind, Multiple Dose Study to Evaluate the Efficacy and Safety of ANB019 in Subjects with Palmoplantar Pustulosis, Protocol Number: ANB019-003
7. Zastosowanie mikroskopii sił atomowych w analizie ultrastruktury i właściwości mechanicznych włosów pacjentów chorujących na łysienie bliznowaciejące i niebliznowaciejące. UR, 2024 r.

Działalność dydaktyczna i organizacyjna

1. Przeprowadzenie warsztatów podczas Kursu obrazowania skóry, organizowanego pod egidą Oddziału Podkarpackiego Polskiego Towarzystwa Dermatologicznego 25-26 stycznia 2024 r. w Rzeszowie
2. Przeprowadzenie warsztatów pt.: „Miarodajne metody oceny zmian skórnych w łuszczycy (PASI, BSA, IGA, NaPSI, PPASI, PPPASI, GPP-PGA, DLQI, CDLQI) – jak stosować, jak interpretować?” podczas konferencji „Podkarpackie Dni Dermatologii | PSORIASIS & LUPUS”, która odbyła się w dniach 17-19 marca 2022 r. w Rzeszowie
3. Członek Komitetu Organizacyjnego i Naukowego „Podkarpackich Dni Dermatologii | PSORIASIS & LUPUS”, Rzeszów 17-19 marca 2022 r.
4. Szkoleniowiec i współorganizator Programu Preceptorship - praktyczne szkolenie dla dermatologów nt. "Leczenie pacjentów z łuszczycą o nasileniu umiarkowanym do ciężkiego lekami systemowymi" Rzeszów 15-16.12.2021 r. oraz 20-21.12.2021 r.

2. Wykaz skrótów

AFM – mikroskopia sił atomowych (ang. *atomic force microscopy*)

AFM-IR – mikroskopia sił atomowych zintegrowana ze spektroskopią w podczerwieni
(ang. *atomic force microscopy-infrared spectroscopy*)

FFA – łysienie czołowe bliznowaciejące (ang. *frontal fibrosing alopecia*)

LPP – liszaj płaski mieszkowy (ang. *lichen planopilaris*)

SD – odchylenie standardowe (ang. *standard deviation*)

SPM – mikroskopia ze skanującą sondą (ang. *scanning probe microscopy*)

3. Wykaz publikacji stanowiących rozprawę doktorską

1. Krawczyk-Wołoszyn K, Roczkowski D, Reich A, Żychowska M. Applying the Atomic Force Microscopy Technique in Medical Sciences—A Narrative Review. *Biomedicines*. 2024; 12(9):2012. doi: 10.3390/biomedicines12092012.
2. Krawczyk-Wołoszyn K, Roczkowski D, Reich A. Evaluation of Surface Structure and Morphological Phenomena of Caucasian Virgin Hair with Atomic Force Microscopy. *Medicina (Kaunas)*. 2024 Feb 9;60(2):297. doi: 10.3390/medicina60020297.
3. Krawczyk-Wołoszyn K, Żychowska M, Reich A. Evaluation of hair surface structure and morphology of patients with lichen planopilaris (LPP) by atomic force microscopy (AFM). *Skin Res Technol*. 2024 Sep;30(9):e70030. doi: 10.1111/srt.70030.

4. Wstęp

Liszaj płaski mieszkowy (LPP) i łysienie czołowe bliznowaciejące (FFA) są dwoma głównymi podtypami pierwotnego łysienia bliznowaciejącego przebiegającego z limfocytarnym naciekiem zapalnym. W obu schorzeniach nacieki złożony głównie z limfocytów T CD8⁺ powoduje niszczenie mieszków włosowych [1,2]. Zarówno LPP, jak i FFA wymagają postawienia diagnozy i wdrożenia leczenia na wczesnym etapie choroby ze względu na praktycznie nieodwracalne uszkodzenie mieszków włosowych i rozwój łysienia bliznowaciejącego [3]. Ponieważ mają tę samą etiopatogenezę, ale różnią się objawami klinicznymi, są uznawane jako dwa warianty tego samego schorzenia [4]. Obecnie diagnozę LPP stawia się na podstawie badania histopatologicznego z inwazyjnej biopsji skóry głowy oraz, pomocniczo, na podstawie szeroko dostępnej i praktycznej dermoskopii, chociaż badania te niekoniecznie muszą być rozstrzygające [5]. W LPP zapalenie okołomieszkowe i późniejsze zwłóknienie mogą deformować mieszek włosowy i powodować nieprawidłowości łodygi włosa [6]. Dermoskopia (trichoskopia) stanowi główne nieinwazyjne narzędzie do wstępnej diagnostyki chorób włosów i skóry owłosionej głowy. Główną nieprawidłowością włosów w LPP, którą można uwidocznic w dermoskopii, jest obecność pili torti, zwanych również „skręconymi włosami” [7]. Należy jednak zdawać sobie sprawę, że rola dermoskopii w ocenie nieprawidłowości ultrastrukturalnych łodyg włosów jest ograniczona. Ponadto, dermoskopia nie umożliwia oceny wpływu zmian w łodydze włosa na jego właściwości mechaniczne.

Dlatego też w ostatnich latach rozpoczęły się badania nad ludzkimi włosami z wykorzystaniem mikroskopii sił atomowych (AFM). Zastosowanie techniki AFM do badania włosów w nanoskali może przyczynić się do poprawy diagnostyki i leczenia chorób skóry głowy [8]. Do tej pory przeprowadzono badania nad obrazowaniem AFM włosów, skupiając się na takich chorobach dermatologicznych jak łuszczyca, łysienie plackowate i łojotokowe zapalenie skóry [9-11].

AFM jest rodzajem mikroskopii z sondą skanującą (scanning probe microscopy-SPM). Służy do obrazowania struktury atomowej poprzez skanowanie próbki zaostrzoną końcówką sondy zamontowaną na elastycznym wsporniku. Technika ta umożliwia obrazowanie próbek w powietrzu, cieczy i wysokiej próżni. Dzięki możliwości rejestrowania obrazów w roztworze buforowym, próbki biologiczne mogą być badane w ich natywnych stanach. Możliwe jest badanie komórek przyżyciowo, bez

konieczności barwienia, utrwalania, odwadniania lub znakowania próbek [12,13]. Umożliwia to badanie dynamicznych zjawisk biologicznych w czasie rzeczywistym, w nanoskali. Ponadto, monitorując ugięcie wspornika, można uzyskać informacje z płaszczyzny Z, zapewniając trójwymiarowe obrazy badanej powierzchni. Umożliwia to scharakteryzowanie morfologii, grubości, chropowatości powierzchni badanej próbki oraz sił atomowych, zwłaszcza sił wzdłużnych. AFM w płaszczyźnie wykazuje rozdzielczość około 1 nm, podczas gdy dla powierzchni żywych komórek może zbliżyć się do 10 nm. Rozdzielczość poza płaszczyznę wykazuje wartości rzędu sub-nanometrów [14,15]. Za pomocą AFM można wykonywać pomiary w mikro- i nanoskali, a nawet rejestrować zdarzenia atomistyczne na krawędziach stopni sieci atomowej. Powierzchnia skanująca umożliwia przeprowadzanie badań do wymiarów rzędu 100 μm w płaszczyźnie poziomej i do 10 μm wysokości. Interakcje mechaniczne sonda-próbka umożliwiają badanie właściwości nanomechanicznych, elektrycznych, magnetycznych i trybologicznych, a także mapowanie powierzchni. AFM jest nowoczesnym, zaawansowanym, wielofunkcyjnym narzędziem, które pozwala na cały szereg pomiarów i testów [16,17]. Ma jednak również kilka wad. Głównym ograniczeniem AFM jako narzędzia diagnostycznego jest to, że AFM nie może być stosowany w żywym ludzkim ciele. Możliwe jest badanie komórek *in vitro* z izolowanych kultur komórkowych lub *ex vivo* z próbek biopsji [18,19]. Kolejnym ograniczeniem metody jest bardzo niska wydajność eksperymentalna ze względu na niską automatyzację procedury i jej czasochłonność [20]. Jednym z ograniczeń jest również techniczne przygotowanie próbki biologicznej, przez co uzyskane wyniki nie mogą być porównywane bez uprzedniej standaryzacji danej procedury. W zależności od przygotowania próbek biologicznych, wyniki mogą różnić się między badaniami, a artefakty mogą wpływać na porównywalność uzyskanych obrazów [21].

5. Cel pracy

Podjęliśmy badania mające na celu:

1. Określenie typowych cech i wyglądu powierzchni zdrowego włosa w nanoskali za pomocą mikroskopii sił atomowych oraz stworzenie schematu referencyjnego włosa zdrowego.
2. Wykazanie wpływu limfocytarnego nacieku zapalnego w mieszkach włosowych i hiperkeratynizacji ujść mieszków włosowych na morfologię łodyg włosów pacjentów z liszajem płaskim mieszkowym.
3. Ocenienie skuteczności zastosowania mikroskopii sił atomowych do wykrywania różnic między włosami zdrowymi a chorymi.

6. Materiały i metody

Do badania na podstawie autorskiej ankiety dotyczącej badania podmiotowego i przedmiotowego włączono 20 osób rasy kaukaskiej. Całość preparatyki próbek przeprowadzono w oparciu o powtarzalną, własną metodę obróbki i badania włosów za pomocą mikroskopu AFM. Projekt uzyskał pozytywną opinię Komisji Bioetycznej Uniwersytetu Rzeszowskiego (uchwała nr 9/10/2020 wydana w dniu 22.10.2020 r.).

Grupa kontrolna składała się z 10 zdrowych uczestników, 9 kobiet i 1 mężczyzny, w średnim wieku 43,8 lat z SD (odchyleniem standardowym) = 15,5. Od każdego badanego pobrano od trzech do pięciu włosów, które nie były poddawane farbowaniu ani innym uszkadzającym zabiegom przez co najmniej 3 miesiące. Żaden z badanych nie cierpiał na jakąkolwiek chorobę skóry lub włosów.

Następnie z grupy czterdziestu pacjentów z histopatologicznie potwierdzoną diagnozą LPP, wybrano 10 pacjentów z największym nasileniem choroby (grupa badana). Nasilenie choroby oceniano na podstawie badania fizykalnego, dermoskopii oraz objawów subiektywnych. Grupa badana składała się z 9 kobiet i 1 mężczyzny, w średnim wieku 56.1 lat z SD = 10,0. 5 osób wykazywało klasyczną postać LPP, 3 osoby klasyczną postać FFA, natomiast u 2 współistniały cechy LPP i FFA. Od każdego z uczestników pobrano od trzech do pięciu włosów z obwodu aktywnych zmian chorobowych.

Czyste włosy zostały wyrwane wraz z korzeniami, a następnie pocięte skalpelem na odcinki o długości 3 cm. Fragmenty włosów przymocowano do szkiełka mikroskopowego za pomocą przezroczystej dwustronnej taśmy. Każdy włos został zeskanowany za pomocą mikroskopu sił atomowych w 9 lokalizacjach (0.5, 1.0, 1.5, 2.0, 3.5, 4.5, 5.5, 6.5 i 7.0 cm od korzenia włosa).

Obrazowanie AFM przeprowadzono przy użyciu mikroskopu DriveAFM z kontrolerem CX (Nanosurf, Liestal, Szwajcaria) w warunkach atmosferycznych (w powietrzu) w temperaturze pokojowej i stabilnej wilgotności (65%-70%). Obrazowanie zostało przeprowadzone w trybie kontaktowym przy użyciu końcówek PPP-FMAuD-10 (NANOSENSORS, Neuchatel, Szwajcaria) zamontowanych na wspornikach ze stałą siłą 1,9 N/m i częstotliwością 75 kHz. Zakres skanowania obejmował obszar od 40×40 μm do 3×3 μm. Prędkość skanowania wynosiła 0,5 s/linię. Rozdzielczość obrazów wynosiła 512-1024 punktów/linię. Końcówka AFM została wyśrodkowana tak, aby znajdowała się nad najwyższym punktem krzywizny włosa.

Skanowała ona włos prostopadle do osi wzdłużnej jego włókna, aby zmniejszyć błędy spowodowane uderzaniem końcówki AFM o zakrzywione boki włókna włosa. W każdej z 9 lokalizacji na włosie, wykonano co najmniej 4 zdjęcia (4-10 zdjęć). Ostatecznie stworzono i przeanalizowano łącznie około 836 zdjęć. Obrazy zostały przetworzone komputerowo przy użyciu oprogramowania Nanosurf CX ver 3.10.3.7. Tworzenie profili liniowych, wizualizacje 3D, przetwarzanie obrazów i wszystkie pomiary metryczne zostały wykonane przy użyciu oprogramowania Gwyddion (64 bit) ver 2.63.

W badaniu wykonano pomiary metryczne łusek włosów, takie jak względna długość, szerokość i wysokość stopnia łuski. Scharakteryzowano cztery różne powierzchnie włókna włosa (łuski o prążkowanej powierzchni, endocuticle, łuski o gładkiej powierzchni i kora), ghost signs oraz zmiany kształtu łusek i ich wolnych krawędzi. Ponadto zaobserwowano zmiany morfologiczne widoczne na powierzchni zdrowych włosów (pitting, oval indentations, rod-like macrofibrillar elements, globules, scratches, wavy edge) oraz chorych włosów (fragmenty okołomieszkowych łusek, wizualizacja AFM obszarów przewężeń i owalnych zagłębień włosów opisywanych w mikroskopie świetlnym oraz takie cechy morfologiczne jak longitudinal cracks oraz indentations). Przeprowadzono analizę ilościową i półilościową stwierdzonych struktur.

Analizę statystyczną przeprowadzono przy użyciu oprogramowania Statistica v.13.0 (TIBCO Software Inc., Kraków, Polska). Obliczono średnie, minimalne i maksymalne wartości parametrów oraz ich odchylenia standardowe (SD). Różnice pomiędzy osiągniętymi wynikami zostały poddane analizie przy pomocy testu t-Studenta, testu U Manna-Whitneya lub testu Chi². Wartości p mniejsze niż 0,05 uznawane były za znaczące statystycznie.

7. Wyniki

Przedstawione badanie umożliwiło ocenę dynamiki zmian powierzchni włosa wraz z odległością od korzenia.

Zidentyfikowano powierzchnie włókna zdrowego włosa, takie jak łuski o prążkowanej powierzchni, endocuticle, łuski o gładkiej powierzchni i kora. Tylko łuski o prążkowanej powierzchni były obecne na początkowych, nieuszkodzonych odcinkach włosów zdrowych. Gdy górna warstwa łusek odrywała się (od wolnego końca łuski) w procesie naturalnej delaminacji włosa, odsłaniane były głębsze warstwy łusek: endocuticle, a następnie gładka powierzchnia następnej warstwy łusek. Zmiany te były najbardziej intensywne w odległości 1,5-6,5 cm od końca korzenia włosa. Gładka powierzchnia zyskiwała przewagę nad prążkowaną powierzchnią w odległości około 4,5 cm od końca korzenia. Kolejna warstwa - kora – była obserwowana jedynie na końcu włosa. Powierzchnia ta była widoczna po całkowitym złuszczeniu się warstwy kutykularnej obejmującej łuski włosa. Ponadto, stopniowe złuszczenie powierzchni leżących łusek odsłaniało wgłębienie na łuskach leżących poniżej - ghost signs. Objaw ten był markerem przejścia między zewnętrzną prążkowaną powierzchnią a głębszą gładką powierzchnią. Dodatkowo łuski włosów tuż u nasady miały gładkie i nieprzerwane krawędzie. Stopniowe odrywanie się wolnych krawędzi łusek powodowało, że ich krawędzie stawały się coraz bardziej postrzępione i połamane. Przez odłamywanie się krawędzi łusek, zmieniał się również ich kształt - od wypukłego przez płaski do wklęsłego. Uzyskane wyniki i stworzony wzór wyglądu włosów podczas naturalnego procesu delaminacji stanowiły punkt odniesienia do oceny chorych włosów.

Obserwowano istotną statystycznie różnicę w nasileniu procesu delaminacji włókien włosów pacjentów z LPP wraz z odległością od korzenia włosa. W grupie LPP stwierdzono statystycznie istotną, mniejszą liczbę łusek z prążkowaną powierzchnią, począwszy od 3,5 cm od nasady, aż do wolnego końca włosa. Dodatkowo obecne było m.in. większe nasilenie wyłamania wolnych brzegów łusek oraz większe występowanie endokulikuli. Ponadto, opisano obszary na włosach chorych, w których zachodził proces patologicznej, nienaturalnej delaminacji włókna włosa. Obszary te dotyczyły owalnych zagłębień i przewężeń włókien włosów, które były widoczne w mikroskopie świetlnym. Nie były one obserwowane na włosach zdrowych. Kolejnymi unikalnymi cechami morfologicznymi, które stwierdzono jedynie na włosach LPP były

zakrzywione, elipsoidalne wgniecenia (indentations), pęknięcia wzdłużne wolnych brzegów łusek (longitudinal cracks) oraz perforowane struktury na powierzchni włosów odpowiadające najpewniej fragmentom okołomieszkowego kołnierzyka widocznego w dermoskopii.

W badaniu porównano również nasilenie występowania zmian morfologicznych obecnych zarówno na włosach zdrowych jak i chorych (pitting, oval indentations, rod-like macrofibrillar elements, globules, scratches, wavy edge). Stwierdzono większą ilość zadrapań (scratches) w początkowych sekcjach włosów LPP (1-5,5 cm), większą intensywność występowania falistych krawędzi (wavy edges) na całej długości włosów LPP (0,5-7 cm) oraz większą liczbę łusek z ubytkami (pitting) w środkowej części włosów LPP (3,5-6,5 cm). Wszystkie te różnice były istotne statystycznie.

W pracy wykonano również pomiary metryczne łusek. W badanych grupach wartość odchylenia łusek włosa wzrastała wraz z odległością od korzenia włosa. Wzrastały również wymiary takie jak długość i szerokość łusek. Tendencja do wzrostu tych wymiarów była bardziej zauważalna w grupie badanej niż w grupie kontrolnej. Różnice między wymiarami łusek w grupie badanej i kontrolnej nie były jednak istotne statystycznie.

8. Dyskusja

Podsumowując, nasilone cechy delaminacji mogły sugerować zwiększone zniszczenie włosów u pacjentów z LPP. Może to wskazywać albo na osłabioną strukturę włosa, który tworzy się w histologicznie zmienionym mieszkcu włosowym, albo pomaga określić moment zadziałania czynnika wpływającego na niszczenie włosów, który doprowadził do rozwoju choroby jeszcze przed wystąpieniem objawów klinicznych. Wavy edges mogły powstawać podczas formowania się włosa w zmienionym zapalnie mieszkcu włosowym i przechodzenia jego włókna przez objęte stanem zapalnym infundibulum oraz poprzez kontakt z powierzchnią wewnętrzną pochewki korzenia. Scratches i pitting mogły być związane z nadmierną podatnością włosa na urazy mechaniczne spowodowaną chorobą lub jako objaw wysokiej traumatyzacji włosa, która mogła przyczynić się do rozwoju choroby. Inną możliwością jest teoria, że infiltracja komórek zapalnych w mieszkcu włosowym, która zaburzyła jego architekturę, może powodować „drapanie” tworzących się miękkich łusek.

Według naszej wiedzy jest to pierwsze badanie porównawcze powierzchni łodygi włosa na całej długości pomiędzy grupą LPP i grupą zdrową przy użyciu AFM. Przedstawione badanie umożliwiło ocenę dynamiki zmian powierzchni włosa wraz z odległością od korzenia. Wyniki przedstawione w niniejszym badaniu stanowią próbę scharakteryzowania zmian morfologicznych w nanoskali, co może być pomocne we wczesnej diagnostyce chorób włosów w przyszłości. Przedstawione wstępne wyniki nadają kierunek dalszym badaniom nad chorobami skóry głowy i włosów. Włosy osób z LPP i zdrowe włosy mają zauważalne różnice w powierzchni. Ze względu na czasochłonność metody i konieczność wykonania wielu pomiarów na długości pojedynczego włosa, badaniem objęto niewielką grupę pacjentów. Nie bez znaczenia dla powyższej publikacji jest fakt, że podobne cechy morfologiczne zaobserwowano już we wcześniejszych, choć nielicznych publikacjach. Uzasadnione wydają się być dalsze badania powierzchni włosów w różnych chorobach zapalnych skóry owłosionej głowy za pomocą AFM.

9. Publikacje stanowiące rozprawę doktorską



biomedicines



Review

Applying the Atomic Force Microscopy Technique in Medical Sciences—A Narrative Review

Karolina Krawczyk-Wołoszyn ^{1,2}, Damian Roczowski ², Adam Reich ^{2,*} and Magdalena Żychowska ^{2,*}

¹ Doctoral School, University of Rzeszów, 35-959 Rzeszów, Poland; karolinakrawczyk10@wp.pl

² Department of Dermatology, Institute of Medical Sciences, Medical College of Rzeszów University, 35-959 Rzeszów, Poland; droczkowski99@gmail.com

* Correspondence: adi_medicalis@go2.pl (A.R.); magdazychowska@gmail.com (M.Ż.)

Abstract: Penetrating deep into the cells of the human body in real time has become increasingly possible with the implementation of modern technologies in medicine. Atomic force microscopy (AFM) enables the effective live imaging of cellular and molecular structures of biological samples (such as cells surfaces, components of biological membranes, cell nuclei, actin networks, proteins, and DNA) and provides three-dimensional surface visualization (in X-, Y-, and Z-planes). Furthermore, the AFM technique enables the study of the mechanical, electrical, and magnetic properties of cells and cell organelles and the measurements of interaction forces between biomolecules. The technique has found wide application in cancer research. With the use of AFM, it is not only possible to differentiate between healthy and cancerous cells, but also to distinguish between the stages of cancerous conditions. For many years, AFM has been an important tool for the study of neurodegenerative diseases associated with the deposition of peptide amyloid plaques. In recent years, a significant amount of research has been conducted on the application of AFM in the evaluation of connective tissue cell mechanics. This review aims to provide the spectrum of the most important applications of the AFM technique in medicine to date.

Keywords: atomic force microscopy (AFM); biomedical research; melanoma; oncology; skin cells



Citation: Krawczyk-Wołoszyn, K.; Roczowski, D.; Reich, A.; Żychowska, M. Applying the Atomic Force Microscopy Technique in Medical Sciences—A Narrative Review. *Biomedicines* **2024**, *12*, 2012. <https://doi.org/10.3390/biomedicines12092012>

Academic Editor: Bing Guo

Received: 30 July 2024

Revised: 25 August 2024

Accepted: 29 August 2024

Published: 3 September 2024



Copyright: © 2024 by the authors. Licensee MDPI, Basel, Switzerland. This article is an open access article distributed under the terms and conditions of the Creative Commons Attribution (CC BY) license (<https://creativecommons.org/licenses/by/4.0/>).

1. Introduction

Modern medicine aims to study single cells, chemical molecules and signaling pathways to understand pathological conditions as deeply as possible. Penetrating deep into the cells of the human body in real time has become increasingly possible with the implementation of modern technologies into medicine—such as atomic force microscopy (AFM). AFM is a type of microscopy that utilizes a scanning probe (Scanning Probe Microscopy—SPM). It allows for the possibility of achieving a resolution of fractions of a nanometer, or even on an atomic scale [1,2]. A lateral spatial resolution for an extracted and immobilized cell membrane patch is approximately 1 nm [3,4], while the resolution for surfaces of living cells can approach ~10 nm [5,6]. The vertical resolution in the Z-plane is about 0.01–0.1 nm, which constitutes one of the main advantages of this technique [7,8]. AFM enables the effective live imaging of the cellular and molecular structures of biological samples (such as cellular surfaces, components of biological membranes, cell nuclei, actin networks, proteins, and DNA) and provides three-dimensional visualization of the surfaces, in the X-, Y- and Z-planes. Testing may take place in a variety of environments (vacuum, air or liquid) [9–15]. Typical images reach 10–100 µm in the X- and Y-planes and up to 10 µm in the Z-plane [9,10].

The AFM method has also been used to study the nanomechanical, electrical and magnetic properties of cellular structures [3,9,16–20]. By examining the mechanical properties of the sample, the stiffness/elasticity, as well as the viscous and adhesive properties of the sample's surface, can be determined, and a tensile or compressive modulus (Young's modulus) can be created [8,9,18,19,21–28]. The AFM is now evolving into a multi-parameter

sensing device, but it originally functioned as a tool for imaging and direct force measurement [29,30].

The spring constant of the cell surface is influenced by extracellular and intracellular factors and can provide information about changes in the cell, e.g., it may be used to evaluate the effect of antibiotics on bacterial cells or the impact of mutations on eukaryotic cells [2,9,14,22,31–38]. In addition, it is possible to measure interaction forces between various biomolecules. The ability to measure the interaction forces between the AFM's scanning tip and the sample provided an opportunity for the use of AFM in force spectroscopy [29,30]. Binding forces between complementary oligonucleotides and interactions in receptor–ligand complexes or between adhesion proteins were all studied using AFM [39–42]. Attaching a specific molecule probe to the AFM tip enables selected molecules of interest to be found; these specifically interact with the probe in the studied sample. Such evaluation is possible thanks to molecular recognition force microscopy (MRFM) or topography and recognition (TREC) microscopy [9,43–46].

The main advantages of AFM are that there is no need for the staining, fixation, dehydration or labeling of samples [8]. Scanning probes can image a variety of materials without destroying them—from delicate, soft biological samples to titanium oxide–metal surfaces [47]. AFM may also be combined with other techniques, such as single-cell force spectroscopy (SCFS), single-molecule force spectroscopy (SMFS), chemical force microscopy (CFM), and atomic force microscope–infrared spectroscopy (AFM-IR), which only extends the potential applications for this method [1,17,48].

2. Construction of the Microscope, the Physical Basis, and the Principle of Its Operation

Unlike classical optical microscopy, in AFM, representing the scanning probe microscopy (SPM) group, measurement is performed by the deflection of the cantilever with the probe attached due to contact with the surface or intermolecular forces [49]. The tip is moved along the surface of the tested material. The forces of interaction of the tip's atoms with the surface are measured by recording the movement of a cantilever, which does not exceed 1 nN. Using a set of electronic sensors, information about the deflection of the cantilever from the equilibrium position is recorded, giving information about the force of interaction between the tip and the sample [50]. The principle of the AFM can be illustrated by van der Waals forces [51]. The interaction energy between a pair of neutral atoms, located at a given distance, also called the Lennard-Jones potential (V), is defined by the following equation:

$$V(r) = 4\epsilon \left[\left(\frac{\sigma}{r} \right)^{12} - \left(\frac{\sigma}{r} \right)^6 \right]$$

where r is the distance between two atoms, and ϵ and σ are the bond energy and bond length, respectively [52].

The diagram below (Figure 1B) shows the operation of the AFM. The laser generates a beam of radiation, which is directed at the top surface of the cantilever and is then reflected from it. The reflected laser beam is collected by a split photodiode [53]. The cantilever is mounted on a piezoelectric scanner that allows movement in the horizontal (x , y) or vertical (z) dimension. The geometry of the scanner is controlled by the value of the applied voltage [54]. A flexible cantilever, consisting of a base, a micro spindle and a sharp cone- or pyramid-shaped tip, is used to interact with the sample. Probes are usually made of silicon, silicon dioxide or silicon nitride, created during nanofabrication processes [55]. By approaching the probe to the sample for a short distance, its deformation resulting from the interaction between the tip and the surface of the test substance is observed. Measurements using AFM are designed to obtain information about forces, so the deflection must be converted to a force (F) of interaction according to the principles of mechanics and Hook's law, which states that the magnitude of the force acting on the tip of the sample is proportional to the deflection of the arm:

$$F = k \times x$$

where x is the deflection of the cantilever and k is the elasticity constant of the cantilever. Deflection (F) is measured in volts [V] converted to units of force [N —newton] using the following formula:

$$F[nN] = I[V] \times invA\left[\frac{nV}{V}\right] \times k\left[\frac{N}{m}\right]$$

where I is the signal recorded in the microscope [V], $invA$ is the sensitivity of the photodetector, k is the elasticity constant, m —meter, and n —nano [56].

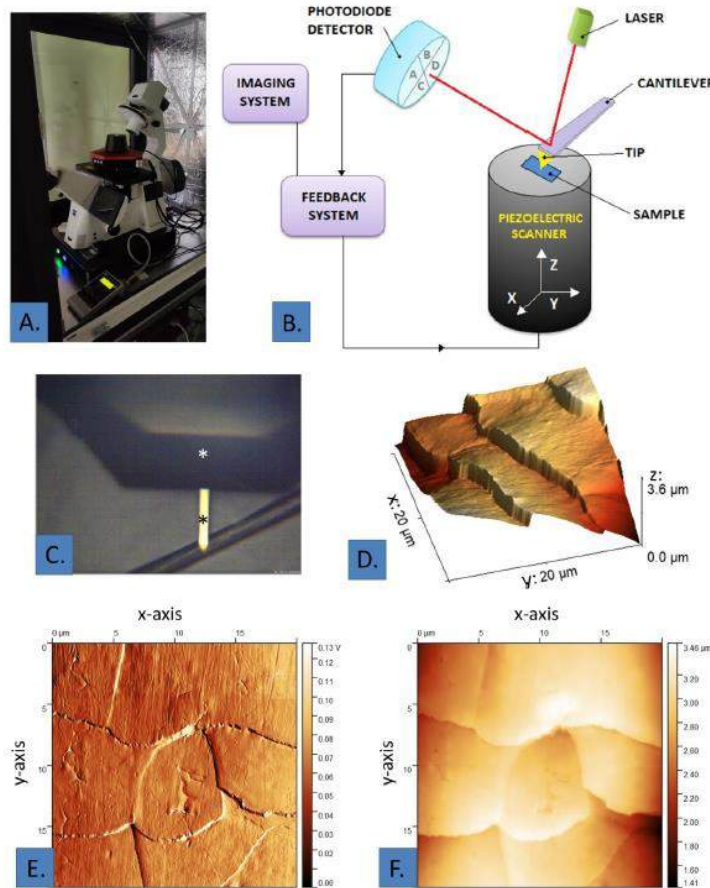


Figure 1. (A) Photograph of the atomic force microscope; (B) schematic of the AFM construction. TIP: tip of the cantilever. (C) cantilever (white asterisk) with AFM tip (black asterisk) scanning hair—optical microscope view; (D) AFM graphic of the hair surface—3D projection: x—the dimension transverse to the longitudinal axis of the hair fiber; y—the dimension parallel to the longitudinal axis of the hair fiber; z—height of hair surface; (E) AFM image of the hair surface—deflection image: x—the dimension transverse to the longitudinal axis of the hair fiber; y—the dimension parallel to the longitudinal axis of the hair fiber; (F) AFM image of the hair surface—Z-axis image: x—the dimension transverse to the longitudinal axis of the hair fiber; y—the dimension parallel to the longitudinal axis of the hair fiber.

The resolution of AFM depends on several factors. These include the radius of curvature of the scanning tip and the precision of the entire scanning system, as well as the nanopositioning system [57]. AFM uses a positioner to place samples under a cantilever with a sharp probe to manipulate objects at the nanoscale. When measuring a sample, the XY nanopositioner is used to move the sample across an area in the system while the Z nanopositioner allows for the positioning of the cantilever and adjustment of the force acting between the tip and the sample [58].

3. AFM Imaging Modes

There are several modes for the imaging of the surface topography with AFM. The most commonly mentioned standard modes are as follows: contact mode, non-contact mode, tapping mode, and atomic force spectroscopy. The modes differ in the range of the interaction force between the AFM tip and the surface (short-range and long-range forces).

Contact mode is the simplest and the most widely used mode developed in AFM [59]. The cantilever tip is in constant physical contact with the sample surface. A feedback mechanism that allows interaction between the tip and the sample should remain constant during scanning. In contact mode, the tip of the probe is applied to the sample surface with a force of 10^{-11} – 10^{-7} N [60]. The cantilever tip constantly changes its position to maintain the same amount of deflection from the surface of the scanned sample. This mode is not particularly suitable for very soft surfaces, but much better results can be obtained for hard materials. The main disadvantage of operating in contact mode includes the susceptibility of the AFM tip to stick to the layer of surface contaminants that are present on the sample surface, which can result in image distortion [61].

In non-contact mode, the AFM tip oscillates at a frequency close to the resonance frequency (typically between 100 and 400 kHz) at a distance of tens to hundreds of angstroms relative to the sample surface. Here, the image is acquired with little or no contact with the sample. The sources of the attractive forces are the van der Waals interactions of atoms on the tested surface and on the surface of the tip [62]. This method is designed for the evaluation of very delicate materials. This mode has several advantages over other modes because the tip does not interact strongly with the sample. Moreover, this model is not subject to tip or sample degradation that can occur during “contact mode” measurements [63].

Positioning the tip close enough to the sample to make short-range forces detectable while also preventing the tip from sticking to the tested surface is the basis for another mode of AFM operations. Tapping mode is a key advancement in AFM. Very soft and delicate samples can be successfully imaged using this mode [64]. During scanning, the cantilever alternately touches the surface and rises at a frequency of about 50–500 kHz. This causes energy loss due to the periodic contact of the tip with the surface, so the amplitude of the vibration varies depending on the topography of the sample surface [65].

Atomic force spectroscopy (AFS) is very similar to contact mode. In this mode, the tip does not leave the surface at all during the oscillation cycle. This mode is used to image the flexibility of the sample and is ideal for imaging composite materials or soft samples on hard substrates, where contrast can be obtained between areas with different flexibilities [66]. AFS is a useful tool for studying adhesion forces, local elastic restoring forces, and local frictional forces [67,68].

4. Biomedical Applications of AFM

The first attempts to image cells using AFM began in the 1990s and involved dried red and white blood cells and *Escherichia coli* at outset, followed by dried *Halobacterium halobium* cells and living plant cells, and then red and white blood cells in buffer solution [69]. Further studies were conducted on mammalian cells, as they did not require additional processing (like dehydration, staining or coating) and fixation, but only immobilization, which did not affect the properties of the cells to any significant extent [29,69,70]. Subsequently, AFM started to be utilized not only to image cell surfaces but also to measure forces in biomolecular systems [26] and the nanomechanical properties of tissues [18,71,72]. In the

late 1990s, it was possible to measure with AFM the forces required to break bonds between selected biomolecules, providing a basis for studying receptor–ligand systems [39,73]. These discoveries enabled further research on the intermolecular forces between antigens and antibodies [74,75].

The possibility of interaction between specific molecules has given origin to topography and recognition microscopy (TREC). This allows for the rapid identification of a specific receptor, the assessment of its location on heterogeneous biosurfaces, and the creation of a visual topography map [76]. In Chitchevlov's study, the extracellular domains of VE cadherin were identified and localized on the surface of vascular endothelium using TREC [76]. This method may find application in oncology, as cell adhesion molecules (CAMs) have been shown to play a key role in tumorigenesis and metastasis [77,78]. CAM expression increases on malignant tumor cells, making their identification with AFM techniques potentially effective. However, studies to date have been limited by the low throughput and mapping time of cells in AFM [18,77,79,80].

Recently, there has been an increasing number of studies in the biomedical field comparing and correlating results obtained with scanning electron microscopy (SEM), transmission electron microscopy (TEM), AFM, confocal microscopy, Raman spectroscopy, and multiphoton microscopy (MPM). These techniques are complementary and are used for nano- to macro-level study. They provide information regarding morphological, chemical, and mechanical properties in order to facilitate a comprehensive understanding of the structure and properties of cells and biological molecules [81–85]. For example, differences between SEM and AFM images in the imaging of the liver's parenchymal structures or ocular nerve fibers have been shown. Each technique revealed different details and subcellular structural information that correlated with each other. These were due to differences in the detection systems and sampling procedures of the two techniques [86,87]. By correlating different microscopic methods, more detailed information can be obtained and the scope of the study can be expanded [81–87].

The interest in the AFM technique in recent years can be seen in the number of studies available. The largest number of publications on the application of AFM in medicine available in PubMed are in fields such as 'DNA research' (approximately 3829 results), 'Oncology' (approximately 2910 results), 'Blood cells and plasma protein' (approximately 1541 results), 'Immunology' (approximately 1152 results), and 'Neurodegenerative disease' (approximately 830 results). A slightly smaller number of publications concerned 'Aging' (approximately 650 results), 'Connective tissue' (approximately 497 results), 'Skin cells' (approximately 339 results), 'Hair' (approximately 197 results), and 'Melanoma' (approximately 136 results).

4.1. Neurodegenerative Diseases

In the following years, the structure of proteins in the bound state and the dissociated state was studied [88–91]. For many years, AFM has been a very important tool for the study of neurodegenerative diseases associated with the deposition of peptide amyloid plaques and it has been the only instrument utilized for evaluating the structural dynamics of amyloid protein aggregates. Initially, Roeters et al. studied the process of the pathological aggregation of peptides and formation of amyloid fibrils [92]. Subsequently, the structure of β -amyloid and its oligomers [93,94], as well as the relationship between its formation and neurotoxicity [95], have been studied. Several authors have recently utilized AFM to assess the potential therapeutic mechanisms in neurodegenerative diseases, including Alzheimer's and Parkinson's disease [96–99]. Shao et al. used tetrahedral DNA nanostructures (TDNs) in their experiment to evaluate their effectiveness in inhibiting neural cell apoptosis. In this case, the AFM technique was used to confirm the correct morphology of the prepared TDNs particles. The authors showed that TDNs, by inhibiting neuronal apoptosis in Alzheimer's disease, can positively improve memory and cognitive function [97].

4.2. DNA Research

AFM has also played a major role in DNA research. More modern AFM techniques, such as AFM biosensing, measure forces between complementary DNA strands or between oligonucleotides using highly specific building blocks [40,41].

There have also been important studies on the DNA mismatch repair (MMR) system using AFM. MMR plays a pivotal role during DNA replication and recombination. The mechanism protects cells from homologous recombination and mutations by signaling DNA damage. Therefore, by maintaining genome stability, it limits carcinogenesis in eukaryotic cells. Defects in the MMR system predispose individuals to certain types of cancer, the formation of birth defects, and infertility. Therefore, some authors studied the interactions between MutS, MutL, MutH, and DNA proteins in this system with AFM techniques [100–102].

4.3. Connective Tissue

Although AFM is mainly utilized in basic science, it has also found wider use in medicine in the diagnosis of cartilage tissue diseases. By examining the functionality of cartilage tissue, AFM may serve as a tool for the early diagnosis of osteoarthritis. Stolz et al. found the degradation of collagen, followed by the softening of the articular cartilage, and thus a reduction in the tissue's nano stiffness in osteoarthritis. Initial changes can be detected only at the nanoscale and differ from those found in healthy tissues that undergo aging [72,103].

Osteoblasts and muscle cells represent other connective tissue cells that have been studied with AFM. Takai et al. analyzed the transduction of mechanical signals in osteoblasts by measuring cell stiffness and adhesion to various substrates [104]. Mathur et al. developed elastic moduli and studied the elastic behavior of cardiac and skeletal muscles [105].

The impact of osteoporosis on the appearance of bone tissue in AFM was assessed in animal models. AFM can evaluate the bone surface in 3D and the geometry of its microstructure, as well as the organization of the bone matrix and collagen fibers in regions with increased resorption [106]. In a recent study utilizing AFM measurements of adhesion forces, collagen fibers were found to swell in osteoporotic bones. This reduces the ability of collagen–apatite interfaces to catalyze the crystallization of hydroxyapatite. This was suggested by the authors of the study to be the crucial mechanism in the development of osteoporosis [107]. It is noteworthy that the aforementioned changes were identified using the AFM technique.

Bone marrow cells have also been of interest to researchers working with AFM. Recent studies have evaluated multipotent mesenchymal stem cells (MSCs), which have an important function in bone and cartilage regeneration processes. MSCs are of focus because they represent a potential source in regenerative medicine. To date, changes in stiffness have been studied and Young's moduli have been developed for these cells. In addition, protocols for AFM measurements of MSCs during their osteogenic differentiation have been developed [108].

AFM has also been used to assess the biomechanics of cardiac tissues in arrhythmogenic cardiomyopathy, among others. It allows for the study of cell elasticity, adhesive forces, and viscoelastic properties. Therefore, AFM represents a promising tool with great potential for future research into fibrotic heart diseases [109].

4.4. Oncology

Recently, applications of AFM as a spectroscopic tool have expanded, especially in evaluating condensed soft matter or thin samples where other standard methods face significant limitations [110]. However, the refinement of this technique has found its most important applications in biomechanics for studying complex biological samples, such as cells and tissues, in terms of cancerous changes. Many biological processes taking place inside a living cell rely on the nanomechanical properties of cell substructures. AFM can

provide information on the integrity and mechanical parameters of cell membranes. The high sensitivity and low force exerted on the sample make AFM a useful, non-destructive tool for studying cellular nanomechanics [111]. Vibrational spectra of neuronal cells and tissues obtained with AFM have made it possible to distinguish healthy and malignant brain tissues in real time [112].

It is worth noting that, with the use of AFM, it is not only possible to differentiate between healthy and cancerous cells, but the technique also makes it possible to distinguish the stages of cancerous conditions. However, the ability to distinguish cancer stages with AFM is still an area of active research and it is not yet fully established [113]. AFM cell imaging, supported by artificial intelligence (AI), can be used to precisely identify the phenotype of a cell. AFM is able to distinguish between two similar human colon cancer cell lines based on the levels of stiffness, which, as they increase, reduce tumor activity [114]. An analysis of specific surface features at the nanoscopic scale using AFM can distinguish pathways to the process of cell death (e.g., apoptosis, necroptosis, and ferroptosis). It allows the observation of distinct features of each regulated form of cell death. While performing mechanobiological elasticity analysis, it is possible to detect the early onset of cell death, which manifests itself as a significant decrease in elasticity [115].

The best-known group of anticancer drugs are cytotoxic substances. Because of their poor specificity, they can also cause damage to healthy cells and lead to a variety of adverse reactions [116]. Phospholipid vesicles and nanomaterials (e.g., lipid nanotubes) with biocompatible and biodegradable characteristics have attracted considerable interest for their potential use as controlled-release systems. Thanks to its ability to assess the physical properties and stability of liposomes, AFM is an effective technique that provides both morphological and metrological information on the properties of liposomes [117]. It is one of the most widely used SPM techniques, which provides information on the interaction between lipid carriers and active compounds, as well as data on the elastic, chemical and adhesive properties of the carriers. AFM also makes it possible to monitor the effect of drug treatments on the nanomechanical properties of solid tumors, which can lead to the identification of biomarkers [118].

4.5. Skin Cells

The study of skin cells made it possible to assess the cytoskeleton, the stiffness of cells in different layers of the epidermis, and the cytoskeleton's differentiation and movement from the basal layer to the skin surface in order to evaluate the cell membrane lipids or nuclear mechanotransduction and to map the elastic moduli of the stratum corneum, epidermis, and dermis [119–122]. Modules of corneocyte elasticity and filaggrin, building a cornified cell envelope, were used to assess the mechanical properties of skin cells in atopic dermatitis [123]. AFM has also found application in studying the mechanical defects of cells caused by defective keratins and damage to the keratin network in blistering skin diseases, i.e., epidermolysis bullosa simplex [124]. By testing the forces of interaction between adhesion molecules, Vielmuth et al. conducted studies on desmogleins in pemphigus [125].

4.6. Aging

In dermatology, the effects of aging on skin and hair have been evaluated using AFM. Studies on skin fibroblasts, which are responsible for maintaining the mechanical properties of the dermal matrix, have shown that fibroblasts undergoing aging processes have reduced cytoskeletal tension and exhibit a considerable loss of traction force. This reinforces other factors associated with skin aging [126]. Other studies on skin photoaging have focused on collagen fiber content, which correlated with cell stiffness. AFM showed the reduced stiffness of skin cells subjected to long-term exposure to sunlight [127]. This parameter was evaluated in studies of drugs that exhibit anti-aging effects (i.e., retinol) [128]. Hairs also show differences in morphology during the process of aging. Jeong et al. showed that, after the age of 30, the diameter of the hair decreases, the surface of the scales is more

undulating and rougher, and the edges of the scales are more broken. They evaluated all these morphological changes using AFM [129].

4.7. Hair

In terms of hair research, the physicochemical and tribological properties of hair fibers, cells, and surface changes were studied. The research focus so far has been mainly concentrated on the effect of conditioners, hair-damaging external factors, and ethnic differences [130–137]. The latest AFM studies of hair utilized hybrid techniques. Among other things, spectroscopic techniques are being used in conjunction with AFM. Fellows et al. used AFM integrated with an infrared spectroscopy (AFM-IR) to study the chemical composition of the cuticle, medulla, and cortex of European hair [138–140].

In 2012, Shin et al. evaluated the morphology of the hair surface in patients with psoriasis vulgaris. They observed pits, increased roughness, and increased thickness of hair scales in patients with psoriasis. By imaging similar nanochanges within patients' hair growing on unaffected scalps, they showed that psoriasis is generalized in nature [141].

4.8. Melanoma

Jeon et al. demonstrated that neoplasia modulates the mechanical properties of melanoma tissue. Representative stiffness maps and elastic modulus histograms were generated using force–distance curve measurements. It was found that benign pigmented nevi showed more stiffness than healthy skin. In contrast, melanoma tissues showed a wide variety of elastic modulus distributions, indicating a high heterogeneity of mechanical properties. In addition, the mechanical properties of all histological melanoma samples were independent of gender, age, anatomical location or Clark grade of invasion [142].

4.9. Immunology

The study of immune cell mechanics appears to be the new application of AFM. The functioning of the immune system is based on complex intercellular interactions, made possible by physical and mechanical forces between cells. To date, AFM has enabled the imaging and study of the formation of neutrophil extracellular traps (NETs), immune synapse formation between T lymphocytes and antigen-presenting cells, macrophage phagocytosis, and the process of membrane pore formation [143]. AFM enabled the real-time imaging of the changes occurring in neutrophils and its organelles during the NETosis reaction. By measuring the forces occurring in neutrophils, the steps indicative of chromatin decondensation and the release of NETs were characterized [144]. In contrast, when analyzing the interactions between T cells and antigen-presenting cells, Babak et al. studied the forces of interaction (adhesion) between the receptors that make up these synapses (complex TCR/CD3 and molecules LFA-1, CD43, F-actin) [145,146]. With the AFM technique, it was also possible to record height profiles and maps of cell membrane adhesion and pore stiffness in lymphocytes. The process of cell membrane remodeling under the influence of mediators such as perforins and gasdermins in tumor cells and the complement-induced membrane attack complex (MAC) in immune cells were visualized using AFM. In addition, the effects of the formation, remodeling, and repair of pores in cell membranes on the processes of cell death (apoptosis) were also studied [147]. Considering the above, one can conclude that recent discoveries are laying the basis for the new branch of medicine that mechanobiology is becoming [143–146]. A combination of the AFM technique and mechanobiology may contribute to the development of immunotherapy for blood cancers and perhaps solid tumors in the future [148].

4.10. Blood Cells and Plasma Protein

Previously, the morphology of red blood cells (RBCs), surface roughness, RBC surface antigen-specific biomolecules, and mechanical properties such as the architecture of the membrane skeleton and elasticity were studied [29]. Using Young's moduli, changes in the stiffness and elasticity or deformability of the RBC cytoskeleton were shown [29,149].

Normal RBC cells were observed to have higher deformability. RBCs of patients with diabetes mellitus, hypertension, coronary disease, hereditary spherocytosis, thalassemia, G6PD deficiency, and sickle cell traits show a higher Young's modulus value (i.e., greater stiffness) [150–152]. Differences in RBC surface roughness have been observed in conditions such as Waldenström macroglobulinemia, multiple myeloma, elliptocytosis, iron deficiency anemia, thalassemia, and diabetes mellitus, as well as during aging and in nicotinism [153–157]. The study of changes in RBC quantitative parameters was also used to evaluate the effect of oxygen concentration on the characteristics of RBCs in a model in vitro in states of normoxemia and hypoxemia. It was found that there is a specific state of imbalance between oxidative and antioxidant substances at a specific level of hypoxemia, which only minimally affects the disruption of RBCs [158]. However, testing RBCs' values still requires the standardization of AFM parameters and sample preparation before AFM can serve as a diagnostic tool [29]. One of the most commonly studied hematological diseases with the use of AFM is malaria. With AFM imaging, it was possible to localize individual *Plasmodium falciparum* parasites in RBCs. AFM also made it possible to observe structural and adhesion changes in RBCs in real time at different stages of infection [29,159,160]. Further force spectroscopy research has opened the topic of targeted malaria drug development [161]. AFM is being used extensively to measure interactions between antibodies and plasma proteins (including fibrinogen) and RBC surface group antigens [29,162–164]. Some authors argue that the use of AFM in immunohematology could lay the groundwork for the development of highly selective and personalized medicine [29]. Also, the study of protein fibril aggregation on RBCs represents a new trend in the search for potential biomarkers of age-related neurodegeneration [165].

5. Limitations, Challenges, and New Trends for AFM Technology in Biomedicine

The main limitation of AFM as a diagnostic tool is that AFM cannot be used in the living human body. It is possible to examine cells in vitro from isolated cell cultures or ex vivo from biopsy samples [166,167]. Another limitation of the method is the very low experimental efficiency due to the low automation of the procedure and its time-consuming nature [116]. One of the limitations is also the technical preparation of the biological sample, so that the results obtained cannot be compared without prior standardization of the procedure in question. Depending on the preparation of the biological samples (cells may be fixed or unfixed but dried or resuspended in a specific solution), results may be different between studies and artifacts may affect the comparability of the images obtained [29]. It has been shown, for example, that the use of different cell preparation protocols affects different values of Young's modulus [149]. In the future, sample processing and technical protocols for working with AFM (choice of probe tip and choice of appropriate equipment parameters) should be standardized for specific tissues or diseases between different research centres [29].

A new direction in biomedical research using AFM is the acquisition of spatial-temporal information. The introduction of high-speed AFM (HS-AFM) to study dynamic changes in biological molecules over time enables an in-depth analysis of the configuration of biomolecules without disturbing their function. It is a technique currently used to study the function of soluble and membrane-bound proteins, the organization of DNA chromatin, and viral replication [168–171]. In addition, another trend in improving the AFM technique is to combine it with other techniques. Hybrid AFM methods lay the groundwork for the targeted study of the chemical, physical, and morphological properties of specific structures that have been located at a nanoscale [1,17,48,139,140]. Currently, hybrid technologies combining AFM functions with other measurement techniques are the most promising. AFM-IR enables nanoscale infrared spectroscopy studies. Contact Resonance AFM uses the vibration of an AFM cantilever that resonates in contact with the sample for testing nanomechanical properties. Chemical force microscopy (CFM) extended the AFM technique to localize selected structures on the sample surface for chemical composition studies.

AFM combined with confocal laser scanning microscopy (CLSM) correlates indentation points directly via fluorescence imaging of subcellular structures [10,116].

6. Conclusions

AFM evolved from the scanning tunneling microscope (STM), which was awarded the Nobel Prize in Physics in 1986 [19]. The STM used a conductive probe to electronically sense the surface of the conductive sample. Because of this, 2D images of biomolecules were unrepresentative and difficult to create [9]. AFM, based on the deflection of a scanning tip in contact or near contact with the surface under examination (without an electric field, as in STM), is more suitable for the visual testing of biological samples. The AFM technique is a future-oriented scientific tool thanks to its continuous improvement. Over the years, its ability to image cells or study their nanomechanical properties has evolved. Due to its highly complex nature, the study of biological samples was very complicated, requiring extensive knowledge in various fields and technical skills. In recent years, however, there have been significant advances and breakthroughs in the sophisticated study of biomechanical properties of human cells using microscopic techniques.

Funding: This research received no external funding. The publication fee was covered by a grant from the University of Rzeszow (grant number DINMCM 113/24).

Conflicts of Interest: The authors declare no conflict of interest.

References

1. Dorobantu, L.S.; Goss, G.G.; Burrell, R.E. Atomic force microscopy: A nanoscopic view of microbial cell surfaces. *Microm* **2012**, *43*, 1312–1322. [\[CrossRef\]](#) [\[PubMed\]](#)
2. Frederix, P.L.; Bosshart, P.D.; Engel, A. Atomic force microscopy of biological membranes. *Biophys. J.* **2009**, *96*, 329–338. [\[CrossRef\]](#) [\[PubMed\]](#) [\[PubMed Central\]](#)
3. Muller, D.J.; Engel, A. Atomic force microscopy and spectroscopy of native membrane proteins. *Nat. Protoc.* **2007**, *2*, 2191–2197. [\[CrossRef\]](#) [\[PubMed\]](#)
4. Miyata, K.; Tracey, J.; Miyazawa, K.; Haapasilta, V.; Spijker, P.; Kawagoe, Y.; Foster, A.S.; Tsukamoto, K.; Fukuma, T. Dissolution Processes at Step Edges of Calcite in Water Investigated by High-Speed Frequency Modulation Atomic Force Microscopy and Simulation. *Nano Lett.* **2017**, *17*, 4083–4089. [\[CrossRef\]](#) [\[PubMed\]](#)
5. Plomp, M.; Leighton, T.J.; Wheeler, K.E.; Hill, H.D.; Malkin, A.J. In vitro high resolution structural dynamics of single germinating bacterial spores. *Proc. Natl. Acad. Sci. USA* **2007**, *104*, 9644–9664. [\[CrossRef\]](#) [\[PubMed\]](#)
6. Trohalaki, S. Multifrequency force microscopy improves sensitivity and resolution over conventional AFM. *MRS Bull.* **2012**, *37*, 545–546. [\[CrossRef\]](#)
7. Sokolov, I.; Dokukin, M.E. Imaging of Soft and Biological Samples Using AFM Ringing Mode. *Methods Mol. Biol.* **2018**, *1814*, 469–482. [\[CrossRef\]](#) [\[PubMed\]](#)
8. Dufrene, Y.F.; Ando, T.; Garcia, R.; Alsteens, D.; Martinez-Martin, D.; Engel, A.; Gerber, C.; Müller, D.J. Imaging modes of atomic force microscopy for application in molecular and cell biology. *Nat. Nanotechnol.* **2017**, *12*, 295–307. [\[CrossRef\]](#)
9. Allison, D.P.; Mortensen, N.P.; Sullivan, C.J.; Doktycz, M.J. Atomic force microscopy of biological samples. *Wiley Interdiscip. Rev. Nanomed. Nanobiotechnol.* **2010**, *2*, 618–634. [\[CrossRef\]](#) [\[PubMed\]](#)
10. Xia, F.; Youcef-Toumi, K. Review: Advanced Atomic Force Microscopy Modes for Biomedical Research. *Biosensors* **2022**, *12*, 1116. [\[CrossRef\]](#) [\[PubMed\]](#) [\[PubMed Central\]](#)
11. Nievergelt, A.P.; Kammer, C.; Brillard, C.; Kurisinkal, E.; Bastings, M.M.C.; Karimi, A.; Fantner, G.E. Large-Range HS-AFM Imaging of DNA Self-Assembly through In Situ Data-Driven Control. *Small Methods* **2019**, *3*, 1900031. [\[CrossRef\]](#)
12. Xu, X.; Nakano, T.; Tsuda, M.; Kanamoto, R.; Hirayama, R.; Uzawa, A.; Ide, H. Direct observation of damage clustering in irradiated DNA with atomic force microscopy. *Nucleic Acids Res.* **2020**, *48*, e18. [\[CrossRef\]](#) [\[PubMed\]](#) [\[PubMed Central\]](#)
13. Viljoen, A.; Foster, S.J.; Fantner, G.E.; Hobbs, J.K.; Dufrene, Y.F. Scratching the Surface: Bacterial Cell Envelopes at the Nanoscale. *mBio* **2020**, *11*, e03020-19. [\[CrossRef\]](#) [\[PubMed\]](#) [\[PubMed Central\]](#)
14. Mortensen, N.P.; Fowlkes, J.D.; Sullivan, C.J.; Allison, D.P.; Larsen, N.B.; Molin, S.; Doktycz, M.J. Effects of colistin on surface ultrastructure and nanomechanics of *Pseudomonas aeruginosa* cells. *Langmuir* **2009**, *25*, 3728–3733. [\[CrossRef\]](#) [\[PubMed\]](#)
15. Wildling, L.; Hinterdorfer, P.; Kusche-Vihrog, K.; Treffner, Y.; Oberleithner, H. Aldosterone receptor sites on plasma membrane of human vascular endothelium detected by a mechanical nanosensor. *Pflug. Arch.* **2009**, *458*, 223–230. [\[CrossRef\]](#)
16. Marszałek, P.E.; Dufrene, Y.D. Stretching single polysaccharides and proteins using atomic force microscopy. *Chem. Soc. Rev.* **2012**, *41*, 3523–3534. [\[CrossRef\]](#)
17. Weisenhorn, A.; Hansma, P.; Albrecht, T.; Quate, C. Forces in atomic force microscopy in air and water. *Appl. Phys. Lett.* **1989**, *54*, 2651–2653. [\[CrossRef\]](#)

18. Dokukin, M.E.; Sokolov, I. Nanoscale compositional mapping of cells, tissues, and polymers with ringing mode of atomic force microscopy. *Sci. Rep.* **2017**, *7*, 11828. [\[CrossRef\]](#) [\[PubMed\]](#) [\[PubMed Central\]](#)
19. Stylianou, A.; Kontomaris, S.V.; Grant, C.; Alexandratou, E. Atomic Force Microscopy on Biological Materials Related to Pathological Conditions. *Scanning* **2019**, *2019*, 8452851. [\[CrossRef\]](#) [\[PubMed\]](#) [\[PubMed Central\]](#)
20. Gaboriaud, E.; Dufrene, Y.F. Atomic force microscopy of microbial cells: Application to nanomechanical properties, surface forces and molecular recognition forces. *Colloids Surf. B Biointerfaces* **2007**, *54*, 10–19. [\[CrossRef\]](#)
21. Zemla, J.; Danilkiewicz, J.; Orzechowska, B.; Pabijan, J.; Seweryn, S.; Lekka, M. Atomic force microscopy as a tool for assessing the cellular elasticity and adhesiveness to identify cancer cells and tissues. *Semin. Cell Dev. Biol.* **2018**, *73*, 115–124. [\[CrossRef\]](#) [\[PubMed\]](#)
22. Benaglia, S.; Gisbert, V.G.; Perrino, A.P.; Amo, C.A.; Garcia, R. Fast and high-resolution mapping of elastic properties of biomolecules and polymers with bimodal AFM. *Nat. Protoc.* **2018**, *13*, 2890–2907. [\[CrossRef\]](#)
23. Rosa-Zeiser, A.; Weilandt, E.; Hild, S.; Marti, O. The simultaneous measurement of elastic, electrostatic and adhesive properties by scanning force microscopy: Pulsed-force mode operation. *Mats. Sci. Technol.* **1997**, *8*, 1333. [\[CrossRef\]](#)
24. Braunsman, C.; Seifert, J.; Rheinlaender, J.; Schäffer, T.E. High-speed force mapping on living cells with a small cantilever atomic force microscope. *Rev. Sci. Instrum.* **2014**, *85*, 073703. [\[CrossRef\]](#)
25. Maver, U.; Velnar, T.; Gabersček, M.; Planinšek, O.; Finšgar, M. Recent progressive use of atomic force microscopy in biomedical applications. *TrAC Trends Anal. Chem.* **2016**, *80*, 96–111. [\[CrossRef\]](#)
26. Wang, Y.; Wang, J. Friction Determination by Atomic Force Microscopy in Field of Biochemical Science. *Micromachines* **2018**, *9*, 313. [\[CrossRef\]](#) [\[PubMed\]](#) [\[PubMed Central\]](#)
27. Charras, G.T.; Horton, M.A. Single cell mechanotransduction and its modulation analyzed by atomic force microscope indentation. *Biophys. J.* **2002**, *82*, 2970–2981. [\[CrossRef\]](#)
28. Sokolov, I.; Zorn, G.; Nichols, J.M. A study of molecular adsorption of a cationic surfactant on complex surfaces with atomic force microscopy. *Analyst* **2016**, *141*, 1017–1026. [\[CrossRef\]](#)
29. Yeow, N.; Tabor, R.F.; Gamier, G. Atomic force microscopy: From red blood cells to immunohaematology. *Adv. Colloid. Interface Sci.* **2017**, *249*, 149–162. [\[CrossRef\]](#) [\[PubMed\]](#)
30. Marti, O.; Drake, B.; Hansma, P.K. Atomic Force Microscopy of Liquid-Covered Surfaces: Atomic Resolution Images. *Appl. Phys. Lett.* **1987**, *51*, 484. [\[CrossRef\]](#)
31. Henderson, E.; Haydon, P.G.; Sakaguchi, D.S. Actin filament dynamics in living glial-cells imaged by atomic force microscopy. *Science* **1992**, *257*, 1944–1946. [\[CrossRef\]](#) [\[PubMed\]](#)
32. Goldmann, W.H.; Galneder, R.; Ludwig, M.; Xu, W.M.; Adamson, E.D.; Wang, N.; Ezzell, R.M. Differences in elasticity of vinculin-deficient F9 cells measured by magnetometry and atomic force microscopy. *Exp. Cell Res.* **1998**, *239*, 235–242. [\[CrossRef\]](#) [\[PubMed\]](#)
33. Sullivan, C.J.; Venkataraman, S.; Retterer, S.T.; Allison, D.P.; Doktycz, M.J. Comparison of the indentation and elasticity of E-coli and its spheroplasts by AFM. *Ultramicroscopy* **2007**, *107*, 934–942. [\[CrossRef\]](#) [\[PubMed\]](#)
34. Yao, X.; Walter, J.; Burke, S.; Stewart, S.; Jericho, M.H.; Pink, D.; Hunter, R.; Beveridge, T.J. Atomic force microscopy and theoretical considerations of Surface properties and turgor pressures of bacteria. *Colloids Surf. B Biointerfaces* **2002**, *23*, 213–230. [\[CrossRef\]](#)
35. Velegol, S.B.; Logan, B.E. Contributions of bacterial Surface polymers, electrostatics, and cell elasticity to the shape of AFM force curves. *Langmuir* **2002**, *18*, 5256–5262. [\[CrossRef\]](#)
36. Cerf, A.; Cau, J.C.; Vieu, C.; Dague, E. Nanomechanical properties of dead or alive single-patterned bacteria. *Langmuir* **2009**, *25*, 5731–5736. [\[CrossRef\]](#)
37. Birukova, A.A.; Arce, E.T.; Moldobaeva, N.; Dudek, S.M.; Garcia, J.G.; Lal, R.; Birukov, K.G. Endothelial permeability is controlled by spatially defined cytoskeletal mechanics: Atomic force microscopy force mapping of pulmonary endothelial monolayer. *Nanomedicine* **2009**, *5*, 30–41. [\[CrossRef\]](#)
38. Roduit, C.; van der Goot, F.G.; De Los Rios, P.; Yersin, A.; Steiner, P.; Dietler, G.; Catsicas, S.; Lafont, F.; Kasas, S. Elastic membrane heterogeneity of living cells revealed by stiff nanoscale membrane domains. *Biophys. J.* **2008**, *94*, 1521–1532. [\[CrossRef\]](#)
39. Florin, E.L.; Moy, V.T.; Gaub, H.E. Adhesion forces between individual ligand-receptor pairs. *Science* **1994**, *264*, 415–417. [\[CrossRef\]](#)
40. Leitner, M.; Brummeir, J.; Plaimer, G.O.; Kefer, I.; Potumayova, A.; Hianik, T.; Ebner, A. DNA building blocks for AFM tip functionalization: An easy, fast and stable strategy. *Methods* **2022**, *197*, 54–62. [\[CrossRef\]](#) [\[PubMed\]](#)
41. Lee, G.U.; Chrisey, L.A.; Colton, R.J. Direct measurement of the forces between complementary strands of DNA. *Science* **1994**, *266*, 771–773. [\[CrossRef\]](#) [\[PubMed\]](#)
42. Benoit, M.; Gabriel, D.; Gerisch, G.; Gaub, H.E. Discrete interactions in cell adhesion measured by single-molecule force spectroscopy. *Nat. Cell Biol.* **2000**, *2*, 313–317. [\[CrossRef\]](#)
43. Chtcheglova, L.A.; Hinterdorfer, P. Simultaneous AFM topography and recognition imaging at the plasma membrane of mammalian cells. *Semin. Cell Dev. Biol.* **2018**, *73*, 45–56. [\[CrossRef\]](#) [\[PubMed\]](#)
44. Jiang, Y.X.; Wang, J.; Fang, X.H.; Bai, C.L. Study of the effect of metal ion on the specific interaction between protein and aptamer by atomic force microscopy. *J. Nanosci. Nanotechnol.* **2004**, *4*, 611–615. [\[CrossRef\]](#)
45. Almqvist, N.; Bhatia, R.; Primbs, G.; Desai, N.; Banerjee, S.; Lal, R. Elasticity and adhesion force mapping reveals real-time clustering of growth factor receptors and associated changes in local cellular rheological properties. *Biophys. J.* **2004**, *86*, 1753–1762. [\[CrossRef\]](#) [\[PubMed\]](#)

46. Schindler, H.; Badt, D.; Hinterdorfer, P.; Kienberger, E.; Raab, A.; Wielert-Badt, S.; Pastushenko, V.P. Optimal sensitivity for molecular recognition MAC-mode, A.F.M. *Ultramicroscopy* **2000**, *82*, 227–235. [\[CrossRef\]](#) [\[PubMed\]](#)
47. Liu, Y.; Zhu, D.; Gilbert, J.L. Sub-nano to nanometer wear and tribocorrosion of titanium oxide-metal surfaces by in situ atomic force microscopy. *Acta Biomater.* **2021**, *126*, 477–484. [\[CrossRef\]](#) [\[PubMed\]](#)
48. Amenabar, I.; Poly, S.; Goikoetxea, M.; Nuansing, W.; Lasch, P.; Hillenbrand, R. Hyperspectral infrared nanoimaging of organic samples based on Fourier transform infrared nanospectroscopy. *Nat. Commun.* **2017**, *8*, 14402. [\[CrossRef\]](#)
49. Jahanmir, J.; Haggag, B.G.; Hayes, J.B. The scanning probe microscope. *Scanning Microsc.* **1992**, *6*, 2.
50. West, P.E. *Introduction to Atomic Force Microscopy Theory, Practice, Applications*; Pacific Nanotechnology: Santa Clara, CA, USA, 2007.
51. Barash, J. *Van der Waals Forces*; Nauka: Nayarit, Mexico, 1988; 344p.
52. Adams, J.B. Bonding Energy Modes. In *Encyclopedia of Materials: Science and Technology*, 2nd ed.; Elsevier: Amsterdam, The Netherlands, 2001; pp. 763–767.
53. Shinato, K.W.; Huang, F.; Jin, Y. Principle and application of atomic force microscopy (AFM) for nanoscale investigation of metal corrosion. *Corros. Rev.* **2020**, *38*, 423–432. [\[CrossRef\]](#)
54. Jung, S.H.; Park, D.; Park, J.H.; Kim, Y.M.; Ha, K.S. Molecular imaging of membrane proteins and microfilaments using atomic force microscopy. *Exp. Mol. Med.* **2010**, *42*, 597–605. [\[CrossRef\]](#)
55. Xia, F.; Quigley, J.; Zhang, X.; Yang, C.; Wang, Y.; Youcef-Toumi, K. A modular low-cost atomic force microscope for precision mechatronics education. *Mechatronics* **2021**, *76*, 102550. [\[CrossRef\]](#)
56. Kubiak, A. The Role of Mechanical Interactions in Prostate Cancer Therapy and Cell Resistance to Anti-Cancer Drugs. Ph.D. Thesis, The Henryk Niewodniczański Institute of Nuclear Physics Polish Academy of Sciences, Kraków, Poland, 2021.
57. Kruk, T. Mikroskopia Sił Atomowych (AFM). *LAB Lab. Apar. Badania* **2013**, *18*, 40–50.
58. Kwon, J.; Hong, J.; Kim, Y.S.; Lee, D.Y.; Lee, K.; Lee, S.M.; Park, S.I. Atomic force microscope with improved scan accuracy, scan speed, and optical vision. *Rev. Sci. Instrum.* **2003**, *74*, 4378–4383. [\[CrossRef\]](#)
59. Binnig, G.; Quate, C.F.; Gerber, C. Atomic force microscope. *Phys. Rev. Lett.* **1986**, *56*, 930. [\[CrossRef\]](#) [\[PubMed\]](#)
60. Moreno-Herrero, F.; Colchero, J.; Gomez-Herrero, J.; Baro, A.M. Atomic force microscopy contact, tapping, and jumping modes for imaging biological samples in liquids. *Phys. Rev. E* **2004**, *69*, 031915. [\[CrossRef\]](#) [\[PubMed\]](#)
61. Schilardi, P.; Diaz, C.; Flores, C.; Alvarez, E.; Fernández, M.; de Mele, L. Atomic force microscopy and optical microscopy: Suitable tools for the study of the initial stages of biofilm formation. In *Current Research, Technology and Education Topics in Applied Microbiology and Microbial Biotechnology*; Formatex Research Center: Badajoz, Spain, 2010; pp. 860–869.
62. Smallman, R.E.; Ngan, A.H.W. Characterization and analysis. In *Modern Physical Metallurgy*; Butterworth-Heinemann Elsevier Ltd.: Oxford, UK, 2014; pp. 159–250.
63. Chelikowsky, J.R.; Fan, D.; Lee, A.J.; Sakai, Y. Simulating noncontact atomic force microscopy images. *Phys. Rev. Mater.* **2019**, *3*, 110302. [\[CrossRef\]](#)
64. Reedijk, J. (Ed.) Reference Module in Chemistry, Molecular Sciences and Chemical Engineering. In *Encyclopedia of Electrochemical Power Sources*; Elsevier: Amsterdam, The Netherlands, 2009; pp. 696–717.
65. Jalili, N.; Laxminarayana, K. A review of atomic force microscopy imaging systems: Application to molecular metrology and biological sciences. *Mechatronics* **2004**, *14*, 907–945. [\[CrossRef\]](#)
66. Maivald, P.; Butt, H.J.; Gould, S.A.C.; Prater, C.B.; Drake, B.; Gurley, J.A.; Elings, V.B.; Hansma, P.K. Using force modulation to image surface elasticities with the atomic force microscope. *Nanotechnology* **1991**, *2*, 103. [\[CrossRef\]](#)
67. Krottil, H.-U.; Stifter, T.; Marti, O. Concurrent measurement of adhesive and elastic surface properties with a new modulation technique for scanning force microscopy. *Rev. Sci. Instrum.* **2000**, *71*, 2765–2771. [\[CrossRef\]](#)
68. Leite, F.L.; Herrmann, P.S.P. Application of atomic force spectroscopy (AFS) to studies of adhesion phenomena: A review. *J. Adhes. Sci. Technol.* **2005**, *19*, 365–405. [\[CrossRef\]](#)
69. Butt, H.J.; Wolff, E.K.; Gould, S.A.C.; Northern, B.D.; Peterson, C.M.; Hansma, P.K. Imaging cells with the atomic force microscope. *J. Struct. Biol.* **1990**, *105*, 54–61. [\[CrossRef\]](#)
70. Radmacher, M.; Tillmann, R.W.; Fritz, M.; Gaub, H.E. From molecules to cells—Imaging soft samples with the atomic force microscope. *Science* **1992**, *257*, 1900–1905. [\[CrossRef\]](#)
71. Rother, J.; Nöding, H.; Mey, I.; Janshoff, A. Atomic force microscopy-based micro rheology reveals significant differences in the viscoelastic response between malign and benign cell lines. *Open Biol.* **2014**, *4*, 140046. [\[CrossRef\]](#) [\[PubMed\]](#)
72. Stolz, M.; Gottardi, R.; Raiteri, R.; Miot, S.; Martin, I.; Imer, R.; Staufer, U.; Raducanu, A.; Düggelein, M.; Baschong, W.; et al. Early detection of aging cartilage and osteoarthritis in mice and patient samples using atomic force microscopy. *Nat. Nanotechnol.* **2009**, *4*, 186–192. [\[CrossRef\]](#)
73. Moy, V.T.; Florin, E.L.; Gaub, H.E. Intermolecular forces and energies between ligands and receptors. *Science* **1994**, *266*, 257–259. [\[CrossRef\]](#) [\[PubMed\]](#)
74. Chen, Y.; Zeng, G.; Chen, S.S.; Feng, Q.; Chen, Z.W. AFM force measurements of the gp120-sCD4 and gp120 or CD4 antigen-antibody interactions. *Biochem. Biophys. Res. Commun.* **2011**, *407*, 301–306. [\[CrossRef\]](#) [\[PubMed\]](#)
75. Lv, Z.; Wang, J.; Chen, G.; Deng, L. Imaging and determining friction forces of specific interactions between human IgG and rat anti-human IgG. *J. Biol. Phys.* **2011**, *37*, 417–427. [\[CrossRef\]](#) [\[PubMed\]](#)
76. Chitchevlova, L.A.; Waschke, J.; Wildling, L.; Drenckhahn, D.; Hinterdorfer, P. Nano-scale dynamic recognition imaging on vascular endothelial cells. *Biophys. J.* **2007**, *93*, L11–L13. [\[CrossRef\]](#)

77. Smart, J.A.; Oleksak, J.E.; Hartsough, E.J. Cell Adhesion Molecules in Plasticity and Metastasis. *Mol. Cancer Res.* **2021**, *19*, 25–37. [\[CrossRef\]](#) [\[PubMed\]](#) [\[PubMed Central\]](#)
78. Labernadie, A.; Kato, T.; Brugués, A.; Serra-Picamal, X.; Derzi, S.; Arwert, E.; Weston, A.; González-Tarragó, V.; Elosegui-Artola, A.; Albertazzi, L.; et al. A mechanically active heterotypic E-cadherin/N-cadherin adhesion enables fibroblasts to drive cancer cell invasion. *Nat. Cell Biol.* **2017**, *19*, 224–237. [\[CrossRef\]](#) [\[PubMed\]](#) [\[PubMed Central\]](#)
79. Dokukin, M.E.; Guz, N.V.; Gaikwad, R.M.; Woodworth, C.D.; Sokolov, I. Cell surface as a fractal: Normal and cancerous cervical cells demonstrate different fractal behavior of surface adhesion maps at the nanoscale. *Phys. Rev. Lett.* **2011**, *107*, 028101. [\[CrossRef\]](#) [\[PubMed\]](#)
80. Guz, N.V.; Dokukin, M.E.; Woodworth, C.D.; Cardin, A.; Sokolov, I. Towards early detection of cervical cancer: Fractal dimension of AFM images of human cervical epithelial cells at different stages of progression to cancer. *Nanomedicine* **2015**, *11*, 1667–1675. [\[CrossRef\]](#)
81. Saadh, M.J.; Shallan, M.A.; Hussein, U.A.; Mohammed, A.Q.; Al-Shuwaili, S.J.; Shikara, M.; Ami, A.A.; Khalil, N.A.M.A.; Ahmad, I.; Abbas, H.H.; et al. Advances in microscopy characterization techniques for lipid nanocarriers in drug delivery: A comprehensive review. *Naunyn-Schmiedeberg's Arch. Pharmacol.* **2024**, *397*, 5463–5481. [\[CrossRef\]](#) [\[PubMed\]](#)
82. Jin, S.E.; Bae, J.W.; Hong, S. Multiscale observation of biological interactions of nanocarriers: From nano to macro. *Microsc. Res. Tech.* **2010**, *73*, 813–823. [\[CrossRef\]](#) [\[PubMed\]](#) [\[PubMed Central\]](#)
83. Labroo, P.; Irvin, J.; Johnson, J.; Sieverts, M.; Miess, J.; Robinson, I.; Baetz, N.; Garrett, C.; Sopko, N. Physical characterization of swine and human skin: Correlations between Raman spectroscopy, Tensile testing, Atomic force microscopy (AFM), Scanning electron microscopy (SEM), and Multiphoton microscopy (MPM). *Skin Res. Technol.* **2021**, *27*, 501–510. [\[CrossRef\]](#) [\[PubMed\]](#)
84. Beekman, P.; Enciso-Martinez, A.; Rho, H.S.; Pujari, S.P.; Lenerink, A.; Zuilhof, H.; Terstappen, L.W.M.M.; Otto, C.; Le Gac, S. Immuno-capture of extracellular vesicles for individual multi-modal characterization using AFM, SEM and Raman spectroscopy. *Lab. Chip* **2019**, *19*, 2526–2536. [\[CrossRef\]](#) [\[PubMed\]](#)
85. Kraus, A.; Rose, V.; Krüger, R.; Sarau, G.; Kling, L.; Schiffer, M.; Christiansen, S.; Müller-Deile, J. Characterizing Intra-individual Podocyte Morphology In Vitro with Different Innovative Microscopic and Spectroscopic Techniques. *Cells* **2023**, *12*, 1245. [\[CrossRef\]](#) [\[PubMed\]](#) [\[PubMed Central\]](#)
86. Melling, M.; Karimian-Teherani, D.; Mostler, S.; Behnam, M.; Hochmeister, S. 3-D morphological characterization of the liver parenchyma by atomic force microscopy and by scanning electron microscopy. *Microsc. Res. Tech.* **2004**, *64*, 1–9. [\[CrossRef\]](#) [\[PubMed\]](#)
87. Melling, M.; Karimian-Teherani, D.; Mostler, S.; Hochmeister, S. Three-dimensional morphological characterization of optic nerve fibers by atomic force microscopy and by scanning electron microscopy. *Microsc. Microanal.* **2005**, *11*, 333–340. [\[CrossRef\]](#) [\[PubMed\]](#)
88. Wakayama, J.; Sugiyama, S. Evaluation of temperature effect on the interaction between β -lactoglobulin and anti- β -lactoglobulin antibody by atomic force microscopy. *Biochemistry* **2012**, *51*, 32–42. [\[CrossRef\]](#)
89. Kim, B.-H.; Palermo, N.Y.; Lovas, S.; Zaikova, T.; Keana, J.F.W.; Lyubchenko, Y.L. Single-molecule atomic force microscopy force spectroscopy study of A β -40 interactions. *Biochemistry* **2011**, *50*, 5154–5162. [\[CrossRef\]](#) [\[PubMed\]](#)
90. Yu, J.; Wamke, J.; Lyubchenko, Y.L. Nanoprobng of α -synuclein misfolding and aggregation with atomic force microscopy. *Nanomed. Nanotechnol. Biol. Med.* **2011**, *7*, 146–152. [\[CrossRef\]](#) [\[PubMed\]](#)
91. Lovas, S.; Zhang, Y.; Yu, J.; Lyubchenko, Y.L. Molecular Mechanism of Misfolding and Aggregation of A β (13–23). *J. Phys. Chem. B* **2013**, *117*, 6175–6186. [\[CrossRef\]](#) [\[PubMed\]](#)
92. Lei, H.; Zhang, X.; Hu, J.; Zhang, Y. Self-assembly of amyloid-like peptides at interfaces investigated by atomic force microscopy. *Sci. Adv. Mater.* **2017**, *9*, 65–76. [\[CrossRef\]](#)
93. Watanabe-Nakayama, T.; Ono, K. High-speed atomic force microscopy of individual amyloidogenic protein assemblies. In *Nanoscale Imaging*; Lyubchenko, Y., Ed.; Vol. 1814 of Methods in Molecular Biology; Humana Press: New York, NY, USA, 2018; pp. 201–212.
94. Han, S.W.; Shin, H.K.; Adachi, T. Nanolithography of amyloid precursor protein cleavage with β -secretase by atomic force microscopy. *J. Biomed. Nanotechnol.* **2016**, *12*, 546–553. [\[CrossRef\]](#)
95. Drolle, E.; Hammond, K.; Hane, F.T.; Lee, B.; Leonenko, Z. Atomic Force Microscopy and Kelvin Probe Force Microscopy to Study Molecular Mechanism of Alzheimer's Disease. In Proceedings of the International Conference on Scanning Probe Microscopy on Soft and Polymeric Materials, Toronto, ON, Canada, 2–6 September 2014.
96. Song, S.; Ma, X.; Zhou, Y.; Xu, M.; Shuang, S.; Dong, C. Studies on the interaction between vanillin and β -amyloid protein via fluorescence spectroscopy and atomic force microscopy. *Chem. Res. Chin. Univ.* **2016**, *32*, 172–177. [\[CrossRef\]](#)
97. Shao, X.; Cui, W.; Xie, X.; Ma, W.; Zhan, Y.; Lin, Y. Treatment of Alzheimer's disease with framework nucleic acids. *Cdl Prolif.* **2020**, *53*, e12787. [\[CrossRef\]](#) [\[PubMed\]](#) [\[PubMed Central\]](#)
98. Han, S.W.; Lee, T.H.; Kang, M.S.; Kim, H.J.; Shin, H.K. Probing Amyloid β and the Antibody Interaction Using Atomic Force Microscopy. *J. Nanosci. Nanotechnol.* **2018**, *18*, 1410–1413. [\[CrossRef\]](#) [\[PubMed\]](#)
99. Watanabe-Nakayama, T.; Ono, K. Acquisition and processing of high-speed atomic force microscopy videos for single amyloid aggregate observation. *Methods* **2022**, *197*, 4–12; Erratum in *Methods* **2022**, *199*, 80. [\[CrossRef\]](#) [\[PubMed\]](#)
100. Josephs, E.A.; Zheng, T.; Marszalek, P.E. Atomic force microscopy captures the initiation of methyl-directed DNA mismatch repair. *DNA Repair.* **2015**, *35*, 71–84. [\[CrossRef\]](#) [\[PubMed\]](#)

101. Beckwitt, E.; Kong, M.; Van Houten, B. Studying Protein-DNA Interactions Using Atomic Force Microscopy. *Semin. Cell Dev. Biol.* **2017**, *73*, 220–230. [\[CrossRef\]](#) [\[PubMed\]](#)
102. Wang, H.; Yang, Y.; Schofield, M.J.; Du, C.; Fridman, Y.; Lee, S.D.; Larson, E.D.; Drummond, J.T.; Alani, E.; Hsieh, P.; et al. DNA Bending and Unbending by MutS Govern Mismatch Recognition and Specificity. *Proc. Natl. Acad. Sci. USA* **2003**, *100*, 14822–14827. [\[CrossRef\]](#)
103. Loparic, M.; Wirz, D.; Daniels, A.U.; Raiteri, R.; VanLandingham, M.R.; Guex, G.; Martin, I.; Aebi, U.; Stolz, M. Micro- and nanomechanical analysis of articular cartilage by indentation-type atomic force microscopy: Validation with a gel-microfiber composite. *Biophys. J.* **2010**, *98*, 2731–2740. [\[CrossRef\]](#)
104. Takai, E.; Costa, K.D.; Shaheen, A.; Hung, C.T.; Guo, X.E. Osteoblast elastic modulus measured by atomic force microscopy is substrate dependent. *Ann. Biomed. Eng.* **2005**, *33*, 963–971. [\[CrossRef\]](#)
105. Mathur, A.B.; Collinworth, A.M.; Reichert, W.M.; Kraus, W.E.; Truskey, G.A. Endothelial, cardiac muscle and skeletal muscle exhibit different viscous and elastic properties as determined by atomic force microscopy. *J. Biomech.* **2001**, *34*, 1545–1553. [\[CrossRef\]](#)
106. Kim, G.J.; Yoo, H.S.; Lee, K.J.; Choi, J.W.; Hee An, J. Image of the Micro-Computed Tomography and Atomic-Force Microscopy of Bone in Osteoporosis Animal Model. *J. Nanosci. Nanotechnol.* **2018**, *18*, 6726–6731. [\[CrossRef\]](#)
107. Gaidash, A.A.; Sinita, L.N.; Babenko, O.A.; Lugovskoy, A.A. Nanoporous Structure of Bone Matrix at Osteoporosis from Data of Atomic Force Microscopy and IR Spectroscopy. *J. Osteoporos.* **2011**, *2011*, 162041. [\[CrossRef\]](#) [\[PubMed\]](#)
108. Yen, M.H.; Chen, Y.H.; Liu, Y.S.; Lee, O.K. Alteration of Young's modulus in mesenchymal stromal cells during osteogenesis measured by atomic force microscopy. *Biochem. Biophys. Res. Commun.* **2020**, *526*, 827–832. [\[CrossRef\]](#)
109. Peña, B.; Abdel-Hafiz, M.; Cavaşin, M.; Mestroni, L.; Sbaizero, O. Atomic Force Microscopy (AFM) Applications in Arrhythmogenic Cardiomyopathy. *Int. J. Mol. Sci.* **2022**, *23*, 3700. [\[CrossRef\]](#) [\[PubMed\]](#) [\[PubMed Central\]](#)
110. Vannozzi, L.; Gouveia, P.; Pingue, P.; Canale, C.; Ricotti, L. Novel ultrathin films based on a blend of PEG-b-PCL and PLLA and doped with ZnO nanoparticles. *ACS Appl. Mater. Interfaces* **2020**, *12*, 21398–21410. [\[CrossRef\]](#) [\[PubMed\]](#)
111. Pelling, A.E.; Sehati, S.; Gralla, E.B.; Valentine, J.S.; Gimzewski, J.K. Local nanomechanical motion of the cell wall of *Saccharomyces cerevisiae*. *Science* **2004**, *305*, 1147–1150. [\[CrossRef\]](#) [\[PubMed\]](#)
112. Nelson, S.L.; Proctor, D.T.; Ghasemloonia, A.; Lama, S.; Zareinia, K.; Ahn, Y.; Al-Saiedy, M.R.; Green, F.H.; Amrein, M.W.; Sutherland, G.R. Vibrational profiling of brain tumors and cells. *Theranostics* **2017**, *7*, 2417. [\[CrossRef\]](#)
113. Zhu, X.; Qin, R.; Qu, K.; Wang, Z.; Zhao, X.; Xu, W. Atomic force microscopy-based assessment of biomechanical cellular properties for classification of graded bladder cancer cells and cancer early diagnosis using machine learning analysis. *Acta Biomater.* **2023**, *158*, 358–373; Erratum in *Acta Biomater.* **2023**, *162*, 324. [\[CrossRef\]](#) [\[PubMed\]](#)
114. Prasad, S.; Rankine, A.; Prasad, T.; Song, P.; Dokukin, M.E.; Makarova, N.; Backman, V.; Sokolov, I. Atomic force microscopy detects the difference in cancer cells of different neoplastic aggressiveness via machine learning. *Adv. NanoBiomed Res.* **2021**, *1*, 2000116. [\[CrossRef\]](#)
115. Van der Meeren, L.; Verduijn, J.; Krysko, D.V.; Skirtach, A.G. AFM analysis enables differentiation between apoptosis, necroptosis, and ferroptosis in murine cancer cells. *iScience* **2020**, *23*, 101816. [\[CrossRef\]](#)
116. Deng, X.; Xiong, F.; Li, X.; Xiang, B.; Li, Z.; Wu, X.; Guo, C.; Li, X.; Li, Y.; Li, G.; et al. Application of atomic force microscopy in cancer research. *J. Nanobiotechnol.* **2018**, *16*, 1–15. [\[CrossRef\]](#) [\[PubMed\]](#)
117. Spyratou, E.; Mourelatou, E.A.; Makropoulou, M.; Demetrios, C. Atomic force microscopy: A tool to study the structure, dynamics and stability of liposomal drug delivery systems. *Expert. Opin. Drug Deliv.* **2009**, *6*, 305–317. [\[CrossRef\]](#) [\[PubMed\]](#)
118. Stylianou, A.; Mpekris, E.; Voutouri, C.; Papoui, A.; Constantinidou, A.; Kitiros, E.; Kailides, M.; Stylianopoulos, T. Nanomechanical properties of solid tumors as treatment monitoring biomarkers. *Acta Biomater.* **2022**, *154*, 324–334. [\[CrossRef\]](#)
119. Miroshnikova, Y.A.; Le, H.Q.; Schneider, D.; Thalheim, T.; Rübsam, M.; Bremicker, N.; Polleux, J.; Kamprad, N.; Tarantola, M.; Wang, L.; et al. Adhesion forces and cortical tension couple cell proliferation and differentiation to drive epidermal stratification. *Nat. Cell Biol.* **2018**, *20*, 69–80. [\[CrossRef\]](#)
120. Connelly, J.T.; Gavara, N.; Sliogeryte, K.; Blowes, L.M. Research Techniques Made Simple: Analysis of Skin Cell and Tissue Mechanics Using Atomic Force Microscopy. *J. Investig. Dermatol.* **2021**, *141*, 1867–1871.e1. [\[CrossRef\]](#) [\[PubMed\]](#)
121. Laly, A.C.; Sliogeryte, K.; Pundel, O.J.; Ross, R.; Keeling, M.C.; Avisetti, D.; Waseem, A.; Gavara, N.; Connelly, J.T. The keratin network of intermediate filaments regulates keratinocyte rigidity sensing and nuclear mechanotransduction. *Sci. Adv.* **2021**, *7*, eabd6187. [\[CrossRef\]](#) [\[PubMed\]](#) [\[PubMed Central\]](#)
122. Boyle, C.J.; Plotczyk, M.; Villalta, S.F.; Patel, S.; Hettiaratchy, S.; Masouros, S.D.; Masen, M.A.; Higgins, C.A. Morphology and composition play distinct and complementary roles in the tolerance of plantar skin to mechanical load. *Sci. Adv.* **2019**, *5*, eaay0244. [\[CrossRef\]](#) [\[PubMed\]](#)
123. Haftek, M.; McAleer, M.A.; Jakasa, I.; McLean, W.I.; Kezic, S.; Irvine, A.D. Changes in nano-mechanical properties of human epidermal cornified cells in children with atopic dermatitis. *Wellcome Open Res.* **2020**, *5*, 97. [\[CrossRef\]](#) [\[PubMed\]](#) [\[PubMed Central\]](#)
124. Homberg, M.; Ramms, L.; Schwarz, N.; Dreissen, G.; Leube, R.E.; Merkel, R.; Hoffmann, B.; Magin, T.M. Distinct Impact of Two Keratin Mutations Causing Epidermolysis Bullosa Simplex on Keratinocyte Adhesion and Stiffness. *J. Investig. Dermatol.* **2015**, *135*, 2437–2445; Erratum in *J. Investig. Dermatol.* **2016**, *136*, 1306. [\[CrossRef\]](#) [\[PubMed\]](#)

125. Vielmuth, F.; Wanuske, M.T.; Radeva, M.Y.; Hiermaier, M.; Kugelmann, D.; Walter, E.; Buechau, F.; Magin, T.M.; Waschke, J.; Spindler, V. Keratins Regulate the Adhesive Properties of Desmosomal Cadherins through Signaling. *J. Investig. Dermatol.* **2018**, *138*, 121–131. [\[CrossRef\]](#) [\[PubMed\]](#)
126. Rebehn, L.; Khalaji, S.; KleinJan, F.; Kleemann, A.; Port, F.; Paul, P.; Huster, C.; Nolte, U.; Singh, K.; Kwapich, L.; et al. The weakness of senescent dermal fibroblasts. *Proc. Natl. Acad. Sci. USA* **2023**, *120*, e2301880120. [\[CrossRef\]](#) [\[PubMed\]](#) [\[PubMed Central\]](#)
127. Peñuela, L.; Negro, C.; Massa, M.; Repaci, E.; Cozzani, E.; Parodi, A.; Scaglione, S.; Quarto, R.; Raiteri, R. Atomic force microscopy for biomechanical and structural analysis of human dermis: A complementary tool for medical diagnosis and therapy monitoring. *Exp. Dermatol.* **2018**, *27*, 150–155. [\[CrossRef\]](#) [\[PubMed\]](#)
128. Shao, Y.; He, T.; Fisher, G.J.; Voorhees, J.J.; Quan, T. Molecular basis of retinol anti-ageing properties in naturally aged human skin in vivo. *Int. J. Cosmet. Sci.* **2017**, *39*, 56–65. [\[CrossRef\]](#) [\[PubMed\]](#) [\[PubMed Central\]](#)
129. Jeong, K.H.; Kim, K.S.; Lee, G.J.; Choi, S.J.; Jeong, T.J.; Shin, M.K.; Park, H.K.; Sim, W.Y.; Lee, M.H. Investigation of aging effects in human hair using atomic force microscopy. *Ski. Res. Technol.* **2011**, *17*, 63–68. [\[CrossRef\]](#) [\[PubMed\]](#)
130. Chen, N.; Bhushan, B. Morphological, nanomechanical and cellular structural characterization of human hair and conditioner distribution using torsional resonance mode with an atomic force microscope. *J. Microsc.* **2005**, *220 Pt 2*, 96–112. [\[CrossRef\]](#) [\[PubMed\]](#)
131. La Torre, C.; Bhushan, B. Nanotribological effects of silicone type, silicone deposition level, and surfactant type on human hair using atomic force microscopy. *J. Cosmet. Sci.* **2006**, *57*, 37–56. [\[PubMed\]](#)
132. Chen, N.; Bhushan, B. Atomic force microscopy studies of conditioner thickness distribution and binding interactions on the hair surface. *J. Microsc.* **2006**, *221 Pt 3*, 203–215. [\[CrossRef\]](#) [\[PubMed\]](#)
133. La Torre, C.; Bhushan, B. Investigation of scale effects and directionality dependence on friction and adhesion of human hair using AFM and macroscale friction test apparatus. *Ultramicroscopy* **2006**, *106*, 720–734. [\[CrossRef\]](#) [\[PubMed\]](#)
134. Lodge, R.A.; Bhushan, B. Effect of physical wear and triboelectric interaction on surface charge as measured by Kelvin probe microscopy. *J. Colloid. Interface Sci.* **2007**, *310*, 321–330. [\[CrossRef\]](#) [\[PubMed\]](#)
135. Clifford, C.A.; Sano, N.; Doyle, P.; Seah, M.P. Nanomechanical measurements of hair as an example of micro-fibre analysis using atomic force microscopy nanoindentation. *Ultramicroscopy* **2012**, *114*, 38–45. [\[CrossRef\]](#) [\[PubMed\]](#)
136. Seshadri, I.P.; Bhushan, B. Effect of ethnicity and treatments on in situ tensile response and morphological changes of human hair characterized by atomic force microscopy. *Acta Mater.* **2008**, *56*, 3585–3597. [\[CrossRef\]](#)
137. Seshadri, I.P.; Bhushan, B. In situ tensile deformation characterization of human hair with atomic force microscopy. *Acta Mater.* **2008**, *56*, 774–781. [\[CrossRef\]](#)
138. Fellows, A.P.; Casford, M.T.L.; Davies, P.B. Nanoscale Molecular Characterization of Hair Cuticle Cells Using Integrated Atomic Force Microscopy-Infrared Laser Spectroscopy. *Appl. Spectrosc.* **2020**, *74*, 1540–1550. [\[CrossRef\]](#) [\[PubMed\]](#) [\[PubMed Central\]](#)
139. Fellows, A.P.; Casford, M.T.L.; Davies, P.B. Using hybrid atomic force microscopy and infrared spectroscopy (AFM-IR) to identify chemical components of the hair medulla on the nanoscale. *J. Microsc.* **2021**, *284*, 189–202. [\[CrossRef\]](#) [\[PubMed\]](#)
140. Fellows, A.P.; Casford, M.T.L.; Davies, P.B. Chemically characterizing the cortical cell nano-structure of human hair using atomic force microscopy integrated with infrared spectroscopy (AFM-IR). *Int. J. Cosmet. Sci.* **2022**, *44*, 42–55. [\[CrossRef\]](#) [\[PubMed\]](#)
141. Shin, M.K.; Kim, K.S.; Ahn, J.J.; Kim, N.I.; Park, H.K.; Haw, C.R. Investigation of the hair of patients with scalp psoriasis using atomic force microscopy. *Clin. Exp. Dermatol.* **2012**, *37*, 156–163. [\[CrossRef\]](#) [\[PubMed\]](#)
142. Jeon, B.; Jung, H.G.; Lee, S.W.; Lee, G.; Shim, J.H.; Kim, M.O.; Kim, B.J.; Kim, S.-H.; Lee, H.; Lee, S.W.; et al. Melanoma Detection by AFM Indentation of Histological Specimens. *Diagnostics* **2022**, *12*, 1736. [\[CrossRef\]](#) [\[PubMed\]](#)
143. Li, J.; Liu, Y.; Yuan, Y.; Huang, B. Applications of atomic force microscopy in immunology. *Front. Med.* **2021**, *15*, 43–52. [\[CrossRef\]](#)
144. Neubert, E.; Meyer, D.; Rocca, E.; Günay, G.; Kwaczala-Tessmann, A.; Grandke, J.; Senger-Sander, S.; Geisler, C.; Egner, A.; Schön, M.P.; et al. Chromatin swelling drives neutrophil extracellular trap release. *Nat. Commun.* **2018**, *9*, 3767. [\[CrossRef\]](#) [\[PubMed\]](#)
145. Hosseini, B.H.; Louban, I.; Djandji, D.; Wabnitz, G.H.; Deeg, J.; Bulbuc, N.; Samstag, Y.; Gunzer, M.; Spatz, J.P.; Hämmerling, G.J. Immune synapse formation determines interaction forces between T cells and antigen-presenting cells measured by atomic force microscopy. *Proc. Natl. Acad. Sci. USA* **2009**, *106*, 17852–17857. [\[CrossRef\]](#) [\[PubMed\]](#)
146. Paeon, S.V.; Govendir, M.A.; Kempe, D.; Biro, M. Mechanoimmunology: Molecular-scale forces govern immune cell functions. *Mol. Biol. Cell* **2018**, *29*, 1919–1926. [\[CrossRef\]](#)
147. Liu, Y.; Zhang, T.; Zhou, Y.; Li, J.; Liang, X.; Zhou, N.; Lv, J.; Xie, J.; Cheng, F.; Fang, Y.; et al. Visualization of perforin/gasdermin/complement-formed pores in real cell membranes using atomic force microscopy. *Cell Mol. Immunol.* **2019**, *16*, 611–620. [\[CrossRef\]](#)
148. Kristi, N.; Gafur, A.; Kong, L.; Ma, X.; Ye, Z.; Wang, G. Atomic Force Microscopy in Mechanoimmunology Analysis: A New Perspective for Cancer Immunotherapy. *Biotechnol. J.* **2020**, *15*, e1900559. [\[CrossRef\]](#)
149. Ciasca, G.; Papi, M.; Di Claudio, S.; Chiarpotto, M.I.C.H.E.L.A.; Palmieri, V.; Maulucci, G.; Nocca, G.; Rossi, C.; De Spirito, M. Mapping viscoelastic properties of healthy and pathological red blood cells at the nanoscale level. *Nanoscale* **2015**, *7*, 17030–17037. [\[CrossRef\]](#)
150. Lekka, M.; Fomal, M.; Pyka-Foćiak, G.; Lebed, K.; Wizner, B.; Grodzicki, T.; Styczeń, J. Erythrocyte stiffness probed using atomic force microscope. *Biorheology* **2005**, *42*, 307–317. [\[PubMed\]](#)

151. Dulińska, I.; Targosz, M.; Strojny, W.; Lekka, M.; Czuba, P.; Balwierz, W.; Szymoński, M. Stiffness of normal and pathological erythrocytes studied by means of atomic force microscopy. *J. Biochem. Biophys. Methods* **2006**, *66*, 1–11. [\[CrossRef\]](#) [\[PubMed\]](#)
152. Maciaszek, J.L.; Lykotrafitis, G. Sickle cell trait human erythrocytes are significantly stiffer than normal. *J. Biomed. Sci.* **2011**, *44*, 657–661. [\[CrossRef\]](#)
153. Pretorius, E.; du Plooy, J.N.; Soma, P.; Keyser, I.; Buys, A.V. Smoking and fluidity of erythrocyte membranes: A high resolution scanning electron and atomic force microscopy investigation. *Nitric Oxide* **2013**, *35*, 42–46. [\[CrossRef\]](#)
154. Jin, H.; Xing, X.; Zhao, H.; Chen, Y.; Huang, X.; Ma, S.; Ye, H.; Cai, J. Detection of erythrocytes influenced by aging and type 2 diabetes using atomic force microscope. *Biochem. Biophys. Res. Commun.* **2010**, *391*, 1698–1702. [\[CrossRef\]](#)
155. Liu, J.; Li, J. Detection of erythrocytes in patients with Waldenström macroglobulinemia using atomic force microscopy. *Acta Biochim. Biophys. Sin.* **2014**, *46*, 420–425. [\[CrossRef\]](#) [\[PubMed\]](#)
156. Xing, X.; Jin, H.; Lu, Y.; Wang, Q.; Pan, Y.; Cai, J.; Wang, H. Detection of erythrocytes in patient with elliptocytosis complicating ITP using atomic force microscopy. *Micron* **2011**, *42*, 42–46. [\[CrossRef\]](#) [\[PubMed\]](#)
157. Zhang, Y.; Zhang, W.; Wang, S.; Wang, C.; Xie, J.; Chen, X.; Xu, Y.; Mao, P. Detection of human erythrocytes influenced by iron deficiency anemia and thalassemia using atomic force microscopy. *Micron* **2012**, *43*, 1287–1292. [\[CrossRef\]](#)
158. Kozlova, E.; Sherstyukova, E.; Sergunova, V.; Grechko, A.; Kuzovlev, A.; Lyapunova, S.; Inozemtsev, V.; Kozlov, A.; Chernysh, A. Atomic Force Microscopy and High-Resolution Spectrophotometry for Study of Anoxemia and Normoxemia in Model Experiment In Vitro. *Int. J. Mol. Sci.* **2023**, *24*, 11043. [\[CrossRef\]](#)
159. Li, A.; Mansoor, A.H.; Tan, K.S.; Lim, C. Observations on the internal and surface morphology of malaria infected blood cells using optical and atomic force microscopy. *J. Microbiol. Methods* **2006**, *66*, 434–439. [\[CrossRef\]](#)
160. Aikawa, M.; Kamanura, K.; Shiraishi, S.; Matsumoto, Y.; Arwati, H.; Torii, M.; Ito, Y.; Takeuchi, T.; Tandler, B. Membrane Knobs of Unfixed Plasmodium falciparum Infected Erythrocytes: New Findings as Revealed by Atomic Force Microscopy and Surface Potential Spectroscopy. *Exp. Parasitol.* **1996**, *84*, 339–343. [\[CrossRef\]](#) [\[PubMed\]](#)
161. Valle-Delgado, J.J.; Urbán, P.; Fernández-Busquets, X. Demonstration of specific binding of heparin to Plasmodium falciparum-infected vs. non-infected red blood cells by single-molecule force spectroscopy. *Nanoscale* **2013**, *5*, 3673–3680. [\[CrossRef\]](#) [\[PubMed\]](#)
162. Carvalho, F.A.; Santos, N.C. Atomic force microscopy-based force spectroscopy—Biological and biomedical applications. *RUBMB Life* **2012**, *64*, 465–472. [\[CrossRef\]](#) [\[PubMed\]](#)
163. Grandbois, M.; Dettmann, W.; Benoit, M.; Gaub, H.E. Affinity imaging of red blood cells using an atomic force microscope. *J. Histochem. Cytochem.* **2000**, *48*, 719–724. [\[CrossRef\]](#)
164. Torres, B.V.; Smith, D.F. Purification of Forssman and human blood group A glycolipids by affinity chromatography on immobilized Helix pomatia lectin. *Anal. Biochem.* **1988**, *170*, 209–219. [\[CrossRef\]](#)
165. Schneider, T.R.; Stöckli, L.; Felbecker, A.; Nirmalraj, P.N. Protein fibril aggregation on red blood cells: A potential biomarker to distinguish neurodegenerative diseases from healthy aging. *Brain Commun.* **2024**, *6*, fcae180. [\[CrossRef\]](#) [\[PubMed\]](#) [\[PubMed Central\]](#)
166. Braet, F.; Wisse, E. AFM imaging of fenestrated liver sinusoidal endothelial cells. *Micron* **2012**, *43*, 1252–1258. [\[CrossRef\]](#) [\[PubMed\]](#)
167. Braet, F.; Taatjes, D.J.; Wisse, E. Probing the unseen structure and function of liver cells through atomic force microscopy. *Semin. Cell Dev. Biol.* **2018**, *73*, 13–30. [\[CrossRef\]](#) [\[PubMed\]](#)
168. Uchihashi, T.; Watanabe, H.; Fukuda, S.; Shibata, M.; Ando, T. Functional extension of high-speed AFM for wider biological applications. *Ultramicroscopy* **2016**, *160*, 182–196. [\[CrossRef\]](#) [\[PubMed\]](#)
169. Roos, W.H. High-speed AFM reveals the dynamics of virus budding. *Biophys. J.* **2022**, *121*, 4022–4023. [\[CrossRef\]](#) [\[PubMed\]](#) [\[PubMed Central\]](#)
170. Kaur, P.; Lu, X.; Xu, Q.; Irvin, E.M.; Pappas, C.; Zhang, H.; Finkelstein, I.J.; Shi, Z.; Tao, Y.J.; Yu, H.; et al. High-speed AFM imaging reveals DNA capture and loop extrusion dynamics by cohesin-NIPBL. *J. Biol. Chem.* **2023**, *299*, 105296. [\[CrossRef\]](#) [\[PubMed\]](#) [\[PubMed Central\]](#)
171. Flechsig, H.; Ando, T. Protein dynamics by the combination of high-speed AFM and computational modeling. *Curr. Opin. Struct. Biol.* **2023**, *80*, 102591. [\[CrossRef\]](#) [\[PubMed\]](#)

Disclaimer/Publisher's Note: The statements, opinions and data contained in all publications are solely those of the individual author(s) and contributor(s) and not of MDPI and/or the editor(s). MDPI and/or the editor(s) disclaim responsibility for any injury to people or property resulting from any ideas, methods, instructions or products referred to in the content.

Article

Evaluation of Surface Structure and Morphological Phenomena of Caucasian Virgin Hair with Atomic Force Microscopy

Karolina Krawczyk-Woloszyn ^{1,2}, Damian Roczowski ² and Adam Reich ^{2,*} ¹ Doctoral School, University of Rzeszów, 35-959 Rzeszów, Poland; karolinakrawczyk10@wp.pl² Department of Dermatology, Institute of Medical Sciences, Medical College of the Rzeszów University, 35-959 Rzeszów, Poland; droczkowski99@gmail.com

* Correspondence: adi_medicalis@go2.pl

Abstract: *Background and Objectives:* Atomic force microscopy (AFM) as a type of scanning microscopy (SPM), which has a resolution of fractions of a nanometer on the atomic scale, is widely used in materials science. To date, research using AFM in medicine has focused on neurodegenerative diseases, osteoporosis, cancer tumors, cell receptors, proteins and the DNA mismatch repair (MMR) system. Only a few small studies of hair imaging have been conducted, mostly in biotechnology or cosmetology. Thanks to the possibilities offered by AFM imaging, dermatologists can non-invasively assess the condition of hair and its possible disorders. Our goal was to capture images and microscopically analyze morphological changes in the surface of healthy hair. *Materials and Methods:* In this study, three to five hairs were collected from each person. Each hair was examined at nine locations (0.5; 1.0; 1.5; 2.0; 3.5; 4.5; 5.5; 6.5 and 7.0 cm from the root). At least 4 images (4–10 images) were taken at each of the 9 locations. A total of 496 photos were taken and analyzed. Metric measurements of hair scales, such as apparent length, width and scale step height, were taken. *Results:* This publication presents the changes occurring in hair during the natural delamination process. In addition, morphological changes visualized on the surface of healthy hair (pitting, oval indentations, rod-shaped macro-fibrillar elements, globules, scratches, wavy edge) are presented. A quantitative analysis of the structures found was carried out. *Conclusions:* The findings of this study can be used in further research and work related to the subject of human hair. They can serve as a reference for research on scalp and hair diseases, as well as hair care.

Keywords: atomic force microscopy; atomic force microscope; AFM; dermatology; hair; human hair; diseases of the hair



Citation: Krawczyk-Woloszyn, K.; Roczowski, D.; Reich, A. Evaluation of Surface Structure and Morphological Phenomena of Caucasian Virgin Hair with Atomic Force Microscopy. *Medicina* **2024**, *60*, 297. <https://doi.org/10.3390/medicina60020297>

Academic Editor: Dietrich Doll

Received: 14 January 2024

Revised: 3 February 2024

Accepted: 7 February 2024

Published: 9 February 2024



Copyright: © 2024 by the authors. Licensee MDPI, Basel, Switzerland. This article is an open access article distributed under the terms and conditions of the Creative Commons Attribution (CC BY) license (<https://creativecommons.org/licenses/by/4.0/>).

1. Introduction

Based on previous studies of hair carried out using scanning electron microscopy (SEM) and transmission electron microscopy (TEM), we have knowledge of hair fiber structure at the microscale, although there are still many unanswered questions in this area. The introduction of atomic force microscopy (AFM) as an alternative method in dermatology research can have great potential in the diagnosis and treatment of various skin and hair disorders [1].

Human scalp hair consists of a central medulla, then cortex and thin layers of cells (cuticle) surrounding it from the outside. Cuticle cells (scales) overlap each other (like tiles on a roof). The casing consists of an average of 5–10 cuticle cells. Each scale is typically 0.3–0.5 µm thick, has an apparent length of 5–10 µm and is separated from the underlying scale by a cell membrane complex [2]. To date, the internal structure and chemical composition of cuticles has been investigated and described using transmission electron microscopy (TEM) of transverse sections of hairs. As a result, we know that each cuticle cell consists of seven layers that differ in composition and tribological properties. These layers are as follows (from the most superficial to the deepest): the upper β-layer, the

A-layer, the exocuticle, the endocuticle, the inner layer, the lower β -layer and the δ -layer. The lower β -layer and δ -layer of one cuticle, together with the upper β -layer of the scale below it, form the cell membrane complex (CMC). CMC is most likely one of the sites of delamination of the cuticle during mechanical wear and tear [3].

Despite some advantages, SEM and TEM also have limitations in terms of accurately visualizing spatial architecture of the hair surface at the nanoscale and the tribological properties of hair, which AFM makes possible. Hair fibers and cells have already been preliminarily examined by AFM in several studies. The researchers studied surface morphology, hair's step heights and scale dimensions in healthy, virgin hair. In addition, they tested the tribological properties of hair [4,5] and mainly focused on the effects of external factors on the above-mentioned hair characteristics. They tested cosmetic preparations for hair care such as conditioners and shampoos, as well as the effects of cosmetic procedures such as coloring and perming [2,6–9].

The invention of AFM by Binnig et al. in 1986 laid the groundwork for imaging atomic structure. AFM is increasingly being used in scientific research, as evidenced by the fact that the number of citations for the inaugural article is now at approximately 23,000 [10]. The AFM technique is constantly improving and is a forward-looking scientific tool. Extending the functions of AFM with other techniques (such as spectroscopy) extended its utility. Various AFM modifications already exist, for example, single-cell force spectroscopy (SCFS), single-molecule force spectroscopy (SMFS), chemical force microscopy (CFM) and AFM-infrared spectroscopy (AFM-IR) [11–13].

In this study, an attempt was made to find such parameters of healthy hair, which can be helpful in a non-invasive, molecular, rapid assessment of the condition of hair and its possible abnormalities. It was proposed to create a characterization of healthy hair based on AFM images, which can be used by dermatologists to examine the hair of patients with various hair diseases. There are few studies focusing on this topic, and the AFM imaging results obtained in them are of inferior quality. The following publication presents the data on this topic more practically so that an attempt can be made to standardize the procedure for assessing the condition of hair for medical purposes. This study is based on a carefully selected control group of dermatologically examined healthy subjects by a dermatologist. Results from hair sections in 0.5–1 cm increments are presented, which is quite accurate for the time-consuming nature of this technique. This work was extended to present a hair diagram that dermatologists could use in their daily work as a reference for future studies on their patients' diseased hair.

2. Material and Methods

2.1. The Objective of the Study

To date, few medical studies have been conducted on AFM imaging of hair diseases. This study demonstrates the appearance of healthy hair under AFM, which can be used for further research and work related to the subject of human hair. The goal of this study was to find the parameters of human healthy hair and map them to quickly assess its condition.

2.2. Subjects

The study group consisted of 10 healthy volunteers, 9 women and 1 man, with a mean age of 43.8 years with SD (Standard Deviation) = 16.19. Three to five virgin hairs, which had not been treated with any dye or other harmful treatments for at least 3 months, were taken from each subject. None of the included subjects suffered from any skin or hair disease.

2.3. Hair Preparation

The clean hairs were pulled out along with their roots and subsequently cut vertically with a scalpel into 3 cm long sections. They were then attached to a microscope slide using a translucent tape.

2.4. Atomic Force Microscopy (AFM)

AFM was performed using a DriveAFM microscope with CX controller (Nanosurf, Liestal, Switzerland) under atmospheric conditions (in air) at room temperature. Imaging was performed in contact mode using PPP-FMAuD-10 tips (NANOSensorTM, Neuchâtel, Switzerland) mounted on cantilevers with a constant force of 1.9 N/m and frequency of 75 kHz. Each hair was imaged at a distance of 0.5, 1.0, 1.5, 2.0, 3.5, 4.5, 5.5, 6.5 and 7.0 cm from the root. The scanning range covered an area from $40 \times 40 \mu\text{m}$ to $3 \times 3 \mu\text{m}$. The scanning velocity was 0.5 s/line. The resolution of the images was 512–1024 points/line.

At least 4 images were taken at each location at different dimensions of the field. The images were computer-processed using Nanosurf CX ver 3.10.3.7. The AFM tip was centered to be on top of the hair fiber upon contact with the cuticle surface. The AFM tip scanned the hair perpendicular to the longitudinal axis of the fiber. This reduced errors due to the AFM tip hitting the sides of the hair.

2.5. Method of Taking Measurements and Analyzing Images Obtained with Atomic Force Microscopy (AFM)

At each of the 9 locations (0.5, 1.0, 1.5, 2.0, 3.5, 4.5, 5.5, 6.5 and 7.0 cm from the root), at least 4 images (4–10 images) were taken. Finally, a total of 496 photos were collected and analyzed.

Line profiles were created by averaging data from 10 adjacent scan lines. Line profile creation, 3D visualizations, image processing and all metric measurements (length, width, and scale step height—Figure 1) were performed using Gwyddion (64 bit) software ver 2.63.

Metric measurements were taken on $30 \times 30 \mu\text{m}$ images from each location and from each subject. A total of 729 scales were evaluated. *Scale length* refers to the dimension parallel to the longitudinal axis of the hair. Due to the tile-like arrangement of the scales, only the portion of the scales available for examination was measured. *Scale width* refers to the transverse dimension to the longitudinal axis of the hair. To measure *scale deviation*, a line profile of adjacent scales was made. Lines were run mostly perpendicular to the free end of each scale. From the resulting profile, the height difference of each step was measured.

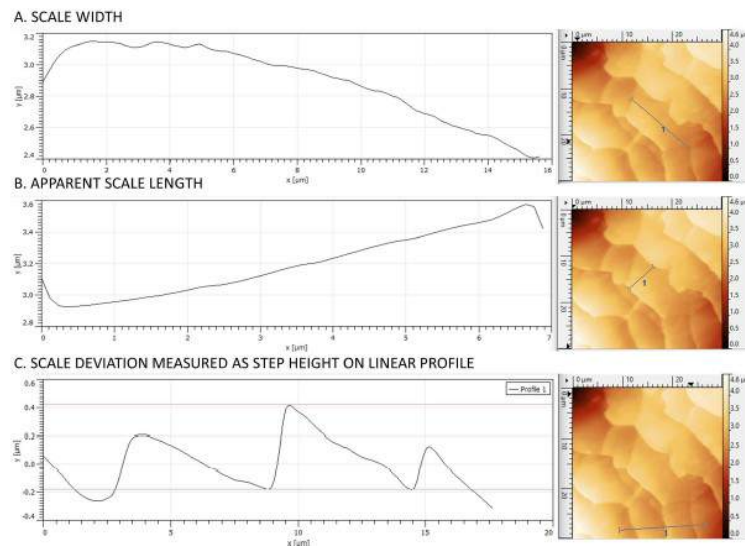


Figure 1. Parameters analyzed with AFM in terms of hair scale (Z-axis images).

The evaluation of features indicative of the natural process of hair delamination (striated surface, endocuticle, smooth surface, cortex, ghost signs, broken edges of scales, shape of edges) was performed in a quantitative and semi-quantitative manner. From the photos, (1) the number of scales with striated surface, (2) the number of scales with smooth surface and (3) the number of cavities corresponding to ghost signs were counted. Then, the above parameters were grouped on a scale from 0 to 5 as in Table 1.

Table 1. Quantitative and descriptive representation of features indicating the natural process of hair delamination.

Feature	Absolute Number—Range or Qualitative Description of the Feature	Corresponding Grade
The number of scales with striated surface	0	0
	1–3	1
	4–7	2
	8–11	3
	12–15	4
	16–20	5
The number of scales with smooth surface	0	0
	1–2	1
	3–4	2
	5–6	3
	7–9	4
	10–12	5
The number of ghost signs	0	0
	1–2	1
	3–4	2
	5–6	3
	7–8	4
	9–10	5
Shape of edges	Convex	1
	Straight	2
	Concave	3
Broken edges	- Edge undamaged, smooth;	0
	- Edge smooth with single small cracks;	1
	- Numerous small cracks, smooth edge visible for less than 40%;	2
	- Lack of smooth edge, numerous larger cracks and scale breakages;	3
	- Deep breakouts, edge like chain saw's teeth;	4
	- Very uneven, deep, different shaped breakouts.	5
Endocuticle	- absent;	0
	- Single nodules 2–4 nm in diameter, located at the base of the scales' edges;	1
	- Single nodules spread over the entire scale surface;	2
	- Granular plaques 3–5 nm wide localized at the base of the scales' edges;	3
	- Granular plaques 4–7 nm wide located across the width of the scales, at the base of the scale edges;	4
	- Granular structure occupying more than 50% of the cuticle surface.	5

Parameters such as (1) broken edges of scales, (2) shape of edges and (3) endocuticle were evaluated in a descriptive manner by grouping a given characteristic in a range, as follows (Table 1):

- From 0 to 5 for the broken edges of scales and the endocuticle (qualification for a given range was made on the basis of a comparison of the trait in question between different subjects and on the basis of the researcher's own experience).

- From 1 to 3 for the shape of the edge (1—convex, 2—straight, 3—concave); the evaluation was based on the researcher's own experience and comparison between different photos.

Assessment of morphological lesions (pitting, oval indentations, rod-like macrofibrillar elements, globules, scratches, wavy edge) on the surface of scales was performed manually on images of the same size, usually $20 \times 20 \mu\text{m}$ and $30 \times 30 \mu\text{m}$, to compare features between patients. At each location, 2–5 images were used for analysis.

2.6. Statistical Analysis

Statistical analysis was performed using *Statistica* software, v. 13.0 (TIBCO Software Inc., Kraków, Poland). Mean, minimal and maximal values along with the standard deviations were calculated for longitudinal parameters.

3. Results

In this study, the hair surface was evaluated for three separate groups of parameters. The first subsection concerns metric measurements of hair scales. The measurements obtained are shown in Table 2. The second subsection focuses on mapping the hair in terms of morphological features of the natural process of hair delamination. The change in the distribution of these features with distance from the root of the hair is presented semi-quantitatively. The third subsection deals with selected non-characteristic morphological features on the surface of healthy hair. These changes were imaged in significantly greater numbers on the surface of hair from patients with diseases, i.e., lichen planopilaris and frontal fibrosing alopecia. However, since it also occurred on the hair of healthy subjects, it is presented descriptively above.

Table 2. Measurements of the hair scales.

Distance from the Root	Scale Step Height—Mean [nm]	Scale Step Height—SD [nm]	Apparent Scale Length—Mean [nm]	Apparent Scale Length—SD [nm]	Scale Width—Mean [nm]	Scale Width—SD [nm]
0.5 cm	512.9	99.5	7879.5	1135.4	17,234.0	3649.5
1.0 cm	509.5	119.2	6847.4	1352.8	16,589.0	2245.0
1.5 cm	480.5	106.2	7562.5	1369.4	17,177.0	2616.2
2.0 cm	494.4	81.4	7673.4	1071.3	20,646.0	3685.4
3.5 cm	522.2	50.5	6719.1	1014.1	19,218.0	2865.8
4.5 cm	531.1	168.3	7855.9	1883.1	19,215.0	4010.3
5.5 cm	530.8	92.2	7495.0	1251.4	18,670.0	3236.4
6.5 cm	530.5	112.6	7255.7	1335.1	20,219.0	4404.2
7.0 cm	500.5	132.3	7589.2	1579.6	19,715.0	4310.5

3.1. Dimensions and Size of the Scale

The hair scales were more-or-less rectangular in shape. The average length and width of the scales, depending on the distance from the root, differed only subtly. The measurements obtained are shown in Table 2. The main difference was observed in the shape of the free edge of each scale. Cells of intact hair show a smooth and convex contour. The edges of the cells, which wear down, become increasingly frayed and concave (Figure 2(a1–a4),b). The cells degenerate by breaking off small fragments from the free edge of the scale. This process is most intense in the center of the hair scales. The study using AFM captured moments of natural exfoliation of hair cells (Figure 2c).

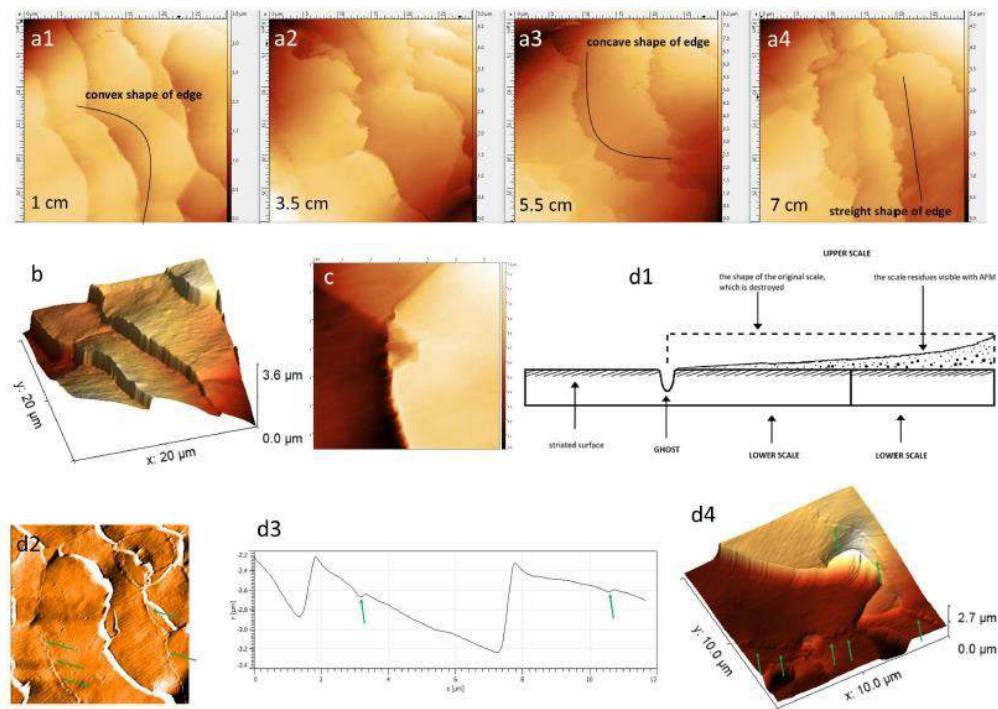


Figure 2. (a1–a4) The process of exfoliation of the scales depending on the distance from the root end of the hair—the black line marks the shapes of the scales' edges; visible smooth (a1) and frayed (a4) edges of scales; Z-axis image. (b) Three-dimensional projection. (c) The beginning of the scale detachment; Z-axis image. (d1) Diagram of ghost sign formation. (d2) Ghost signs—green arrows; deflection image. (d3) Line profile of the scales with the cavity corresponding to the ghost sign marked with a green arrow. (d4) Ghost signs—green arrows; 3D projection.

3.2. Surface Phenomena Resulting from the Natural Delamination Process

In this study, four different scale's surfaces differing in morphology were identified—striated surface, endocuticle, smooth surface and cortex. They were singled out as being key for a further evaluation of the advancement of the delamination process. They formed the basis of the morphological structure of the surface of each healthy hair. As the distance from the root of the hair increased, the individual surfaces were replaced by more hair, forming a kind of continuum of the process of natural wear and tear of hair cells (for maintaining the self-adaptive—disentangling—properties of the hair [2,3]) (Figures 2–5).

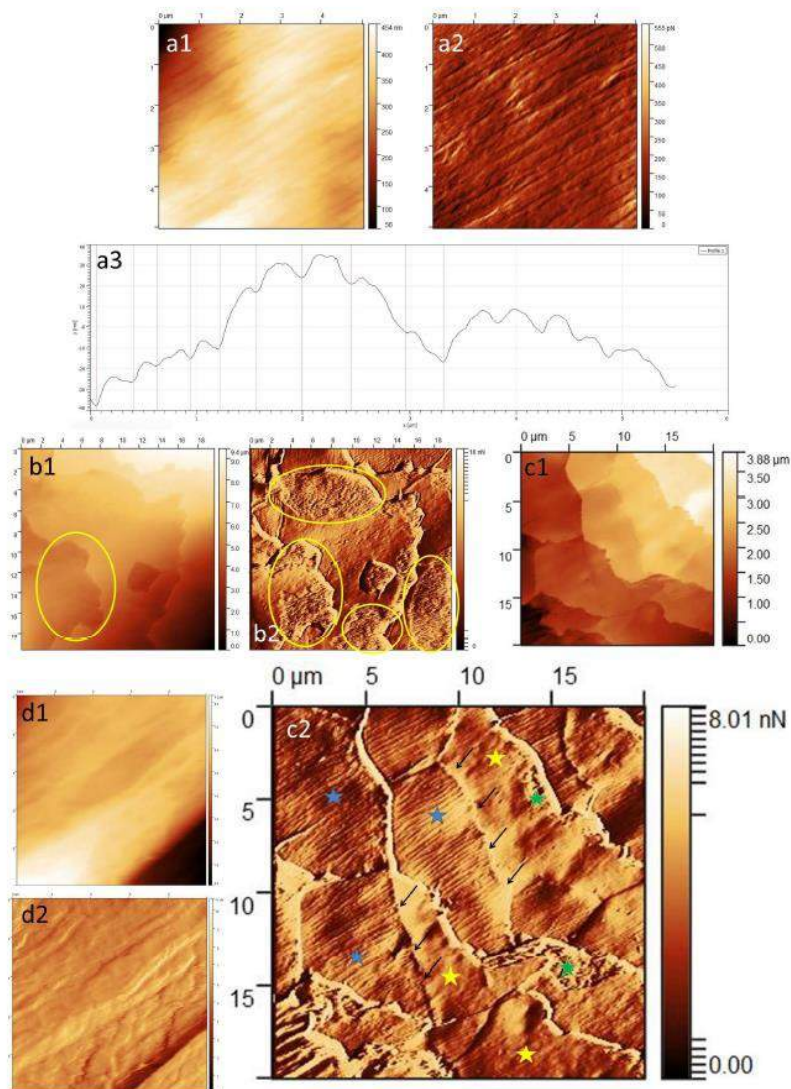


Figure 3. (a1) Striated surface; Z-axis image. (a2) Striated surface; deflection image. (a3) Striated surface; line profile. (b1) Endocuticle at the free edge of the scales—yellow circles; Z-axis image. (b2) Endocuticle at the free edge of the scales—yellow circles; deflection image. (c1) The appearance of the scales during the natural delamination process; Z-axis image. (c2) The appearance of the scales during the natural delamination process: striated scale (blue star), smooth scale (yellow star), ghost signs between the two scales (black arrows), endocuticle (green star); deflection image. (d1) Image of a fully exposed cortex—irregular, rod-shaped cortex surface; Z-axis image. (d2) Image of a fully exposed cortex—irregular, rod-shaped cortex surface; deflection image.

The surface of the intact hair fiber, just near the end of the root, shows a longitudinal *striation*, which is a characteristic of the cuticle's superficial layers (Figure 3(a1–a3)). With a greater distance from the root, such a surface is imaged less and less frequently, indicating gradual destruction of the hair. To visualize this surface, the probe should scan perpendicularly to the long axis of the hair. The striations were cylindrical in shape and parallel in arrangement, along the long axis of the hair. With a greater distance from the root end, they became flatter and began to transition into each other. On average, these striations were 300–450 nm wide and about 10 nm high. A detailed analysis of these striations, their individual differences and their association with scalp diseases will be included in a separate publication.

With a greater distance from the root end, fragments of the harder, outer layers of the cuticle (exocuticle and A-layer) exfoliate gradually and expose the surface of the *endocuticle* (Figure 3(b1,b2)). (Controlled detachment at the level of the soft endocuticle under friction occurs due to lipids—18-methyleicosanoic acid—that cover the outer surface of the cuticle cell [3]). The endocuticle is a granular, irregular surface. It was visible at the base of the free end of the scale, representing its remnant. It laid directly on top of the smooth surface of the scale.

The *smooth surface* is revealed when the outermost layers of the scales exfoliate. It represents cuticle structures such as the inner layer, the lower β -layer and the δ -layer. In this study, it was the surface on which various morphological lesions—scratches, pitting, globules—were more frequently observed. The smooth surface appeared proximal to the line delineating the ghost signs (see below). Viewing a particular scale (Figure 3(c1,c2)), one can see the following at a similar level: a striated surface of the distal scale that extends to the free end of the cell; a transverse line representing the transition of one scale into another (ghost signs); and a smooth surface as a remnant of the proximal scales (in the cephalad direction).

At the end tip of the hair, it was possible to visualize an irregular rod-shaped surface, which most likely corresponds to the hair's *cortical cells* (Figure 3(d1,d2)). In the material studied, this type of cortex surface was found relatively rarely due to the fact that the scope of the study included the first 7 cm of each hair.

The scale exfoliates from the free end, initially showing its deeper layers until it disappears completely. Once the lower cell is exposed, a linear depression of the surface is visible, corresponding to the edge of the higher lying scale that has recently been destroyed. The cavity that is created is referred to as a *ghost sign* (Figure 2(d1–d4)). These ghost signs can be recognized because proximally from the transverse linear depression, the striations disappear and the smoother surface of the inner or lower β -layer is exposed. Ghosts are found in sections of hair, where the process of cuticle delamination begins. As the destruction of the cuticle progresses, ghosts also disappear.

With the distance from the root of the hair, the *free edges* of the cells became damaged. At first, the edges were smooth and undamaged, but gradually became increasingly frayed and broken. The *shape of the cells* also changed. At first, the free edges of the cells were rounded, convex. Then, they became concave, C-shaped.

Figure 6 graphically shows how the above features changed on the hair fibers of the control group subjects (S1–S10). It is possible to see how a particular feature disappeared or increased with distance from the root in a particular subject. You can also see individual differences in the intensity of delamination between subjects. It can be seen that some hairs (S4, S5) only started to show more delamination features towards the end of the hair section studied (so hair was less damaged and better cared for). However, one can see a repeatability and a trend in the formation of the hair fiber.

3.3. Other Morphological Phenomena Visualized on the Hair Surface

Pitting (Figure 4a,b)

One of the characteristic changes observed on all tested hairs was the finding of small, round excavations—pitting. In appearance, they resemble corrosion pits or pitting caused

by friction in systems with grease (in the process of wear). In the healthy hair studied, they were regularly dispersed, did not form clusters on specific scales and were of similar size.

Oval indentations (Figure 4c,d)

The indentations differed from pitting in size and shape. They were about 10–12 times larger and oval in shape.

Scratches (Figure 4e,f)

Scratches and indentations of various shapes were observed along the entire length of the hair. In all samples, short but deeper scratches in the shapes of triangles, lines and commas were visible. In addition, we noted individual scratches along the long axis of the hair extending through several scales in the form of a precise line and with various other unexpected shapes. The lesions described above were less often seen on the striated surface and appeared more often on the deeper and softer layers of the cuticle.

Wavy edge (Figure 5a,b)

In individual samples, perfectly wavy edges of the scales were visible in some places. In addition, at a high magnification, the indentations on the surface of the scales in the ghost sign also take this shape. The cuticle cells with perfectly wavy edges in the proximal regions fracture along the long axis of the hair. As a result, linear cracks running from the base of the wave deep into the scales are visible.

Globules (Figure 5c,d)

The lesions were observed in various sections of the studied hairs in low quantities. The etiology of their formation is not entirely evident. They are probably related to mechanical damage to the hair surface. Globules appeared in the course of physiological delamination and exposing the lower cuticle layers. They were also observed in larger amounts in the immediate areas of sudden destruction of the hair fiber in patients with LPP (personal observation). Three different types of globules were visualized: (1) characteristic of delamination, flat elevation globules with dimensions on the order of hundreds of nanometers; (2) smaller globules (sand) with dimensions in the order of tens of nanometers (encountered less frequently), which were probably part of the cuticle layers underlying the endocuticle; (3) large conglomerates of contaminants lying on the surface of the hair with dimensions comprising thousands of nanometers, which were rather individual, found on the hair of specific patients, at different sections of the hair.

Rod-like macrofibrillar elements (Figure 5e,f)

There were clearly visible structures that were limited to a particular scale. Rod-like macrofibrillar elements were usually below the level of the surrounding cuticle cells. However, individual lesions were visualized at the level of other scales. They differed from the rods in the cortex layer in size and had a more regular, parallel formation.

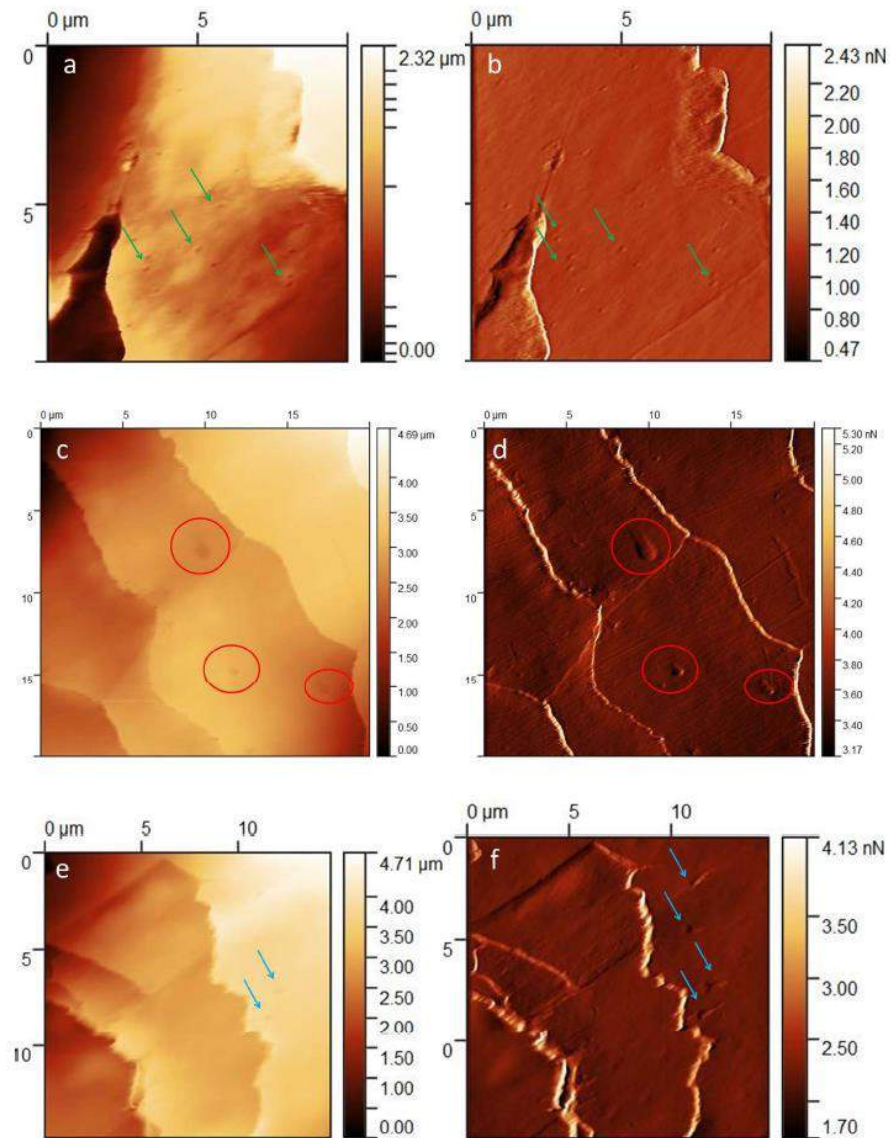


Figure 4. (a) Pitting—green arrows; Z-axis image. (b) Pitting—green arrows; deflection image. (c) Oval indentations—red circles; Z-axis image. (d) Oval indentations—red circles; deflection image. (e) Scratches—blue arrows; Z-axis image. (f) Scratches—blue arrows; deflection image.

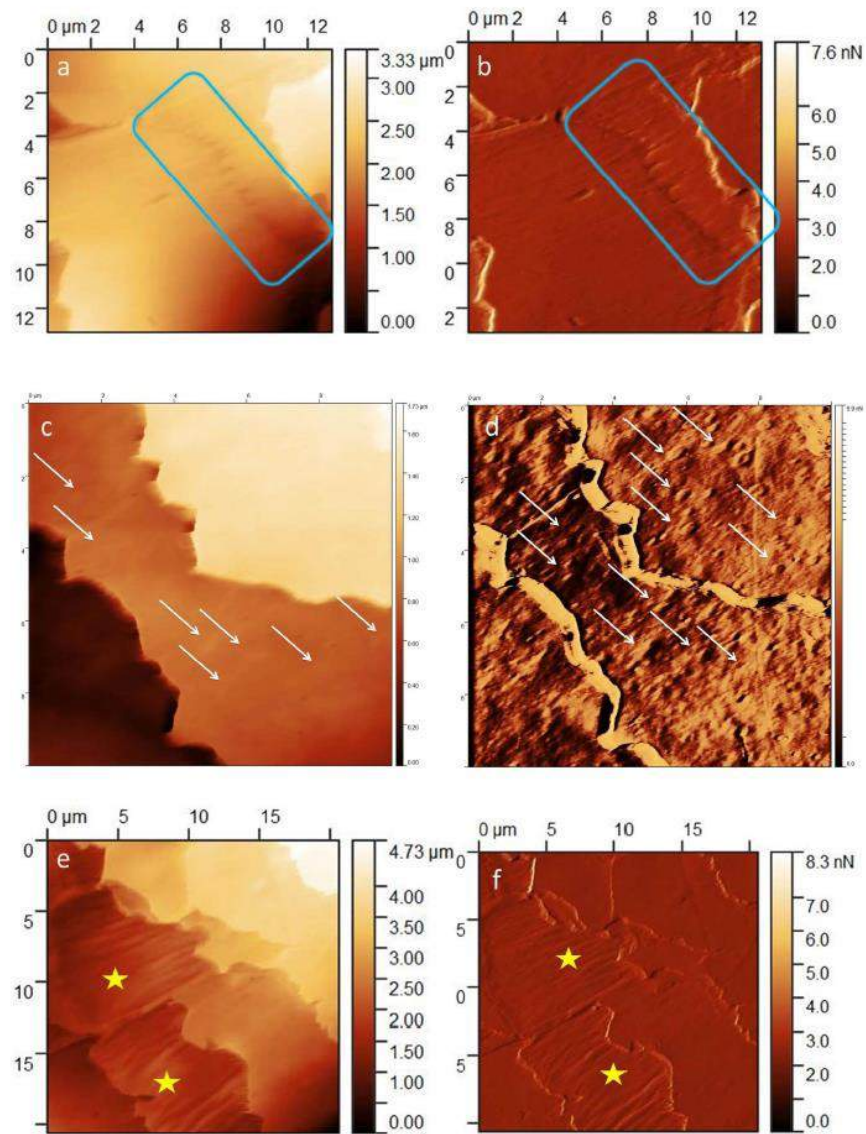


Figure 5. (a) Wavy edges—blue rectangle; Z-axis image. (b) Wavy edges—blue rectangle; deflection image. (c) Globules—white arrows; Z-axis image. (d) Globules—white arrows; deflection image. (e) Rod-like macrofibrillar elements—yellow star; Z-axis image. (f) Rod-like macrofibrillar elements—yellow star; deflection image.

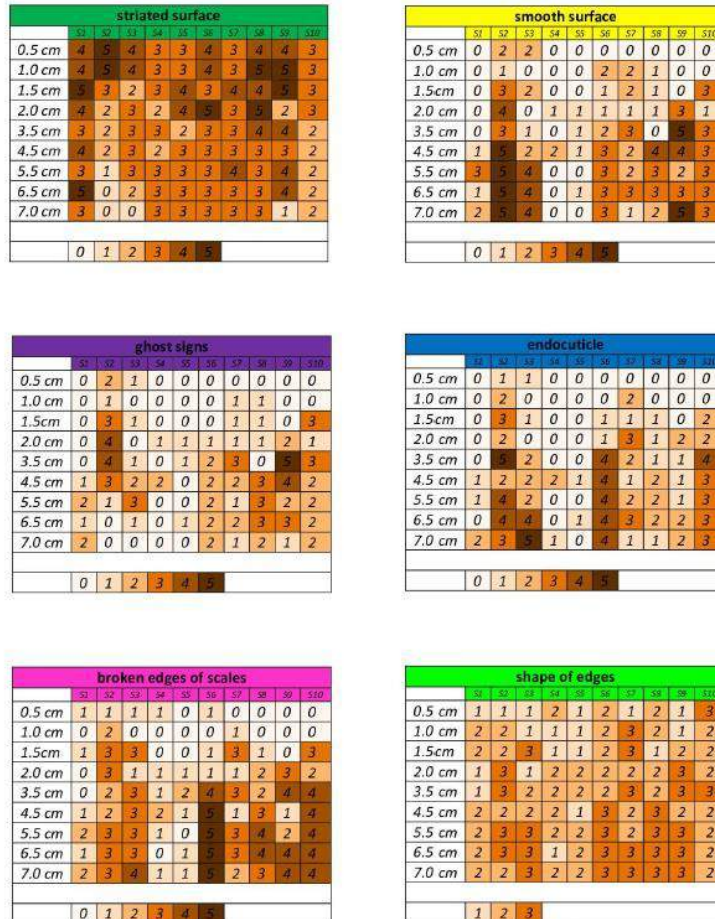


Figure 6. Distribution of delamination features on hair (parameters described in Table 1).

4. Discussion

4.1. Basics of AFM Operation and Functioning

AFM is a type of microscopy with a scanning probe (scanning probe microscopy—SPM). It is used to image atomic structure by scanning a sample with a sharpened tip mounted on a flexible cantilever. The technique allows imaging of samples in air, liquid and high vacuum. With the ability to capture images in a buffer solution, biological samples can be studied in their native states. It is possible to examine cells intravitaly, without the need to stain, fix, dehydrate or label samples. This makes it possible to examine dynamic biological phenomena in a real-time manner, at the nanoscale [10,14,15]. In addition, by scanning the deflection of the cantilever, information from the Z-plane can be obtained, providing 3D images of the surface under examination. This enables us to perform a characterization of the morphology, thickness, surface roughness of the test sample and atomic forces, especially longitudinal forces [16]. In-plane AFM shows a resolution of about 1 nm, while for the

surface of living cells it can approach ~ 10 nm. Out-of-plane resolution is in the order of sub-nanometers. With AFM, measurements can be made at the micro- and nanoscale, and even atomistic events can be recorded at the edges of atomic lattice steps [15,17,18]. The scanning surface enables testing to be performed up to dimensions in the order of $100\ \mu\text{m}$ in the horizontal plane and up to $10\ \mu\text{m}$ in height [14].

The AFM is constructed from a laser, a cantilever with probe tip, a photodiode detector, a nanopositioning system with a piezoelectric scanner and a feedback imaging motion controller. The basis of operation with regard to this method concerns performing a scan with the tip of the probe and the surface of the test sample in the X and Y planes. By detecting the laser beam reflected from the top surface of the deflected cantilever, it is possible to measure the height of the sample in the Z-axis. The nanopositioning system is used to control the relative distance between the probe tip and the sample surface. Depending on the mode of operation, this system adjusts the deflection or oscillation of the cantilever to maintain the same spacing between the tip and the sample during the entire scanning process. Additional control feedback systems between the laser detector and scanner are essential for imaging performance and to avoid the destruction of biological samples [14–16,19]. Depending on whether the tip is in contact or almost in contact with the surface to be tested, AFM can operate in a contact mode, noncontact mode and in an intermediate mode (tapping mode). The AFM imaging mode depends on the characteristics of the samples being studied [17–20].

In *contact mode*, the AFM tip is constantly in contact with the surface to be analyzed. When imaging in contact mode with vertical forces of 10–30 nN, there is usually no cell damage. However, this method does not completely protect delicate biological samples from the deformation or degradation of their surfaces. It performs better with samples that are harder, rougher and that have a stiffer surface [14,21]. The vertical forces compress cell membranes and allow imaging of elements inside the cell. By examining cells without a cell wall, it is possible to image the cell nucleus or cytoskeleton network by increasing the vertical force. However, as the imaging force applied to the cells increases, the resolution of the images obtained decreases [14,22,23]. The force also provides information on the local viscoelasticity of the cell, adhesion forces and nanomechanical properties [24,25]. This is the most suitable mode for testing frictional forces [26]. Scanning can be performed in two modes of operation: constant force mode and constant height mode. The constant force mode provides information about the topography of the surface, considering the changes in the surface height of the sample. The constant height mode is primarily used for quick overview scanning of samples with small height differences [27].

In *noncontact mode*, where the scanner tip does not touch the surface to be tested, a high vacuum environment is required to examine biological samples. Consequently, this mode is not frequently applicable in medical research [20,27,28]. The noncontact mode enables us to detect the interaction forces between biomolecules. Attaching a specific molecule probe to the AFM tip makes it possible to find selected molecules of interest in the sample under study that specifically interact with the selected probe. Such a study is made possible via molecular recognition force microscopy (MRFM) or topography and recognition (TREC) microscopy [29–32]. In the noncontact mode, there is no possibility of testing the mechanical properties of the samples [21].

Given the limitations of the above methods, a *tapping mode* (also known as intermittent mode, dynamic mode) was constructed in 1993. This is the most suitable and most widely used method for testing delicate biological samples and polymers. In tapping mode, the tip cantilever typically oscillates between 100 and 300 kHz, with an amplitude of 30–100 nm. The tip moves toward the sample, touches it, and then moves away from the sample surface during each oscillation period [20,21,27,33–35]. The test can be conducted in any environment and achieves high resolution. Scanning in this mode is fast as in contact mode and, furthermore, there are no shear forces that are responsible for possible surface damage in contact mode. In this mode, topographic images and phase images are obtained [20,36]. The study of the viscoelastic properties, the variations in composition and adhesion is

based on the measurement of the amplitude or phase shift between the free oscillation in air and the oscillation when the tip is tapped against the surface [20,21,37].

Recently, new mechanical imaging techniques based on the tapping mode have emerged, such as contact resonance, multifrequency AFM, multiharmonic mode AFM and viscoelastic mapping. These modes are used to study complex biomolecular and tissue systems due to their ability to provide multi-parametric, quantitative evaluations [26,38–42]. The most suitable for testing the mechanical properties of multicomponent coatings is *force mode*. In this mode, the surface to be tested moves in the direction of the tip. It shows a high resolution and does not damage the surface of samples [27].

AFM enables the creation of images of a sample's surface under examination, providing information on 3D topography. In addition, monitoring cantilever deflection during scanning enables the measurement of the force acting between the tip and the sample [20]. Due to the different forces acting between the AFM tip and the sample surface (overlapping of electron orbitals or van der Waals forces), resultant repulsive or attractive forces are generated [20,27]. In contact mode, where the excursion force is repulsive, the tip is constantly in contact with the sample. In noncontact mode, the tip floats at a certain distance from the surface, and the force is attractive [14,16,20,21,27,40,43]. In tapping mode, the resultant force is alternately attractive or repulsive, while in the force mode, the force is initially attractive until the tip is so close to the sample that the resultant force becomes repulsive [20,27,40]. Probe sample mechanical interactions enable us to study nanomechanical, electrical, magnetic and tribological properties as well as surface mapping [16].

The AFM is a modern, advanced, multifunctional tool that allows for a whole range of measurements and tests. However, it also has several disadvantages. The main disadvantage is the speed of AFM imaging, which is relatively slow, making the AFM technique time-consuming. In addition, the measurement technique is generally complicated. To avoid damaging biological and delicate samples, the right mode, probe properties and controller parameters have to be chosen [15].

4.2. AFM Research on Hair

Previous research has focused on depicting healthy hair in material sciences. You and Yu (1997) were among the first to image human hair using AFM techniques. This was one of the largest studies available on quantitative changes in the hair surface under the influence of external environmental factors. For this purpose, accurate measurements of hair scale deviation were completed on a large control group. The surface of the intact hair imaged by You and Yu had a stepped pattern, where each scale overlapped each other. In order to evaluate the height (deviation) of the scales, they created line profiles, which are line graphs of the longitudinal section of the hair. The *x*-axis of this graph is the long axis of the hair, while the height difference on the surface of the hair is deposited on the *y*-axis, measured in the *Z*-plane of the scanner. The height of each step on the line graph represents the value of the scale's deviation. This study showed that the height of each step in a profile line (scale deviation) varies greatly and changes even within a single hair fiber measured at different locations. Statistically, the step height of untreated hair statistically was $340.72 \text{ nm} \pm 90.57 \text{ nm}$ ($n = 210$) [4]. In this study, the scale's step height was relatively constant at approx. 480.5–531.1 nm. You and Yu also showed the dependence of scale deviation on pH and high temperature. In addition, this study described the changes occurring on the surface of heat-treated hair. The structural changes were mainly rough and uneven cuticle edges and granules [4]. In the following years, when step heights became a quantitative parameter for assessing hair, Smith (1998) developed a computational method for conducting rapid measurements from AFM-derived images. Based on 10 AFM images of brown European hair, thousands of line profiles were made in image analysis software (Topo-Metrix SPM Lab. 1996, Version 3.06.06, TopoMetrix Corporation, Santa Clara, CA, USA.). It was then possible to measure the cuticle step height using a computer method. The results obtained using the automated method coincided with those obtained using

manual measurement. A wide distribution of results and similar step height values were obtained, similar to the study by You and Yu [5].

Swift et al. (2000) were the first to describe the overall morphology of the hair surface using AFM techniques. This is one of the most comprehensive and still current studies of the surface appearance of healthy hair. They found that the architecture of the hair surface changed gradually from the root to the tip. At 1 cm from the root, the scales were slightly curved and had a smooth edge. The surface of the scales themselves showed a slight undulation (striations), which developed when the hair cells passed through the inner root sheath. With distance from the root, small fragments broke off from individual scales causing the edges to be angularly serrated. As short as 3 cm from the root, most scales lost their smooth edge and granular remnants of exfoliated scales and exposed one of the inner layers of cuticular hair cells (endocuticle) appeared. At this distance from the root, the ghost sign was most often observed. Swift et al. explained that this is the imprint of a pre-existing scale, which has completely exfoliated, on the existing basal scale surface beneath it. With distance from the root, there was an increasing erosion of the scales until they completely disappeared, and the cortical surface was revealed near the tip of the hair. It had the appearance of longitudinally arranged rod-shaped elements. One of the main discoveries of their work was the imaging of striations on the surface of intact cuticle cells, which were not well visible using previous hair imaging methods (TEM, SEM). These occurred mainly at root ends. They had a parallel arrangement and comb shape. Each ridge was about 350 nm wide and up to about 9 nm high above the surface of the substrate [3]. The striated scaly surface has also been described in animal (mammalian) hair in other biological studies [44]. The above authors attributed this species-independent feature to all mammals. Swift et al. also studied the process of hair deterioration. They found that with external factors and dry friction, the hair cuticle delaminates at the cell boundary at the site of the so-called cell membrane complex (CMC). The new surface dominating the greater length of the hair has different chemical and physical properties. Additional signs of hair destruction included areas of exposed endocuticle in the form of granules covering 1/2 the thickness of a normal cuticle cell. These, however, are transient and quickly undergo complete exfoliation. In this work, Swift et al. distinguished between the two hair surfaces described above (with striations and the one formed after cuticular delamination). The difference in the angle of the two surfaces was also noted. These features may prove helpful in assessing the degree of hair damage [3].

Chen and Bhushan (2005) accurately imaged ghost signs on the hair surface and explained its genesis. In addition, they visualized the cuticle and cortex layers in cross sections [7].

The above morphological features of the surface of human hair were described in publications that aimed to demonstrate the feasibility of studying human hair with AFM. The authors did not assign specific properties to these features. They did not focus on the visual description of the hair and the importance of discrete morphological features such as pitting, globules or scratches. Although they are visible in some of their published photographs.

In contrast, Shin et al. (2012) studied the hair of patients, using AFM, with one of the most important dermatological diseases, psoriasis. They described morphological changes such as micropits and macropits. Micropits were described as indentations in diameter $<0.5 \mu\text{m}$ or area $<0.25 \mu\text{m}^2$, while macropits were described as indentations in diameter $>0.5 \mu\text{m}$ or area $>0.25 \mu\text{m}^2$. On hair taken from active psoriasis patches, the researchers found twice as many pits as on hair samples belonging to patients with psoriasis in comparison to unchanged skin. On the hair samples from active patches, the majority of pits were macropits, while micropits predominated over macropits on the hair from apparently unaltered skin. Micropits were also rarely observed in the control group. In addition, the hair of patients with psoriasis showed greater scale thickness and greater scale surface roughness. This was one of the few AFM studies of the hair surface in the field of skin and hair diseases. In addition, this study made it possible to visualize abnormalities at the nanoscale, as the same changes on the hair surface were found in patients with

psoriasis—on the hairs taken from disease lesions and from apparently (clinically) healthy skin [45].

The studies cited above involved the imaging of the cuticle surface of human hair. This is still the most up-to-date research on this subject, as further work has begun to evolve into the study of nanomechanical properties, among other things. In this study, however, morphological features provide a reference point of what healthy hair is expected to look like. The characterization of hair on the basis of relatively well-imaged surface features can be helpful for comparing healthy hair with diseased hair.

In subsequent years, other studies have mainly focused on the effects of conditioners and hair care products on the hair damaged from cosmetic treatments. In addition, many studies have considered the assessment of tribological features, mechanical properties of hair cells and physical interactions on their surface [2,5–9,46]. Seshadri and Bhushan (2008) and Lu et al. (2019) studied virgin hair of different races and the hair damaged by cosmetic treatments, i.e., coloring or perming. Hair imaging was designed to assess the effectiveness of commercial conditioners and cosmetics [47–49].

The latest AFM studies of hair are being carried out mainly by physicists and engineers, with a trend away from simply imaging the surface of hair towards a deeper understanding of its structure, chemical composition and physico-mechanical properties. From 2020 to 2022, Fellows et al. used the AFM-IR technique to assess the chemical composition and chemical bonds of human hair. They showed the existing significant differences between the medulla, cortex and cuticle layer of human hair [50–52]. A few years earlier, Marcott et al. performed a similar but smaller study of the lipid composition of human hair using the AFM-IR technique [53]. In their study, Fellows et al. and Marcott et al. confirmed the great potential of combining infrared spectroscopy with the AFM technique to study complex biological samples.

5. Conclusions

This publication attempts to characterize the surface of healthy hair. On the basis of the authors' own observations and the available literature, seven features were identified that may indicate the natural process of hair delamination (striated surface, endocuticle, smooth surface, cortex, ghost signs, broken edges of scales, shape of edges). The observation along the length of the hair of the above features made it possible to characterize the appearance of the reference hair in a descriptive and semi-quantitative way. The natural process of delamination is evidenced by the gradual breakaway of the scales and the change in shape of the edges from convex to concave. With detachment, the top layer of striated cuticle disappears, and the endocuticle and ghosts are gradually exposed, on average, at a distance of 2–5.5 cm from the root. With the distance from the tip root, in successive stages of delamination, the ghosts also disappear, and the surface of the endocuticle decreases until it disappears. Deeper smooth layers of the cuticle are exposed until the cortex at the end of the hair is uncovered. Based on the above observations, a preliminary conclusion can be drawn that the hairs' delamination process between us is similar. This process can vary in intensity and its starting point (distance from the root).

Accurate measurements were taken of the length, width and height of the scaly deviation. The scale step height was relatively constant. The apparent scale length was maximal at the root end of the hair. The scale width, in contrast, was greatest at the tip end of hair. Both values changed only subtly. No significant differences were shown between individual subjects. However, the measurements were made on too small a group of subjects to perform a standardization of normal scale dimensions. To do so, measurements would have to be made in a group at least ten times larger.

While the results of the measurements do not have a significant impact on the assessment of healthy hair, subtle morphological changes on the surface of the hair scales may provide a direction for further research. In the physical sciences, such changes can be ignored. However, in medicine, clinical features and qualitative variables are more often given importance. Specifically, descriptive morphological changes are used in dermatology

in examinations such as dermoscopy and reflectance confocal microscopy, for example. In the above publication, morphological lesions found on the surface of healthy hair, i.e., pitting, oval indentations, rod-like macrofibrillar elements, globules, scratches and wavy edges, are described. These features were visible in all healthy hairs, but in insignificant quantities. They occurred much more frequently on the hair of patients with scalp diseases (personal observation)—which will be a topic for future publications. Therefore, an attempt has been made to characterize morphological lesions at the nanoscale, which may be helpful in the early diagnosis of hair diseases in the future. The presented results will serve as a reference for the authors to conduct further research on the diseases of the scalp and hair (i.e., lichen planopilaris, frontal fibrosing alopecia and alopecia areata).

The main limitations of this study were its focus on morphological assessment of the hair surface only and its small sample size. Mechanical properties of the hair surface were not measured. The image capture time was 6 min at 256 points/line, 12 min at 512 points/line and about 20 min at 1024 points/line. Due to the time-consuming nature of the method and the need to take multiple measurements on the length of a single hair, a small group of subjects was studied. Patients selected for this study had not undergone hair treatments (i.e., hair coloring, keratin straightening or other treatments affecting the hair surface) in the last 3 months prior to this study. However, compliance with this requirement was based only on patients' declarations. No other verification was possible. The selected patients clinically, and on a dermoscopic examination, did not present symptoms of scalp diseases. However, a subclinical course of a disease or a predisposition to develop a disease in the future, which could have affected the appearance of the hair at the nanoscale, could not be excluded. Moreover, the first 7 cm of each hair was examined. Due to the imaging of the cortex in some samples at this distance, further sections of hair were not examined. At greater distances from the end of the root, the hair structure is increasingly altered by external influences. In addition, the hair of patients with scalp diseases is short, and the results presented here were compared to a control group in a study of patients with lichen planopilaris and frontal fibrosing alopecia.

The limitations of the technique for working with AMF comprised the difficulty in scanning damaged areas of hair. In these areas, the AFM probe tip very often broke down due to unstable hair fragments that stuck to the probe. In addition, the diameter of the hair fiber decreased with distance from the root end. This caused a difficulty in positioning the probe tip over the hair, hitting it and centering the probe on the top of the hair. Consequently, each new point on which the probe landed was tested by performing pre-scans, which prolonged the procedure.

Future improvements to this study could include performing a nanomechanical characterization and investigating tribological properties of hair fibers. Parameters such as the roughness and stiffness of the hair scales and the elasticity of the hair fiber could be studied. This study could be improved by normalizing semi-quantitative variables in a more optimal manner and by taking more pictures and measurements. This could be possible by examining more patients, examining the hair along its entire length and taking measurements at smaller intervals. If the right equipment is available, it would be very interesting to combine nanoscale imaging techniques with the study of nanomechanical properties and spectrometric measurements.

Author Contributions: Conceptualization, A.R. and K.K.-W.; methodology, K.K.-W. and A.R.; validation, K.K.-W. and A.R.; formal analysis, K.K.-W. and A.R.; investigation, K.K.-W.; resources, K.K.-W. and A.R.; data curation, A.R., D.R. and K.K.-W.; writing—original draft preparation, K.K.-W.; writing—review and editing, A.R. and D.R.; visualization, K.K.-W. and D.R.; supervision, A.R. All authors have read and agreed to the published version of the manuscript.

Funding: This research received no external funding.

Institutional Review Board Statement: Ethical review and approval were waived for this study due to the fact that all devices used within it are currently commercially available, and as atomic force microscopy is a non-invasive device.

Informed Consent Statement: Informed consent was obtained from all subjects involved in this study.

Data Availability Statement: Data are available from the corresponding author upon reasonable request.

Conflicts of Interest: The authors declare no conflicts of interest.

References

1. McMullen, R.L.; Zhang, G. Investigation of the Internal Structure of Human Hair with Atomic Force Microscopy. *J. Cosmet. Sci.* **2020**, *71*, 117–131.
2. Chen, N.; Bhushan, B. Morphological, nanomechanical and cellular structural characterization of human hair and conditioner distribution using torsional resonance mode with an atomic force microscope. *J. Microsc.* **2005**, *220 Pt 2*, 96–112. [\[CrossRef\]](#) [\[PubMed\]](#)
3. Swift, J.A.; Smith, J.R. Atomic force microscopy of human hair. *Scanning* **2000**, *22*, 310–318. [\[CrossRef\]](#) [\[PubMed\]](#)
4. You, H.; Yu, L. Atomic force microscopy as a tool for study of human hair. *Scanning* **1997**, *19*, 431–437. [\[CrossRef\]](#) [\[PubMed\]](#)
5. Smith, J.R. A quantitative method for analysing AFM images of the outer surfaces of human hair. *J. Microsc.* **1998**, *191 Pt 3*, 223–228. [\[CrossRef\]](#)
6. La Torre, C.; Bhushan, B. Nanotribological effects of silicone type, silicone deposition level, and surfactant type on human hair using atomic force microscopy. *J. Cosmet. Sci.* **2006**, *57*, 37–56.
7. Chen, N.; Bhushan, B. Atomic force microscopy studies of conditioner thickness distribution and binding interactions on the hair surface. *J. Microsc.* **2006**, *221 Pt 3*, 203–215. [\[CrossRef\]](#)
8. La Torre, C.; Bhushan, B. Investigation of scale effects and directionality dependence on friction and adhesion of human hair using AFM and macroscale friction test apparatus. *Ultramicroscopy* **2006**, *106*, 720–734. [\[CrossRef\]](#)
9. Lodge, R.A.; Bhushan, B. Effect of physical wear and triboelectric interaction on surface charge as measured by Kelvin probe microscopy. *J. Colloid Interface Sci.* **2007**, *310*, 321–330. [\[CrossRef\]](#)
10. Binnig, G.; Quate, C.E.; Gerber, C. Atomic force microscope. *Phys. Rev. Lett.* **1986**, *56*, 930–933. [\[CrossRef\]](#)
11. Dorobantu, L.S.; Goss, G.G.; Burrell, R.E. Atomic force microscopy: A nanoscopic view of microbial cell surfaces. *Micron* **2012**, *43*, 1312–1322. [\[CrossRef\]](#)
12. Weisenhorn, A.; Hansma, P.; Albrecht, T.; Quate, C. Forces in atomic force microscopy in air and water. *Appl. Phys. Lett.* **1989**, *54*, 2651–2653. [\[CrossRef\]](#)
13. Amenabar, I.; Poly, S.; Goikotxea, M.; Nuansing, W.; Lasch, P.; Hillenbrand, R. Hyperspectral infrared nanoimaging of organic samples based on Fourier transform infrared nanospectroscopy. *Nat. Commun.* **2017**, *8*, 14402. [\[CrossRef\]](#)
14. Allison, D.P.; Mortensen, N.P.; Sullivan, C.J.; Doktycz, M.J. Atomic force microscopy of biological samples. *Wiley Interdiscip. Rev. Nanomed. Nanobiotechnol.* **2010**, *2*, 618–634. [\[CrossRef\]](#) [\[PubMed\]](#)
15. Xia, F.; Youcef-Toumi, K. Review: Advanced Atomic Force Microscopy Modes for Biomedical Research. *Biosensors* **2022**, *12*, 1116. [\[CrossRef\]](#) [\[PubMed\]](#)
16. Wang, Y.; Wang, J. Friction Determination by Atomic Force Microscopy in Field of Biochemical Science. *Micromachines* **2018**, *9*, 313. [\[CrossRef\]](#) [\[PubMed\]](#)
17. Muller, D.J.; Engel, A. Atomic force microscopy and spectroscopy of native membrane proteins. *Nat. Protoc.* **2007**, *2*, 2191–2197. [\[CrossRef\]](#) [\[PubMed\]](#)
18. Miyata, K.; Tracey, J.; Miyazawa, K.; Haapasilta, V.; Spijker, P.; Kawagoe, Y.; Foster, A.S.; Tsukamoto, K.; Fukuma, T. Dissolution Processes at Step Edges of Calcite in Water Investigated by High-Speed Frequency Modulation Atomic Force Microscopy and Simulation. *Nano Lett.* **2017**, *17*, 4083–4089. [\[CrossRef\]](#) [\[PubMed\]](#)
19. Ando, T.; Uchihashi, T.; Scheuring, S. Filming Biomolecular Processes by High-Speed Atomic Force Microscopy. *Chem. Rev.* **2014**, *114*, 3120–3188. [\[CrossRef\]](#) [\[PubMed\]](#)
20. Stylianou, A.; Kontomaris, S.V.; Grant, C.; Alexandratou, E. Atomic Force Microscopy on Biological Materials Related to Pathological Conditions. *Scanning* **2019**, *2019*, 8452851. [\[CrossRef\]](#)
21. Rosa-Zeiser, A.; Weilandt, E.; Hild, S.; Marti, O. The simultaneous measurement of elastic, electrostatic and adhesive properties by scanning force microscopy: Pulsed-force mode operation. *Mas. Sci. Technol.* **1997**, *8*, 1333. [\[CrossRef\]](#)
22. Fritz, M.; Radmacher, M.; Gaub, H.E. Granula motion and membrane spreading during activation of human platelets imaged by atomic-force microscopy. *Biophys. J.* **1994**, *66*, 1328–1334. [\[CrossRef\]](#)
23. Radmacher, M.; Fritz, M.; Hansma, P.K. Imaging soft samples with the atomic-force microscope—Gelatin in water and propanol. *Biophys. J.* **1995**, *69*, 264–270. [\[CrossRef\]](#)
24. Hassan, E.; Heinz, W.F.; Antonik, M.D.; D’Costa, N.P.; Nageswaran, S.; Schoenenberger, C.A.; Hoh, J.H. Relative microelastic mapping of living cells by atomic force microscopy. *Biophys. J.* **1998**, *74*, 1564–1578. [\[CrossRef\]](#)
25. Radmacher, M.; Cleveland, J.P.; Fritz, M.; Hansma, H.G.; Hansma, P.K. Mapping interaction forces with the atomic force microscope. *Biophys. J.* **1994**, *66*, 2159–2165. [\[CrossRef\]](#) [\[PubMed\]](#)
26. Raman, A.; Trigueros, S.; Cartagena, A.; Stevenson, A.P.Z.; Susilo, M.; Nauman, E.; Contera, S.A. Mapping nanomechanical properties of live cells using multi-harmonic atomic force microscopy. *Nat. Nanotechnol.* **2011**, *6*, 809–814. [\[CrossRef\]](#) [\[PubMed\]](#)
27. Maver, U.; Velnar, T.; Gaberšček, M.; Planinšek, O.; Finšgar, M. Recent progressive use of atomic force microscopy in biomedical applications. *TrAC Trends Anal. Chem.* **2016**, *80*, 96–111. [\[CrossRef\]](#)

28. Altman, E.I.; Baykara, M.Z.; Schwarz, U.D. Noncontact atomic force microscopy: An emerging tool for fundamental catalysis research. *Acc. Chem. Res.* **2015**, *48*, 2640–2648. [\[CrossRef\]](#) [\[PubMed\]](#)
29. Chtcheglova, L.A.; Hinterdorfer, P. Simultaneous AFM topography and recognition imaging at the plasma membrane of mammalian cells. *Semin. Cell Dev. Biol.* **2018**, *73*, 45–56. [\[CrossRef\]](#) [\[PubMed\]](#)
30. Benoit, M.; Gabriel, D.; Gerisch, G.; Gaub, H.E. Discrete interactions in cell adhesion measured by single-molecule force spectroscopy. *Nat. Cell Biol.* **2000**, *2*, 313–317. [\[CrossRef\]](#) [\[PubMed\]](#)
31. Almqvist, N.; Bhatia, R.; Primbs, G.; Desai, N.; Banerjee, S.; Lal, R. Elasticity and adhesion force mapping reveals real-time clustering of growth factor receptors and associated changes in local cellular rheological properties. *Biophys. J.* **2004**, *86*, 1753–1762. [\[CrossRef\]](#)
32. Schindler, H.; Badt, D.; Hinterdorfer, P.; Kienberger, E.; Raab, A.; Wielert-Badt, S.; Pastushenko, V.P. Optimal sensitivity for molecular recognition MAC-mode AFM. *Ultramicroscopy* **2000**, *82*, 227–235. [\[CrossRef\]](#) [\[PubMed\]](#)
33. Sokolov, I.; Dokukin, M.E. Imaging of Soft and Biological Samples Using AFM Ringing Mode. *Methods Mol. Biol.* **2018**, *1814*, 469–482. [\[CrossRef\]](#) [\[PubMed\]](#)
34. Trohalaki, S. Multifrequency force microscopy improves sensitivity and resolution over conventional AFM. *MRS Bull.* **2012**, *37*, 545–546. [\[CrossRef\]](#)
35. Braunsma, C.; Seifert, J.; Rheinlaender, J.; Schäfer, T.E. High-speed force mapping on living cells with a small cantilever atomic force microscope. *Rev. Sci. Instrum.* **2014**, *85*, 073703. [\[CrossRef\]](#) [\[PubMed\]](#)
36. Morris, V.J.; Kirby, A.R.; Gunning, A.P. *Atomic Force Microscopy for Biologists*; Imperial College Press: London, UK, 2008.
37. Burnham, N.A.; Behrend, O.P.; Oulevey, F.; Germaud, G.; Gallo, P.-J.; Gourdon, D.; Dupas, E.; Kulik, A.J.; Pollok, H.M.; Briggs, G.A.D. How does a tip tap? *Nanotechnology* **1997**, *8*, 67–75. [\[CrossRef\]](#)
38. Krisenko, M.O.; Cartagena, A.; Raman, A.; Geahlen, R.L. Nanomechanical property maps of breast cancer cells as determined by multi-harmonic atomic force microscopy reveal SYK-dependent changes in microtubule stability mediated by map1b. *Biochemistry* **2015**, *54*, 60–68. [\[CrossRef\]](#) [\[PubMed\]](#)
39. Harcombe, D.M.; Ruppert, M.G.; Ragazzon, M.R.P.; Fleming, A.J. Higher-harmonic AFM imaging with a high-bandwidth multifrequency Lyapunov filter. In Proceedings of the IEEE International Conference on Advanced Intelligent Mechatronics (AIM), Munich, Germany, 3–7 July 2017; pp. 725–730.
40. Benaglia, S.; Gisbert, V.G.; Perrino, A.P.; Amo, C.A.; Garcia, R. Fast and high-resolution mapping of elastic properties of biomolecules and polymers with bimodal AFM. *Nat. Protoc.* **2018**, *13*, 2890–2907. [\[CrossRef\]](#) [\[PubMed\]](#)
41. Garcia, R.; Proksch, R. Nanomechanical mapping of soft matter by bimodal force microscopy. *Eur. Polym. J.* **2013**, *49*, 1897–1906. [\[CrossRef\]](#)
42. Soares, S.D.; An, S.; Long, C.J. Multi-frequency tapping-mode atomic force microscopy beyond three eigenmodes in ambient air. *Beilstein J. Nanotechnol.* **2014**, *5*, 1637–1648. [\[CrossRef\]](#)
43. Dufrene, Y.F.; Ando, T.; Garcia, R.; Alsteens, D.; Martinez-Martin, D.; Engel, A.; Gerber, C.; Müller, D.J. Imaging modes of atomic force microscopy for application in molecular and cell biology. *Nat. Nanotechnol.* **2017**, *12*, 295–307. [\[CrossRef\]](#) [\[PubMed\]](#)
44. Wolfram, L.J. Topography of some cuticle cells. *Text. Res. J.* **1972**, *42*, 252–254. [\[CrossRef\]](#)
45. Shin, M.K.; Kim, K.S.; Ahn, J.J.; Kim, N.I.; Park, H.K.; Haw, C.R. Investigation of the hair of patients with scalp psoriasis using atomic force microscopy. *Clin. Exp. Dermatol.* **2012**, *37*, 156–163. [\[CrossRef\]](#) [\[PubMed\]](#)
46. Clifford, C.A.; Sano, N.; Doyle, P.; Seah, M.P. Nanomechanical measurements of hair as an example of micro-fibre analysis using atomic force microscopy nanoindentation. *Ultramicroscopy* **2012**, *114*, 38–45. [\[CrossRef\]](#)
47. Seshadri, I.P.; Bhushan, B. Effect of ethnicity and treatments on in situ tensile response and morphological changes of human hair characterized by atomic force microscopy. *Acta Mater.* **2008**, *56*, 3585–3597. [\[CrossRef\]](#)
48. Seshadri, I.P.; Bhushan, B. In situ tensile deformation characterization of human hair with atomic force microscopy. *Acta Mater.* **2008**, *56*, 774–781. [\[CrossRef\]](#)
49. Lu, H.; Wen, Y.; Zhang, H.; Xie, H.; Shen, Y. 360° multiparametric imaging atomic force microscopy: A method for three-dimensional nanomechanical mapping. *Ultramicroscopy* **2019**, *196*, 83–87. [\[CrossRef\]](#)
50. Fellows, A.P.; Casford, M.T.L.; Davies, P.B. Nanoscale Molecular Characterization of Hair Cuticle Cells Using Integrated Atomic Force Microscopy-Infrared Laser Spectroscopy. *Appl. Spectrosc.* **2020**, *74*, 1540–1550. [\[CrossRef\]](#)
51. Fellows, A.P.; Casford, M.T.L.; Davies, P.B. Using hybrid atomic force microscopy and infrared spectroscopy (AFM-IR) to identify chemical components of the hair medulla on the nanoscale. *J. Microsc.* **2021**, *284*, 189–202. [\[CrossRef\]](#) [\[PubMed\]](#)
52. Fellows, A.P.; Casford, M.T.L.; Davies, P.B. Chemically characterizing the cortical cell nano-structure of human hair using atomic force microscopy integrated with infrared spectroscopy (AFM-IR). *Int. J. Cosmet. Sci.* **2022**, *44*, 42–55. [\[CrossRef\]](#) [\[PubMed\]](#)
53. Marcott, C.; Lo, M.; Kjoller, K.; Fiat, F.; Baghdadi, N.; Balooch, G.; Luengo, G.S. Localization of Human Hair Structural Lipids Using Nanoscale Infrared Spectroscopy and Imaging. *Appl. Spectrosc.* **2014**, *68*, 564–569. [\[CrossRef\]](#) [\[PubMed\]](#)

Disclaimer/Publisher's Note: The statements, opinions and data contained in all publications are solely those of the individual author(s) and contributor(s) and not of MDPI and/or the editor(s). MDPI and/or the editor(s) disclaim responsibility for any injury to people or property resulting from any ideas, methods, instructions or products referred to in the content.

Evaluation of hair surface structure and morphology of patients with lichen planopilaris (LPP) by atomic force microscopy (AFM)

Karolina Krawczyk-Wołoszyn^{1,2} | Magdalena Żychowska² | Adam Reich² 

¹Doctoral School, University of Rzeszów, Rzeszów, Poland

²Department of Dermatology, Institute of Medical Sciences, Medical College of Rzeszów University, Rzeszów, Poland

Correspondence

Adam Reich, Department of Dermatology, Institute of Medical Sciences, Medical College of Rzeszów University, 35-959 Rzeszów, Poland.

Email: adamandrzejreich@gmail.com

Abstract

Background: Lichen planopilaris (LPP) is a chronic lymphocytic skin disease manifested by progressive scarring alopecia. The diagnosis of LPP is made based on histopathological examination, although it is not always definite. The current study evaluates the effectiveness of non-invasive atomic force microscopy (AFM) hair examination in detecting morphological differences between healthy and diseased hair.

Materials and methods: Here, three to five hairs from lesional skin of 10 LPP patients were collected and examined at nine locations using AFM. At least four images were taken at each of the nine sites. Metric measurements were taken and metric (length, width, and scale step height) and morphological features (striated and smooth surface of scales, the presence of endocuticle and cortex, shape of scales edges, scratches, pitting, cracks, globules, and wavy edge) were compared with hair from healthy controls. In addition, areas on diseased hair where the process of pathological, unnatural delamination of the hair fiber occurs are described.

Results: There was a statistically significant difference in the number of scratches in the initial sections of the LPP hair, in the intensity of wavy edges along the entire length of the tested hair, and in the number of scales with pitting in the middle section of the hair. In addition, a statistically significant higher number of scales with striated surface was found in LPP group starting at 3.5 cm from the root continuing towards the free end of the hair. Other morphological changes such as presence of cortex, globules, oval indentations, and rod-like macrofibrillar elements were also assessed, however, detailed results are not presented, as the differences shown in the number of these morphological changes were not significantly different.

Conclusion: This publication outlines the differences between virgin, healthy Caucasian hair, and the hair of LPP patients. The results of this study can be used for further research and work related to LPP. This is the first attempt to characterize the hair of LPP patients using AFM.

This is an open access article under the terms of the [Creative Commons Attribution License](https://creativecommons.org/licenses/by/4.0/), which permits use, distribution and reproduction in any medium, provided the original work is properly cited.

© 2024 The Author(s). *Skin Research and Technology* published by John Wiley & Sons Ltd.

Skin Res Technol. 2024;30:e70030.
<https://doi.org/10.1111/srt.70030>

[wileyonlinelibrary.com/journal/srt](https://onlinelibrary.wiley.com/journal/srt) | 1 of 13

KEYWORDS

AFM, atomic force microscope, atomic force microscopy, dermatology, FFA, frontal fibrosing alopecia, human hair, lichen planopilaris, LPP, trichoscopy

1 | INTRODUCTION

Lichen planopilaris (LPP) is a primary lymphocytic skin disease with a multifactorial, incompletely understood pathogenesis. An autoimmune basis has been postulated. An inflammatory infiltrate of the scalp skin leads to damage of the hair follicle structures leading to atrophy and fibrosis. A band-like subepidermal perifollicular lymphocytic infiltrate located in the follicular isthmus and infundibulum is seen in histopathology, although the histopathology is not always diagnostic. The disease is manifested by progressive patches of scarring alopecia. Clinically, there is an active inflammation at their periphery, which presents as perifollicular erythema and scaling. An additional symptom includes hyperkeratosis of the hair follicle, which causes exfoliation, creating a kind of 'collar' on the proximal part of the hair. Currently, the diagnosis of LPP is made based on histopathological examination from an invasive scalp biopsy and, supportively, on widely available and practical dermoscopy, although these examinations do not necessarily have to be conclusive.^{1,2} Currently, the use of novel non-invasive procedures such as optical coherence tomography (OCT) and reflectance confocal microscopy are being studied as an aid in the diagnosis.^{3,4} In recent years, research has also begun on healthy human hair using atomic force microscopy (AFM).^{5–7} The employment of the AFM technique for nanoscale hair examination may contribute to improved diagnosis and treatment of scalp diseases.⁸ To date, a limited studies have been conducted on AFM imaging of hair diseases, limited to psoriasis, alopecia areata, and seborrheic dermatitis.^{9–11} The current study evaluates the potential usefulness of AFM hair examination in detecting morphological differences between healthy and LPP hairs. It has been hypothesized that due to the lymphocytic folliculitis and hyperkeratinization of the follicle's orifices, the hair morphology might differ from normal hair.

2 | MATERIAL AND METHODS

The study used the method established in the authors' previous study on healthy, virgin Caucasian hair.¹²

2.1 | Subjects

From a group of forty patients with a histopathologically confirmed diagnosis of LPP, 10 patients with the highest disease severity were selected (Table 1). The disease severity was assessed by physical examination, dermoscopy, and subjective symptoms. Then, three to five hairs, from the periphery of active lesions, were collected from each subject. The control group consisted of 10 healthy Caucasian subjects who had not dyed their hair for at least 3 months prior to the

study (Table 1). In this case, three to five hairs were taken from the same skull areas as in LPP patients.

2.2 | Hair preparation

The clean hairs were pulled out along with their roots and subsequently cut vertically with a scalpel into 3 cm long sections. They were then attached to a microscope slide using a translucent tape.

2.3 | Atomic force microscopy (AFM)

AFM was performed using a DriveAFM microscope with CX controller (Nanosurf, Liestal, Switzerland) under atmospheric conditions (in air)

TABLE 1 Comparison of patients suffering from lichen planopilaris and healthy controls.

Characteristics	Study group	Control group	p
Sex, n (%)			
Women	9 (90.0)	9 (90.0)	N/A
Men	1 (10.0)	1 (10.0)	
Age (years), mean \pm standard deviation (SD)	56.1 \pm 10.0	43.8 \pm 15.5	0.11
Range (years)	39–71	26–72	
Race, n (%)			
Caucasian	10 (100.0)	10 (100.0)	N/A
Age of diagnosis (years), mean \pm SD	51.4 \pm 14.7	–	N/A
Range (years)	15–66		
Disease duration (months), mean \pm SD	56.0 \pm 103.1	–	N/A
Range, months	4–360		
Clinical subtype of LPP, n (%)			
Classic LPP	5 (50.0)	–	N/A
Classic FFA	3 (30.0)		
Coexistence of LPP and FFA	2 (20.0)		
Locations outside the scalp, n (%)			
Involvement of the mucous membranes	0 (0.0)	–	N/A
Involvement of the nails	1 (10.0)		
Involvement of the face and armpits	1 (10.0)		

Abbreviation: N/A, not applicable.

at room temperature and stable humidity (65%–70%). Imaging was performed in contact mode using PPP-FMAuD-10 tips (NANOSEN-SORS, Neuchatel, Switzerland) mounted on cantilevers with a constant force of 1.9 N/m and frequency of 75 kHz. Each hair was imaged at 0.5, 1.0, 1.5, 2.0, 3.5, 4.5, 5.5, 6.5, and 7.0 cm from the root. The scanning range covered an area from 40×40 μm to 3×3 μm. The scanning velocity was 0.5 s/line. The resolution of the images was 512–1024 points/line.

The images were computer-processed using Nanosurf CX ver 3.10.3.7. The AFM tip was centered to be on top of the hair fiber upon contact with the cuticle surface. The AFM tip scanned the hair perpendicular to the longitudinal axis of the fiber to reduce errors due to the AFM tip hitting the sides of the hair. For each of nine locations (0.5, 1.0, 1.5, 2.0, 3.5, 4.5, 5.5, 6.5, and 7.0 cm from the root), at least four images were taken. Line profile creation, 3D visualizations, image processing, and all metric measurements (length, width, and scale step height) were performed using Gwyddion (64 bit) software ver 2.63. Line profiles were created by averaging data from 10 adjacent scan lines.

Assessment of morphological lesions on the surface of scales was performed manually on images of the same size to compare features between patients. The number of scales with striated surface and the scratches on the surface of scales were counted. Then, the above parameters were grouped on a scale from 0 to 5 as shown in Table 2. Parameters such as endocuticle, broken edges of scales shape of edges of scales, wavy edges of scales, the number of scales with smooth surface, presence of cortex, pitting, globules, oval indentations, and rod-like macrofibrillar elements were evaluated in a descriptive manner by grouping a given characteristic in a range, as shown in Table 2.

2.4 | Statistical analysis

Statistical analysis was performed using Statistica software v.13.0 (TIBCO Software Inc., Kraków, Poland). Mean, minimal, and maximal values along with the standard deviations were calculated for longitudinal parameters. Student *t* test, Mann-Whitney *U* test, or Chi² test was used as appropriate. *p* values less than 0.05 were considered significant.

3 | RESULTS

3.1 | Dimensions and size of the hair scales

In the study group, the scale step height increased with distance from the root. The values of the apparent scale length and the scale width also increased. The tendency for these dimensions to increase was more noticeable in the study group than in the control group. However, the differences between the scale dimensions of the study group and the control group were not statistically significant. The measurements obtained are shown in Table 3.

TABLE 2 Quantitative and descriptive representation of crucial features in the LPP patient group.

Feature	Absolute number-range or qualitative description of the feature	Corresponding grade
The number of scales with striated surface	0	0
	1–3	1
	4–7	2
	8–11	3
	12–15	4
	>15	5
Scratches	0	0
	1–9	1
	10–19	2
	20–29	3
	30–39	4
	>40	5
Endocuticle	Absent	0
	Single nodules 2–4 nm in diameter, located at the base of the scales' edges.	1
	Single nodules spread over the entire scale surface.	2
	Granular plaques 3–5 nm wide localized at the base of the scales' edges.	3
	Granular plaques 4–7 nm wide located across the width of the scales, at the base of the scale edges.	4
	Granular structure occupying more than 50% of the cuticle surface.	5
Broken edges	Edge undamaged, smooth.	0
	Edge smooth with single small cracks.	1
	Numerous small cracks, smooth edge visible for less than 40%.	2
	Lack of smooth edge, numerous larger cracks, and scale breakages.	3
	Deep breakouts, edge like chain saw's teeth.	4
	Very uneven, deep, different shaped breakouts.	5
Shape of edges	Convex	1
	Streight	2
	Concave	3
Wavy edges	Edge undamaged, smooth.	0
	Gentle undulation, U-shaped wave ridges.	1
	Deeper and more marked undulations.	2
	Increased undulations and breaks between individual wave crests.	3

TABLE 3 Metric measurements of healthy and diseased hair scales.

Distance from the root	Scale step height (μm)			Apparent scale length (μm)			Scale width (μm)		
	LPP	Controls	<i>p</i>	LPP	Controls	<i>p</i>	LPP	Controls	<i>p</i>
0.5 cm	0.5 \pm 0.18	0.51 \pm 0.1	0.83	7.1 \pm 1.9	7.9 \pm 1.1	0.26	19.3 \pm 6.8	17.2 \pm 3.6	0.4
1.0 cm	0.5 \pm 0.16	0.51 \pm 0.12	0.88	7.0 \pm 2.0	6.8 \pm 1.4	0.87	19.5 \pm 5.6	16.6 \pm 2.2	0.16
1.5 cm	0.51 \pm 0.16	0.48 \pm 0.11	0.64	7.0 \pm 1.8	7.6 \pm 1.4	0.45	19.6 \pm 4.8	17.2 \pm 2.6	0.18
2.0 cm	0.5 \pm 0.17	0.49 \pm 0.08	0.88	6.5 \pm 1.2	7.7 \pm 1.1	0.03	22.3 \pm 5.1	20.6 \pm 3.7	0.42
3.5 cm	0.61 \pm 0.14	0.52 \pm 0.05	0.11	6.7 \pm 0.8	6.7 \pm 1.0	0.96	21.8 \pm 5.6	19.2 \pm 2.9	0.21
4.5 cm	0.59 \pm 0.16	0.53 \pm 0.17	0.44	7.5 \pm 1.4	7.9 \pm 1.9	0.65	22.2 \pm 5.3	19.2 \pm 4.0	0.18
5.5 cm	0.67 \pm 0.2	0.53 \pm 0.09	0.06	7.7 \pm 1.8	7.5 \pm 1.3	0.79	21.9 \pm 5.2	18.7 \pm 3.2	0.12
6.5 cm	0.61 \pm 0.14	0.53 \pm 0.11	0.16	7.7 \pm 1.8	7.3 \pm 1.3	0.58	21.2 \pm 6.1	20.2 \pm 4.4	0.68
7.0 cm	0.63 \pm 1.62	0.5 \pm 0.13	0.07	7.8 \pm 2.1	7.6 \pm 1.6	0.83	21.2 \pm 5.7	19.7 \pm 4.3	0.52

Results demonstrated as means and standard deviations.

Abbreviation: LPP, Lichen planopilaris.

3.2 | Comparison of morphological features between the study and control groups

Features mentioned in Table 2 were analyzed, as already done in our previous publication on the evaluation of virgin Caucasian hair.¹² Figure 1 shows the distribution of the most notable features in the hair surface morphology of LPP patients. The scoring of the features is characterized in Table 2.

There was a statistically significant difference in the number of scratches in the initial sections of the LPP hair (1–5.5 cm) (Figure 2A), in the intensity of wavy edges along the entire length of the tested hair (0.5–7 cm), and in the number of scales with pitting in the middle section of the hair (3.5–6.5 cm) (Figure 2B). In addition, a statistically significant higher number of scales with striated surface was found in LPP group starting at 3.5 cm from the root continuing toward the free end of the hair (Figure 3). Other morphological changes such as presence of cortex, globules, oval indentations, and rod-like macrofibrillar elements were also assessed; however, detailed results are not presented, as the differences shown in the number of these morphological changes were not statistically different.

Scratches were the most prominent feature on the hair of LPP patients. They took various forms and shapes—triangles, lines, and commas. The scratches were usually arranged parallel to the long axis of the hair fiber (Figure 4A–C). Another important feature visualized on the surface of LPP patients' hair was small, circular excavations, so called pits (Figure 5A–D). In our study, pitting occurred along the entire length of LPP hair, but was most commonly located 1.5–4.5 cm from the root end. Single pits were also observed in healthy hair; however, pitting on LPP hair was characterized by a high density of larger and smaller holes. Their clusters were located on specific scales: in some hairs, pitting was also observed in the area where two scales joined (at the base of another scale) or in a characteristic linear arrangement. In contrast, pits on healthy hair were dispersed in nature, far fewer, and all were in comparable size.

Globules were observed in larger numbers in the areas of sudden hair fiber destruction in LPP patients. Three distinct types of globules

were visualized: (1) globules with flat elevation and dimensions of hundreds of nanometers; (2) smaller globules (sand-like) with dimensions of tens of nanometers; and (3) large conglomerates with dimensions of thousands of nanometers. Sand-like globules were more frequently observed in the LPP group, while the typical flat-elevation globules were often found in the control group (Figure 5E,F).

3.3 | Morphological changes unique to the hair of LPP patients

3.3.1 | AFM visualization of areas of narrowing and cavities identified by light microscopy

Using AFM, we found areas of sudden architectural disruption and greater fraying of the edges of the scales compared to further sections of the hair (where the edges of the cells should become increasingly serrated with distance from the root). These areas on lower magnification light microscopy included the narrowing area of the hair fiber and the oval cavities (Figure S1). The oval structures imaged by light microscopy varied in magnitude. We imaged cavities having sizes of 60–100 μm in the long axis and 10 μm in the short axis, as well as with smaller sizes of 10 \times 10 μm . With AFM, in areas of LPP hair fiber narrowing and around oval cavities, we detected the acceleration of the delamination process confirmed by ghost signs, increased exfoliation of the cuticle surface, and exposure of the endocuticle. Ghost signs were observed in larger amount in LPP hair compared to healthy hair. The exfoliation was so intense that areas of globules formation were visible, despite prior processing of the preparations. Structural changes in the immediate area of the oval cavities were even more evident. At AFM microscope magnifications, no ghost sign was detected anymore, but only the completely exfoliated top layers of the cuticle and the exposure of the layer beneath the endocuticle (the hair inner layer). The endocuticle itself was visible as a very thin fragment right at the edge of the next scale. Interestingly, the area included either intact scales with smooth contours and superficial striations or much lower

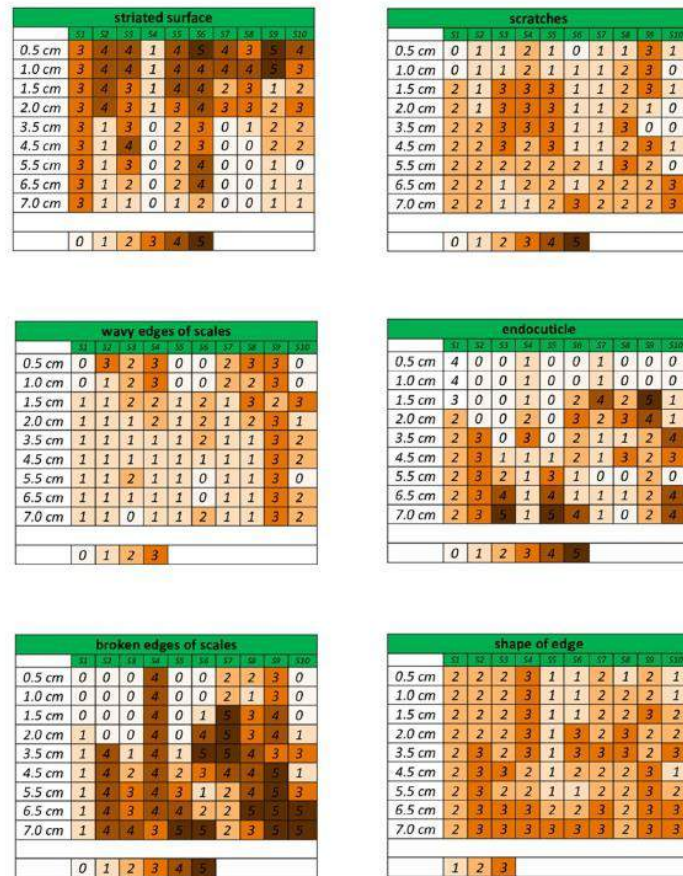


FIGURE 1 Distribution of crucial features of hairs obtained from patients with lichen planopilaris (scoring of parameters described in Table 2).

areas of the exposed inner layer covered with irregularities (globules) (Figure 6).

3.3.2 | Fragments of perifollicular scaling on the surface of the hair

At 0.5 and 1 cm from the root end, undulating soft structures lying on the surface of the hair fiber were visualized. These structures resembled the epithelial cells that were visualized in other studies.¹³ This was also confirmed by the fact that AFM images were taken at the site of the visible collar in the light microscope. At further distances (approximately 3.5 cm), similar structures were observed lying on the surface of the scales, which differed in their perforated texture (Figure 7C).

These are fragments of collar epithelial cells that were systematically destroyed as the hair grew. The 3D model showed that these structures protruded above the surface of the hair scale, rather than being embedded in it. This analysis argues more in favor of the fact that the described hair features were remnants of scalp epithelial cells.

3.3.3 | Linear indentations and longitudinal cracks

In the study group, single linear indentations arranged in an ellipse shape and in various other unexpected shapes were noted (Figure 7A,B). The lesions described above were less frequently seen on the striated surface and more frequently on the deeper and softer layers of the cuticle.

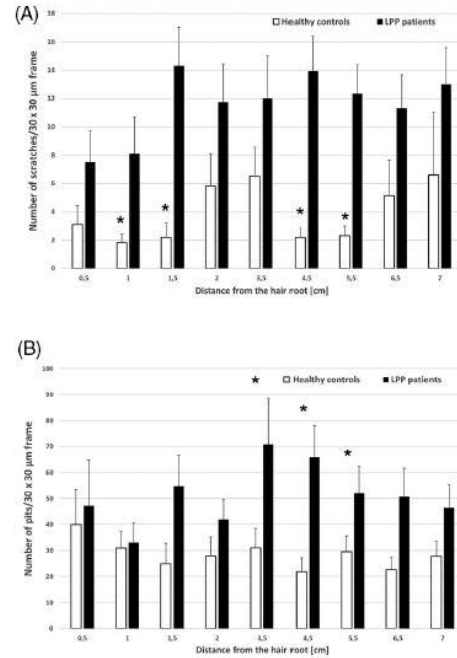


FIGURE 2 Comparison of lichen planopilaris hairs and healthy hairs regarding the (A) number of scratches, (B) number of pits within the hair scales (results demonstrate as means and standard errors, * $p < 0.05$).

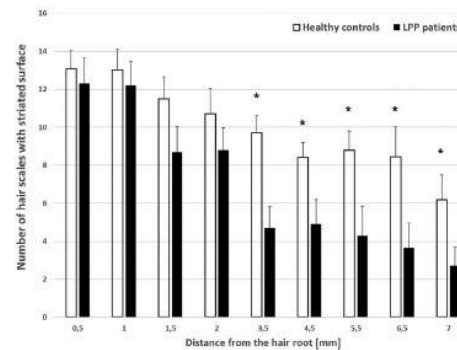


FIGURE 3 Comparison of lichen planopilaris hairs and healthy hairs regarding the number of scales with striated surface (results demonstrate as means and standard errors, * $p < 0.05$).

Cracks were not previously revealed in healthy hair. In diseased hair, it runs parallel to the long axis of the hair fiber. They started from the free end of the scale and fractured inwards. Moreover, cracks were frequently observed in scales with wavy edges (Figure 8A-C).

4 | DISCUSSION

LPP and FFA (frontal fibrosing alopecia) constitute major inflammatory lymphocytic subtypes of primary scarring alopecia. As they share the same etiopathogenesis but differ in the clinical presentations, these two variants are "two branches of the same tree."^{14,15} In both conditions, lymphocytic infiltrate composed mainly of CD8+ T-cells is implicated in the destruction of hair follicles. LPP and FFA also share other pathogenic mechanisms involving epidermal-mesenchymal transition and abnormal peroxisome proliferators-activated receptors (PPAR)- γ -mediated signaling.¹⁶ On the other hand, genetic differences and the influence of environmental factors may be responsible for varying clinical presentation. In classical LPP, the scalp vertex is predominantly involved, while in FFA, the involvement of the frontal and parietal regions leads to the recession of frontal hairline (Figure S2). Both LPP and FFA require early diagnosis and treatment due to largely irreversible damage of the hair follicles and development of scarring alopecia.¹⁵

In LPP, the perifollicular inflammation and subsequent fibrosis may deform the hair follicle and generate hair shaft abnormalities.^{17,18} Dermoscopy (trichoscopy) constitutes major non-invasive tool for the preliminary diagnosis of hair and scalp conditions.^{19,20} The main hair abnormality in LPP that may be visualized under dermoscopy is the presence of pili torti, also referred to as "twisted hair."¹⁷ Pili torti are defined as irregularly flattened and twisted hair shafts. They may be encountered in genetic diseases such as Netherton syndrome, as well as in acquired conditions, including LPP, discoid lupus erythematosus, folliculitis decalvans, alopecia areata, and primary cutaneous lymphomas.^{17,19,21} However, it should be realized that the role of dermoscopy in assessing the ultrastructural abnormalities of hair shafts is limited. In addition, dermoscopy does not enable the evaluation of the impact of hair shaft changes on its mechanical properties.

In our previous study, we characterized the appearance of healthy hair and defined features indicative of the natural process of hair delamination and destruction as it grows.¹² The study was performed on the control group presented in this publication (Table 1). The previous results and the created pattern of hair appearance during natural delamination provided a reference for the evaluation of diseased hair. Four different hair fiber surfaces, ghost marks, and changes in the shape of the scales and their free edges were characterized. Hair fiber surfaces such as scales with striated surface, endocuticle, scales with smooth surface, and cortex were identified. Only scales with a striated surface were present on the initial, undamaged sections of the hair. As the top layer of scales detaches (from the free end of the scale), the deeper layers of scales are exposed: endocuticle followed by the smooth surface of the next layer of scales. These lesions were most intense at 1.5–6.5 cm from the root end. The smooth surface gained

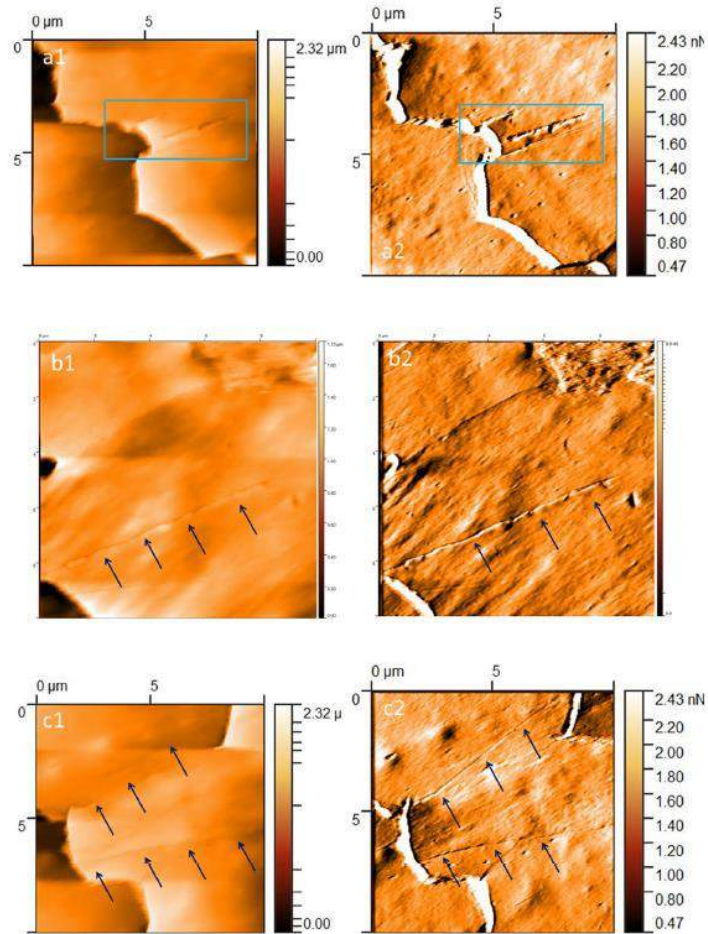


FIGURE 4 Atomic force microscopy of the hair from patient with lichen planopilaris. (a1-a2) 3.5 cm from the root end. Deep linear scratches (blue frames). Image size $10 \times 10 \mu\text{m}$; a1 Z-axis image; a2 deflection image. (b1-b2) 2 cm from the root end. Long linear scratches (black arrows). Images size $10 \times 10 \mu\text{m}$; b1 Z-axis image; b2 deflection image. (c1-c2) 2 cm from the root end. Long linear scratches (black arrows). Images size $10 \times 10 \mu\text{m}$; c1 Z-axis image; c2 deflection image.

an advantage over the striated surface at approximately 4.5 cm from the root end. The next layer—the cortex—can be examined at the end tip of the hair. This surface was visible after complete delamination of the cuticular layer with hair scales. In addition, the gradual peeling of the superficially lying scales exposes a depression on the underlying scales—a ghost sign. This symptom was a marker of the transition between the outer striated surface and the deeper smooth surface. The hair scales just at the root end had smooth and unbroken edges. Gradual detachment of the free edges of the scales caused their edges to

become increasingly frayed and broken. By breaking off the edges of the scales, the shape of the scales also changed—from convex through flat to concave.¹²

Increased signs of delamination may suggest increased hair destruction in patients with LPP. This may indicate either a weakened hair structure that forms in the histologically altered hair follicle, or it helps to emphasize the timing of the factor influencing hair destruction, which led to the development of the disease even before the onset of clinical symptoms. Wavy edges may develop during hair

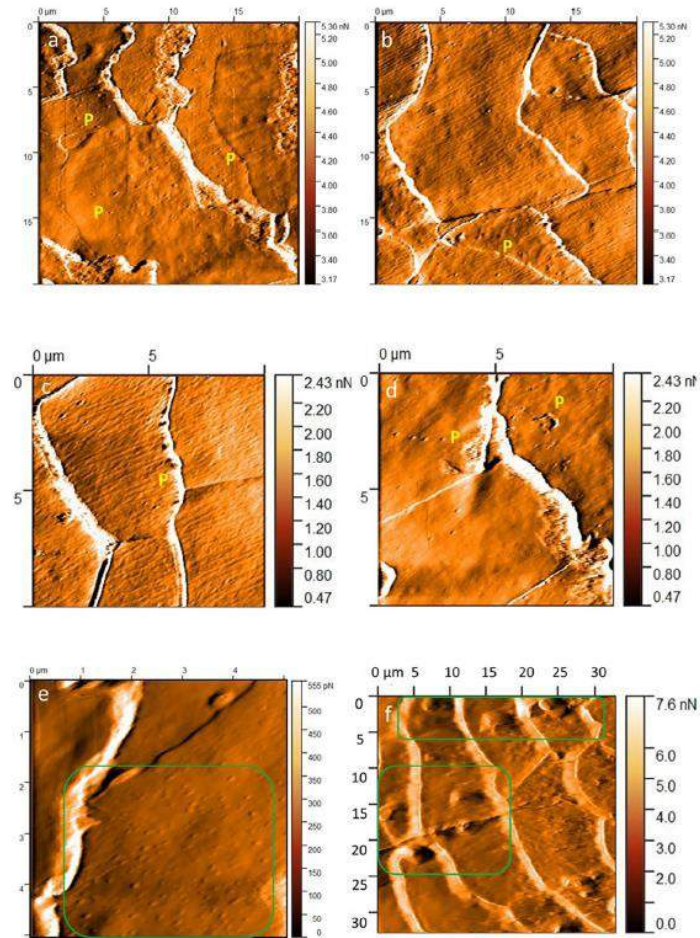


FIGURE 5 Atomic force microscopy of the hair from patient with lichen planopilaris. (A) 4.5 cm from the root end. Pitting (P). Image size $20 \times 20 \mu\text{m}$; deflection image. (B) 2.0 cm from the root end. Dispersed pitting (P). Image size $20 \times 20 \mu\text{m}$; deflection image. (C) 1.5 cm from the root end. Pitting in the junction area of two scales (P). Image size $10 \times 10 \mu\text{m}$; deflection image. (D) 4.5 cm from the root end. Pitting in linear layout (P). Image size $10 \times 10 \mu\text{m}$; deflection image. (E) 3.5 cm from the root end. Absence of striations, absence of ghosts, absence of endocuticle remnants. Small sand-like globules of 92.5–185.1 nm (green frame). Image size $5 \times 5 \mu\text{m}$; deflection image. (F) 0.5 cm from the root end. Globule conglomerates of 4290 nm size (green frames). Image size $30 \times 30 \mu\text{m}$; deflection image.

formation in the hair follicle and the passage of the hair through the inflamed infundibulum and through contact with the surface of the inner root sheath. The scratches and pitting may have been related to the hair's excessive susceptibility to mechanical trauma caused by the disease or as a symptom of high traumatization of the hair, which may happen during the disease. Another possibility is the theory that infiltration of inflammatory cells in the hair follicle, which

disrupted its architecture, might cause scratching of the scales that formed.

In 2009, hair surface changes were described in one of the most common types of alopecia—alopecia areata (AA); this was the first study comparing the morphological changes of the hair surface along its length between patients with alopecia areata and a group of healthy individuals.¹⁰ AA presents with a lymphocytic inflammatory infiltrate

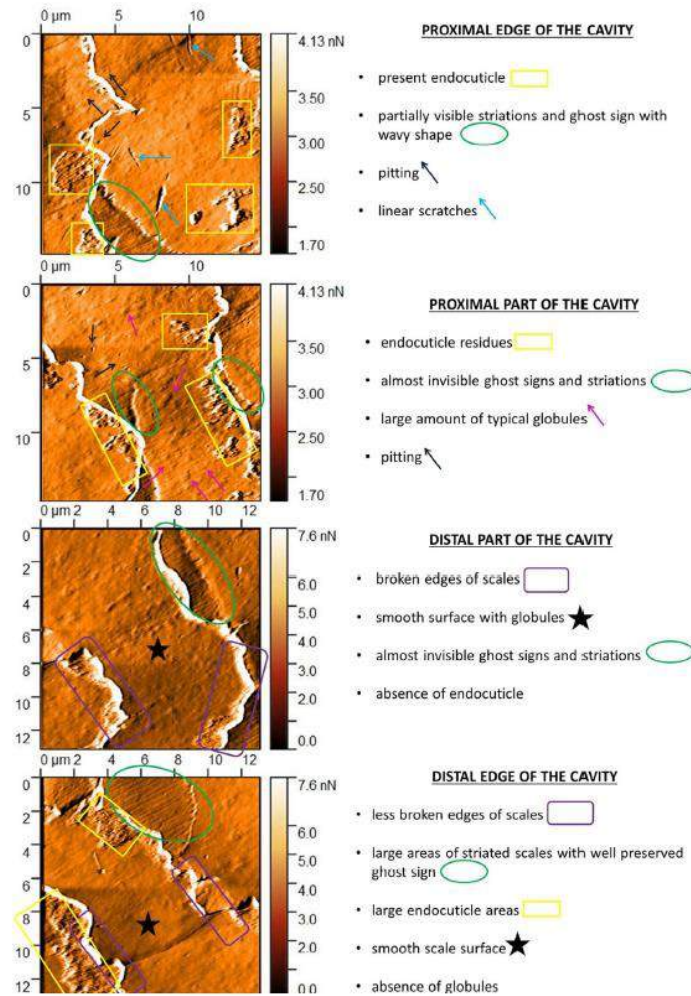


FIGURE 6 Visualization of surface changes from the area and center of the cavity. Images size from $12.0 \times 12.0 \mu\text{m}$ to $15.0 \times 15.0 \mu\text{m}$; deflection images.

in anagen hair follicles, abnormal hair shaft structure, and hair loss occurring without scarring.²² Although the disease affects approximately 2% of the general population, few publications are available on the application of the AFM technique in this disease entity. Lee et al.¹⁰ compared cuticle surface extracted parameters and morphology between a group of healthy hair and hair obtained from patients with AA ($n = 12$ each). They found that the hair surface of patients with AA was more damaged than the control group. Following morphological changes on the surface of the hair scales were described: crack of scale,

longitudinal striation, endocuticular ghost, and debris.¹⁰ These lesions were classified as hair scale damage, but to our knowledge, longitudinal striation is the normal surface of undamaged mammalian hair scales. Scale cracks and endocuticular ghost were also recognized in our study as features indicative of the process of damage to the hair surface. The "debris" described by the authors may correspond to the globules we have observed. In addition, metric measurements of hair scales were taken in the above study. Parameters such as the top distance and step height of cuticle and the curvature of cuticle edge were created and

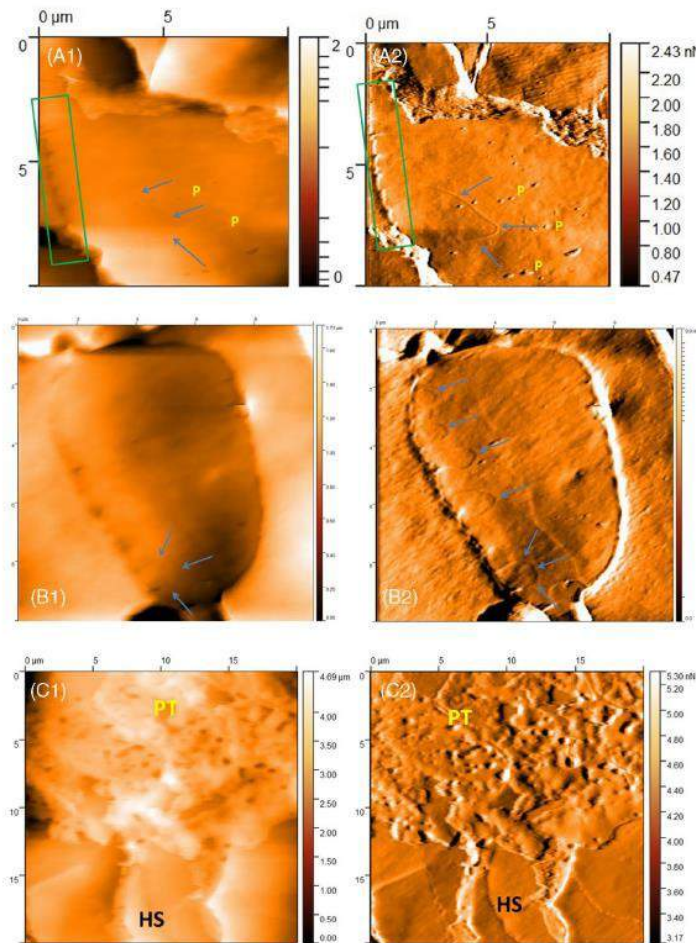


FIGURE 7 Atomic force microscopy of the hair from patient with lichen planopilaris. (a1-a2) 2.0 cm from the root end. Linear dent (blue arrows). Wavy edge (green frames). Pitting in linear layout (P). Images size $10 \times 10 \mu\text{m}$; a1 Z-axis image; a2 deflection image. (b1-b2) 2.0 cm from the root end. Ellipsoidal structures (blue arrows). Images size $10 \times 10 \mu\text{m}$; b1 Z-axis image; b2 deflection image. (c1-c2) 3.5 cm from the root end. Hair scales (HS). Perforated texture on the surface of the hair (PT) (most probably fragments of collar epithelial cells that were destroyed as the hair grew). Image size $20 \times 20 \mu\text{m}$; c1 Z-axis image; c2 deflection image.

evaluated. Compared to the control group, top distance and step height of cuticle were lower in the group with AA. Meanwhile, the curvature of cuticle edge was higher in the group with AA. In our study, we also used a parameter such as scale deviation measured as scale step heights to assess the hair of LPP patients.¹⁰ In 2013, Kim et al.¹¹ compared the morphology and mechanical properties of the scales of patients with scalp psoriasis ($n = 14$), seborrheic dermatitis ($n = 28$) with a control group ($n = 50$). Scans were performed at one location on each hair (1 cm

from the root end). Therefore, it was not possible to follow the dynamics of hair changes with distance from the root in the above study. The researchers described and assessed features such as the pits, the scale thickness, and the surface roughness. They described the pits as a depression in the hair surface. Pits were divided into micropits (diameter $< 0.5 \mu\text{m}^2$ or area $< 0.25 \mu\text{m}^2$) and macropits (diameter $> 0.5 \mu\text{m}^2$ or area $> 0.25 \mu\text{m}^2$). Pits were rarely observed in the control group and in patients with seborrheic dermatitis, while it was a common feature

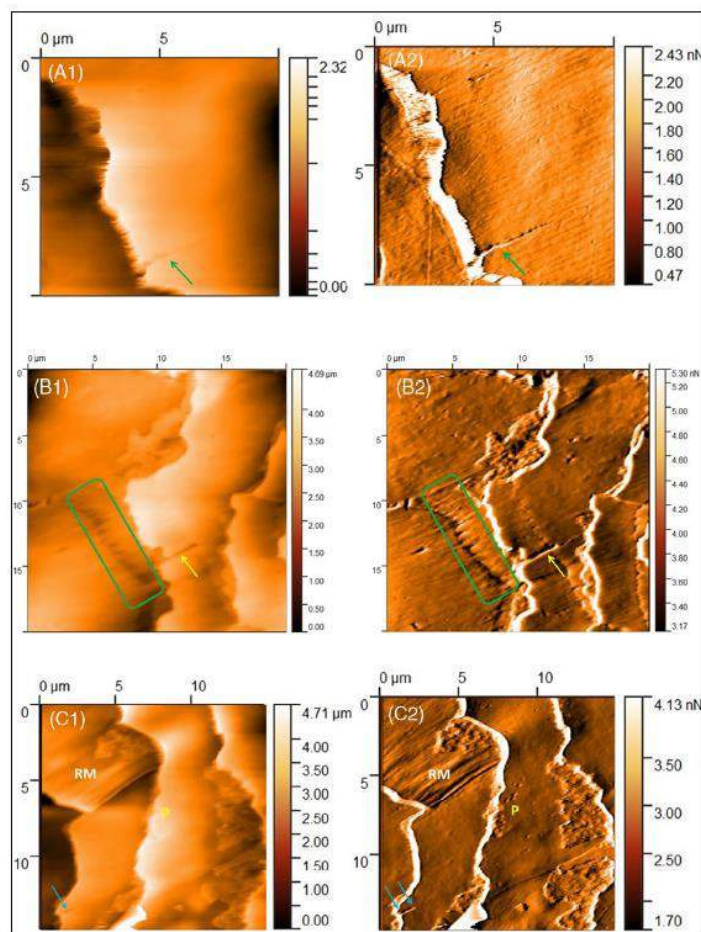


FIGURE 8 Atomic force microscopy of the hair from patient with lichen planopilaris. (a1-a2) 1.5 cm from the root end. Linear crack (green arrows). Image size $10 \times 10 \mu\text{m}$; a1 Z-axis image; a2 deflection image. (b1-b2) 2.0 cm from the root end. Wavy edge (green frames). Linear crack (yellow arrows). Image size $20 \times 20 \mu\text{m}$; b1 Z-axis image; b2 deflection image. (c1-c2) 2.0 cm from the root end. Linear crack (blue arrows). Rod-like macrofibrillar elements on the side edge of the scale (RM). Smaller and larger holes resembling corrosion pitting (P). Image size $15 \times 15 \mu\text{m}$; c1 Z-axis image; c2 deflection image.

in hair with psoriasis. Macropits were demonstrated in 100% of hair samples from psoriasis patients, whereas in the seborrheic dermatitis patients and control group, many of the cavities were micropits. In our LPP group, most of the cavities were macropits (92%). In addition, the researchers showed differences in hair scale thickness between patients with dermatological diseases and hair of healthy subjects.¹¹ A similar scale thickness was found in the psoriasis and seborrheic dermatitis patient group. It was approximately four times greater than in the control group. In contrast, the roughness of the hair surface dif-

fered significantly between the psoriasis group, where it was greatest, and the control and seborrheic dermatitis groups.¹¹ A similar study by Shin et al. in 2012²⁷ evaluated the morphology of the hair surface in patients with psoriasis vulgaris. Pitting, roughness, and thickness of hair scales were assessed. They examined hair from healthy subjects and hair from patients with psoriasis vulgaris. In addition, they compared hair from psoriasis patients extracted from active lesions on the scalp and from areas not clinically occupied by the disease process. The researchers found increased scale thickness and a greater num-

ber of macro pits in psoriasis patients compared to hair from healthy subjects. These features were observed more frequently in both from active psoriasis lesions and hair from non-lesional skin in the psoriasis patient group. Importantly, by imaging similar nanosized changes in hair growing on the non-lesional scalp, they showed that psoriasis is generalized.⁹

5 | CONCLUSION

LPP is difficult to treat, so advances in understanding the molecular mechanisms may contribute to the discovery of new treatments and the possibility of remission in the near future. This is to our knowledge the first comparison study about hair shaft surfaces over the whole lengths between LPP and healthy group using AFM. The study presented here made it possible to assess the dynamics of hair surface changes with distance from the root. This is related to hair growth and different disease onset in different patients. Examining a long section of hair reduced errors due to omission of areas where changes due to disease pathogenesis could potentially be seen.

The results presented in this study attempt to characterize morphological changes at the nanoscale, which may be helpful for early diagnosis of hair diseases in the future. The preliminary results provided give direction for further research into scalp and hair diseases. Our observations indicate that the same structures are present in healthy and diseased hair. The hair does not have a smooth, uniform surface, but a characteristic pattern. The hair of people with LPP and healthy hair have noticeable differences in their surface area. In diseased hair, regions with an increase in structures indicative of damage can be observed, which may suggest the onset of disease. In addition, we observed several structures in LPP absent in healthy hair. The etiology of the structures shown remains to be further discussed. The main limitations of this study were the focus on morphological assessment of the hair surface only and the small sample size. Mechanical properties of the hair surface were not assessed. The lack of software to automatically measure structures on the hair limits the acquisition of numerical data, since the size of the scales, as well as their deviation, is an individual feature. They vary even in a single person depending on the region of the scalp from which the hair was taken and the phase of hair growth. AFM in contact mode is limited to providing images of the top surface of a single fiber. The main limitation of the method is its duration. Image capture time was 6 min at 256 points/line, 12 min at 512 points/line, and approximately 20 min at 1024 points/line. It took about 20 h to examine a single hair, making it unattainable to perform the test on hundreds of patients. Due to the time-consuming nature of the method and the need to take multiple measurements along the length of a single hair, a small group of individuals was included in the study.

Of value for the above publication is the fact that similar morphological features have already been observed in previous, though few, publications. The pathogenesis of previously tested diseases is similar to LPP, so previous results confirm part of our observations. Therefore, further research in this direction seems reasonable.

ACKNOWLEDGMENTS

This research received no external funding.

CONFLICT OF INTEREST STATEMENT

The authors declare no conflicts of interest.

DATA AVAILABILITY STATEMENT

Data are available from the corresponding author upon reasonable request.

ETHICS STATEMENT

The study was approved by the Ethics Committee of the Rzeszów University (Decision No 9/10/2020 and 6/11/2020). Patients underwent all examinations after they signed informed consent.

ORCID

Adam Reich  <https://orcid.org/0000-0002-5573-1754>

REFERENCES

- Alessandrini A, Bruni F, Piraccini BM, Starace M. Common causes of hair loss—clinical manifestations, trichoscopy and therapy. *J Eur Acad Dermatol Venereol*. 2021;35:629–640. doi:10.1111/jdv.17079
- Svigos K, Yin L, Fried L, Lo Sico K, Shapiro J. A practical approach to the diagnosis and management of classic Lichen planopilaris. *Am J Clin Dermatol*. 2021;22:681–692. doi:10.1007/s40257-021-00630-7
- Kurzeja M, Czuwara J, Walecka I, Olszewska M, Rudnicka L. Features of classic lichen planopilaris and frontal fibrosing alopecia in reflectance confocal microscopy: a preliminary study. *Skin Res Technol*. 2021;27:266–271. doi:10.1111/srt.12940
- Kurzeja M, Warszawik-Hendzel O, Rakowska A, et al. Line-field confocal optical coherence tomography: a new diagnostic method in hair loss associated with folliculitis decalvans. *J Eur Acad Dermatol Venereol*. 2024;38:e267–e270. doi:10.1111/jdv.19575
- Fellows AP, Casford MTL, Davies PB. Nanoscale molecular characterization of hair cuticle cells using integrated atomic force microscopy-infrared laser spectroscopy. *Appl Spectrosc*. 2020;74:1540–1550.
- Fellows AP, Casford MTL, Davies PB. Using hybrid atomic force microscopy and infrared spectroscopy (AFM-IR) to identify chemical components of the hair medulla on the nanoscale. *J Microsc*. 2021;284:189–202.
- Fellows AP, Casford MTL, Davies PB. Chemically characterizing the cortical cell nano-structure of human hair using atomic force microscopy integrated with infrared spectroscopy (AFM-IR). *Int J Cosmet Sci*. 2022;44:42–55.
- Mcmullen RL, Zhang G. Investigation of the internal structure of human hair with atomic force microscopy. *J Cosmet Sci*. 2020;71:117–131.
- Shin MK, Kim KS, Ahn JJ, Kim NI, Park HK, Haw CR. Investigation of the hair of patients with scalp psoriasis using atomic force microscopy. *Clin Exp Dermatol*. 2012;37:156–163. doi:10.1111/j.1365-2230.2011.04212.x
- Lee GJ, Kim HJ, Eo YH, et al. AFM imaging analysis of alopecia areata by edge detection. *Tissue Engineer Regen Med*. 2009;6:360–364.
- Kim KS, Shin MK, Ahn JJ, Haw CR, Park HK. A comparative study of hair shafts in scalp psoriasis and seborrheic dermatitis using atomic force microscopy. *Skin Res Technol*. 2013;19:e60–e64. doi:10.1111/j.1600-0846.2011.00608.x
- Krawczyk-Wołoszyn K, Roczowski D, Reich A. Evaluation of surface structure and morphological phenomena of Caucasian virgin hair with atomic force microscopy. *Medicina (Mex)*. 2024;60:297.

13. Yadavalli VK, Ehrhardt CJ. Atomic force microscopy as a biophysical tool for nanoscale forensic investigations. *Sci Justice*. 2021;61:1-12. doi:10.1016/j.scijus.2020.10.004
14. Harries MJ, Jimenez F, Izeta A, et al. Lichen planopilaris and frontal fibrosing alopecia as model epithelial stem cell diseases. *Trends Mol Med*. 2018;24:435-448.
15. Kinoshita-Ise M, Fukuyama M, Ohyama M. Recent advances in understanding of the etiopathogenesis, diagnosis, and management of hair loss diseases. *J Clin Med*. 2023;12:3259.
16. Harries M, Hardman J, Chaundry I, Poblet E, Paus R. Profiling the human hair follicle immune system in lichen planopilaris and frontal fibrosing alopecia: can macrophage polarization differentiate these two conditions microscopically? *Br J Dermatol*. 2020;183:537-547.
17. Hoffman A, Waśkiel-Burnat A, Żółkiewicz J, et al. Pili torti: A feature of numerous congenital and acquired conditions. *J Clin Med*. 2021;10:3901.
18. Whiting DA. Hair shaft defects. In: Olsen EA, ed. *Disorders of Hair Growth: Diagnosis and Treatment*, 2nd ed. McGraw Hill; 2003:123-175.
19. Żychowska M, Żychowska M. Dermoscopy of discoid lupus erythematosus—a systematic review of the literature. *Int J Dermatol*. 2021;60:818-828.
20. Kolcz K, Kaznowska E, Reich A, Żychowska M. Trichoscopy-guided biopsy for the evaluation of scarring alopecia due to discoid lupus erythematosus. *Forum Dermatol*. 2023;9:167-171.
21. Żychowska M, Reich A. Chronic cutaneous lupus erythematosus in a white population: Dermoscopic characteristics by clinical subtype, lesion location and disease duration. *Dermatol Ther (Heidelb)*. 2022;12:2117-2133.
22. Pratt CH, King LE Jr, Messenger AG, Christiano AM, Sundberg JP. Alopecia areata. *Nat Rev Dis Primers*. 2017;3:17011. doi:10.1038/nrdp.2017.11

SUPPORTING INFORMATION

Additional supporting information can be found online in the Supporting Information section at the end of this article.

How to cite this article: Krawczyk-Wołoszyn K, Żychowska M, Reich A. Evaluation of hair surface structure and morphology of patients with lichen planopilaris (LPP) by atomic force microscopy (AFM). *Skin Res Technol*. 2024;30:e70030. <https://doi.org/10.1111/srt.70030>

10. Wnioski

W przedstawionej pracy dokonano przeglądu piśmiennictwa dotyczącego zastosowania techniki mikroskopii sił atomowych w naukach medycznych, a w oparciu o uzyskane wyniki badań wyciągnięto następujące wnioski:

1. W zdrowym włosie można wyróżnić cztery podstawowe powierzchnie morfologiczne (prążkowana powierzchnia, gładka powierzchnia, endokutikula, kora), które odzwierciedlają proces naturalnej delaminacji włosa, oraz kilka cech morfologicznych typowych dla wszystkich włosów (pitting, oval indentations, rod-shaped macro-fibrillar elements, globules, scratches, wavy edge).
2. Nasiloną obecność zmian morfologicznych takich jak: scratches, pitting, wavy edges i perforowane struktury we włosach pobranych od osób chorych mogą być efektem zmian w architektonice mieszka włosowego spowodowanych naciekiem zapalnym.
3. Niniejsze badanie stanowi porównanie pomiędzy dziewiczymi, zdrowymi włosami rasy kaukaskiej, a włosami pacjentów z liszajem płaskim mieszkowym za pomocą mikroskopii sił atomowych. Włosy osób z liszajem płaskim mieszkowym i zdrowe włosy mają zauważalne różnice widoczne w zakresie ich powierzchni. Wyniki tego badania mogą być wykorzystane do dalszych badań i prac związanych z liszajem płaskim mieszkowym.

11. Piśmiennictwo

1. Harries MJ, Jimenez F, Izeta A, et al. Lichen planopilaris and frontal fibrosing alopecia as model epithelial stem cell diseases. *Trends Mol Med*. 2018;24:435-448.
2. Kinoshita-Ise M, Fukuyama M, Ohyama M. Recent advances in understanding of the etiopathogenesis, diagnosis, and management of hair loss diseases. *J Clin Med*. 2023;12:3259.
3. Alessandrini A, Bruni F, Piraccini BM, Starace M. Common causes of hair loss—clinical manifestations, trichoscopy and therapy. *J Eur Acad Dermatol Venereol*. 2021;35:629-640. doi:10.1111/jdv.17079
4. Harries M, Hardman J, Chaundry I, Poblet E, Paus R. Profiling the human hair follicle immune system in lichen planopilaris and frontal fibrosing alopecia: can macrophage polarization differentiate these two conditions microscopically? *Br J Dermatol*. 2020;183:537-547.
5. Svigos K, Yin L, Fried L, Lo Sicco K, Shapiro J. A practical approach to the diagnosis and management of classic Lichen planopilaris. *Am J Clin Dermatol*. 2021;22:681-692. doi:10.1007/s40257-021-00630-7.
6. Whiting DA. Hair shaft defects. In: Olsen EA, ed. *Disorders of Hair Growth: Diagnosis and Treatment*, 2nd ed. McGraw Hill; 2003:123-175.
7. Hoffman A, Waśkiel-Burnat A, Żółkiewicz J, et al. Pili torti: A feature of numerous congenital and acquired conditions. *J Clin Med*. 2021;10:3901.
8. McMullen RL, Zhang G. Investigation of the internal structure of human hair with atomic force microscopy. *J Cosmet Sci*. 2020;71:117-131.
9. Shin MK, Kim KS, Ahn JJ, Kim NI, Park HK, Haw CR. Investigation of the hair of patients with scalp psoriasis using atomic force microscopy. *Clin Exp Dermatol*. 2012;37:156-163. doi:10.1111/j.1365-2230.2011.04212.x
10. Lee GJ, Kim HJ, Eo YH, et al. AFM imaging analysis of alopecia areata by edge detection. *Tissue Engineer Regener Med*. 2009;6:360-364.
11. Kim KS, Shin MK, Ahn JJ, Haw CR, Park HK. A comparative study of hair shafts in scalp psoriasis and seborrheic dermatitis using atomic force microscopy. *Skin Res Technol*. 2013;19:e60-e64. doi:10.1111/j.1600-0846.2011.00608.x
12. Dorobantu L.S, Goss G.G, Burrell R.E. Atomic force microscopy: A nanoscopic view of microbial cell surfaces. *Micron* 2012; 43:1312–1322.
13. Frederix P.L, Bosshart P.D, Engel A. Atomic force microscopy of biological

membranes. *Biophys. J.* 2009; 96:329–338.

14. Plomp M, Leighton T.J, Wheeler K.E, Hill H.D, Malkin A.J. In vitro high resolution structural dynamics of single germinating bacterial spores. *Proc. Natl. Acad. Sci.* 2007; 104:9644–9964.

15. Trohalaki S. Multifrequency force microscopy improves sensitivity and resolution over conventional AFM. *MRS Bull.* 2012; 37:545–546.

16. Xia F, Youcef-Toumi K. Review: Advanced Atomic Force Microscopy Modes for Biomedical Research. *Biosensors.* 2022; 12:1116.

17. Allison D.P, Mortensen N.P, Sullivan C.J, Doktycz M.J. Atomic force microscopy of biological samples. Wiley Interdiscip. *Rev.Nanomed. Nanobiotechnol.* 2010; 2:618–634.

18. Braet F, Taatjes D.J, Wisse E. Probing the unseen structure and function of liver cells through atomic force microscopy. *Semin. Cell Dev. Biol.* 2018;73:13–30.

19. Braet F, Wisse E. AFM imaging of fenestrated liver sinusoidal endothelial cells. *Micron* 2012;43:1252–1258.

20. Deng X, Xiong F, Li X, Xiang B, Li Z, Wu X, Guo C, Li X, Li Y, Li G. et al. Application of atomic force microscopy in cancer research. *J. Nanobiotechnol.* 2018;16:1–15.

21. Yeow N, Tabor R.F, Garnier G. Atomic force microscopy: From red blood cells to immunohaematology. *Adv. Colloid. Interface Sci.* 2017;249:149–162.

12. Streszczenie w języku polskim

Liszaj płaski mieszkowy (LPP) jest przewlekłą limfocytową chorobą skóry objawiającą się postępującym łysieniem bliznowaciejącym. Diagnozę LPP stawia się na podstawie badania histopatologicznego, choć nie zawsze jest ono jednoznaczne. Obecne badanie ocenia skuteczność nieinwazyjnego badania włosów za pomocą mikroskopii sił atomowych (AFM) w wykrywaniu różnic morfologicznych między włosami zdrowymi i chorymi.

Pierwsza praca podsumowuje kwestie techniczne i podstawy działania mikroskopii sił atomowych. Zawiera również przegląd wcześniejszych badań z wykorzystaniem AFM w naukach medycznych, w tym w badaniach włosów. Dzięki możliwościom, jakie daje obrazowanie AFM, możliwa jest nieinwazyjna ocena stanu włosów i ich ewentualnych zaburzeń. W zakresie badań nad włosami oceniano właściwości fizykomechaniczne i trybologiczne włókien włosów, pojedynczych komórek oraz zmiany powierzchniowe. Dotychczasowe badania koncentrowały się głównie na wpływie odżywek, czynnikach zewnętrznych uszkadzających włosy oraz różnicach etnicznych. Najnowsze badania AFM włosów wykorzystują techniki hybrydowe. Są to między innymi techniki spektroskopowe, które są wykorzystywane w połączeniu z AFM. Fellows i wsp. wykorzystali AFM zintegrowaną ze spektroskopią w podczerwieni (AFM-IR) do badania składu chemicznego kutikuli, rdzenia i kory europejskich włosów. W 2012 roku Shin i wsp. ocenili morfologię powierzchni włosów u pacjentów z łuszczycą pospolitą. Zaobserwowali oni ubytki, zwiększoną szorstkość i zwiększoną grubość łusek włosów u pacjentów z łuszczycą.

W związku z powyższym, w obecnym badaniu zdecydowano się ocenić powierzchnię włosów pacjentów z LPP i porównać je z grupą kontrolną. Pierwsze badanie miało na celu zbadanie i ocenę powierzchni zdrowych, dziewiczych włosów rasy kaukaskiej za pomocą AFM. W tym badaniu od każdej osoby pobrano od trzech do pięciu włosów. Każdy włos był badany w dziewięciu lokalizacjach (0,5; 1,0; 1,5; 2,0; 3,5; 4,5; 5,5; 6,5 i 7,0 cm od korzenia). W każdej z 9 lokalizacji wykonano co najmniej 4 zdjęcia (4-10 zdjęć). Łącznie wykonano i przeanalizowano 496 zdjęć. Wykonano pomiary metryczne łusek włosów, takie jak długość, szerokość i wysokość stopnia łuski. W trakcie badania wykazano zmiany zachodzące we włosach podczas naturalnego procesu rozwarstwiania. Ponadto przedstawiono zmiany morfologiczne uwidocznione na powierzchni zdrowych włosów (pitting, oval indentations, rod-shaped

macro-fibrillar elements, globules, scratches, wavy edge). Przeprowadzono analizę ilościową znalezionych struktur. Wyniki badań mogą być wykorzystane w dalszych badaniach i pracach związanych z tematyką włosów ludzkich. Mogą służyć jako punkt odniesienia do badań nad chorobami skóry głowy i włosów, a także pielęgnacji włosów. W drugim badaniu oceniano strukturę i morfologię powierzchni włosów pacjentów z liszajem płaskim mieszkowym (LPP) za pomocą AFM. W tym przypadku pobrano od trzech do pięciu włosów ze zmienionej chorobowo skóry 10 pacjentów z LPP i zbadano je w dziewięciu lokalizacjach za pomocą AFM. W każdym z dziewięciu miejsc wykonano co najmniej cztery zdjęcia. Wykonano pomiary metryczne (długość, szerokość i wysokość stopnia łuski) oraz oceniono cechy morfologiczne (prążkowana i gładka powierzchnia łusek, obecność endokutikuli i kory, kształt krawędzi łusek, scratches, pitting, cracks, globules, wavy edge) porównano z włosami pochodzącymi od zdrowych osób z grupy kontrolnej. Ponadto opisano obszary na chorych włosach, w których zachodzi proces patologicznego, nienaturalnego rozwarstwienia włókna włosa. Stwierdzono istotną statystycznie różnicę w liczbie scratches w początkowych sekcjach włosów LPP, w intensywności wavy edges na całej długości badanych włosów oraz w liczbie łusek z obecnym pittingiem w środkowej sekcji włosa. Ponadto, w grupie LPP stwierdzono statystycznie istotnie mniejszą liczbę łusek z prążkowaną powierzchnią, począwszy od 3,5 cm od nasady, aż do wolnego końca włosa.

Według naszej wiedzy jest to pierwsze badanie porównawcze powierzchni łodygi włosa na całej długości pomiędzy grupą LPP i grupą zdrową przy użyciu AFM. Przedstawione badanie umożliwiło ocenę dynamiki zmian powierzchni włosa wraz z odległością od korzenia. Wyniki przedstawione w niniejszym badaniu stanowią próbę scharakteryzowania zmian morfologicznych w nanoskali, co może być pomocne we wczesnej diagnostyce chorób włosów w przyszłości. Przedstawione wstępne wyniki nadają kierunek dalszym badaniom nad chorobami skóry głowy i włosów. Włosy osób z LPP i zdrowe włosy mają zauważalne różnice w powierzchni. Ze względu na czasochłonność metody i konieczność wykonania wielu pomiarów na długości pojedynczego włosa, badaniem objęto niewielką grupę pacjentów. Nie bez znaczenia dla powyższej publikacji jest fakt, że podobne cechy morfologiczne zaobserwowano już we wcześniejszych, choć nielicznych publikacjach. Uzasadnione wydają się być dalsze badania powierzchni włosów w różnych chorobach zapalnych skóry owłosionej głowy za pomocą AFM.

13. Abstract (streszczenie w języku angielskim)

Lichen planopilaris (LPP) is a chronic lymphocytic skin disease manifested by progressive scarring alopecia. The diagnosis of LPP is made based on histopathological examination, although it is not always definite. The current study evaluates the effectiveness of non-invasive atomic force microscopy (AFM) hair examination in detecting morphological differences between healthy and diseased hair.

The first paper summarizes the technical issues and operating basics of AFM. It also provides a review of previous studies using AFM in medical sciences, including hair research. Thanks to the possibilities offered by AFM imaging, the condition of hair and its possible disorders can be noninvasively assessed. In terms of hair research, the physicochemical and tribological properties of hair fibers, cells, and surface changes were studied. The research has been mainly concentrated on the effect of conditioners, hair-damaging external factors, and ethnic differences. The latest AFM studies of hair utilized hybrid techniques. Among other things, spectroscopic techniques are being used in conjunction with AFM. Fellows et al. used AFM integrated with an infrared spectroscopy (AFM-IR) to study the chemical composition of the cuticle, medulla, and cortex of European hair. In 2012, Shin et al. evaluated the morphology of the hair surface in patients with psoriasis vulgaris. They observed pits, increased roughness, and increased thickness of hair scales in patients with psoriasis.

Therefore, here it was decided to assess the hair surface of LPP patients and compare them with a control group. The first study was aimed at investigating and assessing the surface of healthy, virgin Caucasian hair by AFM. In this study, three to five hairs were collected from each person. Each hair was examined at nine locations (0.5; 1.0; 1.5; 2.0; 3.5; 4.5; 5.5; 6.5 and 7.0 cm from the root). At least 4 images (4–10 images) were taken at each of the 9 locations. A total of 496 photos were taken and analyzed. Metric measurements of hair scales, such as apparent length, width and scale step height, were taken. This publication presents the changes occurring in hair during the natural delamination process. In addition, morphological changes visualized on the surface of healthy hair (pitting, oval indentations, rod-shaped macro-fibrillar elements, globules, scratches, wavy edge) are presented. A quantitative analysis of the structures found was carried out. The findings of this study can be used in further research and work related to the subject of human hair. They can serve as a reference for research on

scalp and hair diseases, as well as hair care.

The second study evaluated the structure and morphology of the hair surface of patients with lichen planus (LPP) by atomic force microscopy. Here, three to five hairs from lesional skin of 10 LPP patients were collected and examined at nine locations using AFM. At least four images were taken at each of the nine sites. Metric measurements were taken and metric (length, width, and scale step height) and morphological features (striated and smooth surface of scales, the presence of endocuticle and cortex, shape of scales edges, scratches, pitting, cracks, globules, and wavy edge) were compared with hair from healthy controls. In addition, areas on diseased hair where the process of pathological, unnatural delamination of the hair fiber occurs are described. There was a statistically significant difference in the number of scratches in the initial sections of the LPP hair, in the intensity of wavy edges along the entire length of the tested hair, and in the number of scales with pitting in the middle section of the hair. In addition, a statistically significant fewer number of scales with striated surface was found in LPP group starting at 3.5 cm from the root continuing towards the free end of the hair.

This is to our knowledge the first comparison study about hair shaft surfaces over the whole lengths between LPP and healthy group using AFM. The study presented here made it possible to assess the dynamics of hair surface changes with distance from the root. The results presented in this study attempt to characterize morphological changes at the nanoscale, which may be helpful for early diagnosis of hair diseases in the future. The preliminary results provided give direction for further research into scalp and hair diseases. The hair of people with LPP and healthy hair have noticeable differences in their surface area. The etiology of the structures shown remains to be further discussed. Due to the time-consuming nature of the method and the need to take multiple measurements along the length of a single hair, a small group of individuals was included in the study. Of value for the above publication is the fact that similar morphological features have already been observed in previous, though few, publications. The pathogenesis of previously tested diseases is similar to LPP, so previous results confirm part of our observations. Therefore, further research in this direction seems reasonable.

14. Oświadczenia współautorów

Rzeszów, 2 grudnia 2024 r.

Prof. dr hab. n. med. Adam Reich

Zakład i Klinika Dermatologii

Uniwersytet Rzeszowski

OŚWIADCZENIE WSPÓŁAUTORA

Oświadczam, że w pracy: *Krawczyk-Wołoszyn K, Roczkowski D, Reich A, Żychowska M. Applying the Atomic Force Microscopy Technique in Medical Sciences—A Narrative Review. Biomedicines 2024; 12: 2012.* mój wkład merytoryczny w przygotowanie, przeprowadzenie i opracowanie badań oraz przedstawienie pracy w formie publikacji to: **nadzór merytoryczny oraz korekta i weryfikacja finalnej wersji manuskryptu.**

Jednocześnie wyrażam zgodę na przedłożenie ww. pracy przez lek. Karolinę Krawczyk-Wołoszyn, jako część rozprawy doktorskiej w formie spójnego tematycznie zbioru artykułów naukowych opublikowanych w czasopismach naukowych na temat oceny zastosowania mikroskopii sił atomowych jako metody obrazowania i diagnostyki chorób włosów.

Oświadczam, iż samodzielna i możliwa do wyodrębnienia część ww. pracy wykazuje indywidualny wkład lek. Karoliny Krawczyk-Wołoszyn przy opracowywaniu koncepcji oraz opracowaniu i interpretacji wyników tej pracy.

Prof. dr hab. n. med. Adam Reich
KIEROWNIK KLINIKI DERMATOLOGII
Uniwersytecki Szpital Kliniczny
im. Emalii Chybińskiej w Rzeszowie

Podpis

Rzeszów, 2 grudnia 2024 r.

Dr hab. n. med. Magdalena Żychowska
Zakład i Klinika Dermatologii
Uniwersytet Rzeszowski

OŚWIADCZENIE WSPÓŁAUTORA

Oświadczam, że w pracy: *Krawczyk-Wołoszyn K, Raczkowski D, Reich A, Żychowska M. Applying the Atomic Force Microscopy Technique in Medical Sciences—A Narrative Review. Biomedicines 2024; 12: 2012.* mój wkład merytoryczny w przygotowanie, przeprowadzenie i opracowanie badań oraz przedstawienie pracy w formie publikacji to: **nadzór merytoryczny, opracowanie koncepcji publikacji (wspólnie z doktorantką) oraz korekta i weryfikacja finalnej wersji manuskryptu.**

Jednocześnie wyrażam zgodę na przedłożenie ww. pracy przez lek. Karolinę Krawczyk-Wołoszyn, jako część rozprawy doktorskiej w formie spójnego tematycznie zbioru artykułów naukowych opublikowanych w czasopismach naukowych na temat oceny zastosowania mikroskopii sił atomowych jako metody obrazowania i diagnostyki chorób włosów.

Oświadczam, iż samodzielna i możliwa do wyodrębnienia część ww. pracy wykazuje indywidualny wkład lek. Karoliny Krawczyk-Wołoszyn przy opracowywaniu koncepcji oraz opracowaniu i interpretacji wyników tej pracy.


.....
Podpis

Rzeszów, 2 grudnia 2024 r.

Mgr Damian Roczkowski

OŚWIADCZENIE WSPÓŁAUTORA

Oświadczam, że w pracy: *Krawczyk-Wołoszyn K, Roczkowski D, Reich A, Żychowska M. Applying the Atomic Force Microscopy Technique in Medical Sciences—A Narrative Review. Biomedicines 2024; 12: 2012.* mój wkład merytoryczny w przygotowanie, przeprowadzenie i opracowanie badań oraz przedstawienie pracy w formie publikacji to:

- przygotowanie podrozdziałów pt. **"Construction of the Microscope, the Physical Basis, and the Principle of Its Operation", "AFM Imaging Modes" oraz "Oncology".**

Jednocześnie wyrażam zgodę na przedłożenie ww. pracy przez lek. Karolinę Krawczyk-Wołoszyn, jako część rozprawy doktorskiej w formie spójnego tematycznie zbioru artykułów naukowych opublikowanych w czasopiśmie naukowym na temat oceny zastosowania mikroskopii sił atomowych jako metody obrazowania i diagnostyki chorób włosów.

Oświadczam, iż samodzielna i możliwa do wyodrębnienia część ww. pracy wykazuje indywidualny wkład lek. Karoliny Krawczyk-Wołoszyn przy opracowywaniu koncepcji oraz opracowaniu i interpretacji wyników tej pracy.



Podpis

Rzeszów, 2 grudnia 2024 r.

Prof. dr hab. n. med. Adam Reich

Zakład i Klinika Dermatologii

Uniwersytet Rzeszowski

OŚWIADCZENIE WSPÓŁAUTORA

Oświadczam, że w pracy: *Krawczyk-Wołoszyn K, Roczkowski D, Reich A. Evaluation of Surface Structure and Morphological Phenomena of Caucasian Virgin Hair with Atomic Force Microscopy. Medicina 2024; 60: 297.* mój wkład merytoryczny w przygotowanie, przeprowadzenie i opracowanie badań oraz przedstawienie pracy w formie publikacji to:

opracowanie koncepcji badania klinicznego (wspólnie z doktorantką), nadzór merytoryczny, analiza wyników wspólnie z doktorantką oraz weryfikacja finalnej wersji manuskryptu.

Jednocześnie wyrażam zgodę na przedłożenie ww. pracy przez lek. Karolinę Krawczyk-Wołoszyn, jako część rozprawy doktorskiej w formie spójnego tematycznie zbioru artykułów naukowych opublikowanych w czasopiśmie naukowym na temat oceny zastosowania mikroskopii sił atomowych jako metody obrazowania i diagnostyki chorób włosów.

Oświadczam, iż samodzielna i możliwa do wyodrębnienia część ww. pracy wykazuje indywidualny wkład lek. Karoliny Krawczyk-Wołoszyn przy opracowywaniu koncepcji oraz opracowaniu i interpretacji wyników tej pracy.

Prof. dr hab. n. med. Adam Reich
KIEROWNIK KLINIKI DERMATOLOGII
Uniwersyteckiego Szpitala Klinicznego
im. Fryderyka Chopina w Rzeszowie

Podpis

Rzeszów, 2 grudnia 2024 r.

Mgr Damian Roczkowski

OŚWIADCZENIE WSPÓŁAUTORA

Oświadczam, że w pracy: *Krawczyk-Wołoszyn K, Roczkowski D, Reich A. Evaluation of Surface Structure and Morphological Phenomena of Caucasian Virgin Hair with Atomic Force Microscopy. Medicina 2024; 60: 297.* mój wkład merytoryczny w przygotowanie, przeprowadzenie i opracowanie badań oraz przedstawienie pracy w formie publikacji to: **korekta finalnej wersji manuskryptu oraz grafik.**

Jednocześnie wyrażam zgodę na przedłożenie ww. pracy przez lek. Karolinę Krawczyk-Wołoszyn, jako część rozprawy doktorskiej w formie spójnego tematycznie zbioru artykułów naukowych opublikowanych w czasopiśmie naukowym na temat oceny zastosowania mikroskopii sił atomowych jako metody obrazowania i diagnostyki chorób włosów.

Oświadczam, iż samodzielna i możliwa do wyodrębnienia część ww. pracy wykazuje indywidualny wkład lek. Karoliny Krawczyk-Wołoszyn przy opracowywaniu koncepcji oraz opracowaniu i interpretacji wyników tej pracy.



Podpis

Rzeszów, 2 grudnia 2024 r.

Prof. dr hab. n. med. Adam Reich
Zakład i Klinika Dermatologii
Uniwersytet Rzeszowski

OŚWIADCZENIE WSPÓŁAUTORA

Oświadczam, że w pracy: *Krawczyk-Wołoszyn K, Żychowska M, Reich A. Evaluation of hair surface structure and morphology of patients with lichen planopilaris (LPP) by atomic force microscopy (AFM). Skin Res Technol. 2024 Sep;30(9):e70030.* mój wkład merytoryczny w przygotowanie, przeprowadzenie i opracowanie badań oraz przedstawienie pracy w formie publikacji to:

nadzór merytoryczny, opracowanie koncepcji badania klinicznego wspólnie z doktorantką, analiza wyników wspólnie z doktorantką, przygotowanie grafik dotyczących statystyki oraz weryfikacja finalnej wersji manuskryptu.

Jednocześnie wyrażam zgodę na przedłożenie ww. pracy przez lek. Karolinę Krawczyk-Wołoszyn, jako część rozprawy doktorskiej w formie spójnego tematycznie zbioru artykułów naukowych opublikowanych w czasopismach naukowych na temat oceny zastosowania mikroskopii sił atomowych jako metody obrazowania i diagnostyki chorób włosów.

Oświadczam, iż samodzielna i możliwa do wyodrębnienia część ww. pracy wykazuje indywidualny wkład lek. Karoliny Krawczyk-Wołoszyn przy opracowywaniu koncepcji oraz opracowaniu i interpretacji wyników tej pracy.

Prof. dr hab. n. med. Adam Reich
KIEROWNIK KLINIKI DERMATOLOGII
Uniwersytecki Szpital Kliniczny
im. Fryderyka Chopina w Rzeszowie

Podpis

Rzeszów, 2 grudnia 2024 r.

Dr hab. n. med. Magdalena Żychowska

Zakład i Klinika Dermatologii

Uniwersytet Rzeszowski

OŚWIADCZENIE WSPÓŁAUTORA

Oświadczam, że w pracy: *Krawczyk-Wołoszyn K, Żychowska M, Reich A. Evaluation of hair surface structure and morphology of patients with lichen planopilaris (LPP) by atomic force microscopy (AFM). Skin Res Technol. 2024 Sep;30(9):e70030.* mój wkład merytoryczny w przygotowanie, przeprowadzenie i opracowanie badań oraz przedstawienie pracy w formie publikacji to:

nadzór merytoryczny, przygotowanie części dyskusji i grafik oraz weryfikacja finalnej wersji manuskryptu.

Jednocześnie wyrażam zgodę na przedłożenie ww. pracy przez lek. Karolinę Krawczyk-Wołoszyn, jako część rozprawy doktorskiej w formie spójnego tematycznie zbioru artykułów naukowych opublikowanych w czasopismach naukowych na temat oceny zastosowania mikroskopii sił atomowych jako metody obrazowania i diagnostyki chorób włosów.

Oświadczam, iż samodzielna i możliwa do wyodrębnienia część ww. pracy wykazuje indywidualny wkład lek. Karoliny Krawczyk-Wołoszyn przy opracowywaniu koncepcji oraz opracowaniu i interpretacji wyników tej pracy.



Podpis

15. Załączniki



KOMISJA BIOETYCZNA UNIwersYTETU RZESZOWSKIEGO
UNIwersYTET RZESZOWSKI
Kolegium Nauk Medycznych
al. mjr. W. Kopisto 2a, 35-959 Rzeszów

UCHWAŁA Nr 9/10/2020

Komisji Bioetycznej przy Uniwersytecie Rzeszowskim

22/10/2020

Komisja Bioetyczna przy Uniwersytecie Rzeszowskim, działając na podstawie art. 29 ust. 3 pkt 2 ustawy z dnia 5 grudnia 1996 roku o zawodzie lekarza (Dz. U. z dnia 26 marca 1997 roku, Nr 28, poz. 152), zgodnie z rozporządzeniem Ministra Zdrowia i Opieki Społecznej z dnia 11 maja 1999 roku (Dz. U. Nr 47 poz. 480 z 1999 roku) w sprawie szczegółowych zasad powoływania i finansowania oraz trybu działania Komisji Bioetycznych oraz działając zgodnie z zasadami GCP (Good Clinical Practice) i ustawą z dnia 6 września 2001 roku Prawo farmaceutyczne (Dz. U. z 2019 r. poz. 499 z późn. zm.), po zapoznaniu się z wnioskiem złożonym przez wnioskodawcę, w wyniku przeprowadzonej dyskusji i głosowania (dn. 22 października 2020 r.) przeprowadzonych w formie zdalnej liczbą 9 głosów akceptujących spośród 9 oddanych głosów

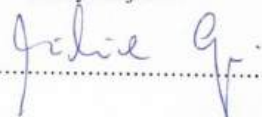
postanawia

projekt badawczy: „Zastosowanie spektroskopii w podczerwieni (FTIR) i spektroskopii ramanowskiej w schorzeniach dermatologicznych.”

zaopiniować pozytywnie.

Uwagi: Uchwała jest ważna na okres objęty planem badań.

Zastępca Przewodniczącego Komisji
Bioetycznej UR


.....

Do wiadomości:

Wnioskodawca: Mgr inż. Kornelia Lach, dr inż. Grzegorz Gruzeł, mgr Kamil Szmuc, lek. Karolina Krawczyk, dr n. med. Magdalena Żychowska, dr.hab. n. med. Józef Cebulski, prof. dr. hab. n. med. Adam Reich



Karolina Krawczyk-Wołoszyn
Imię i nazwisko Doktoranta UR

Rzeszów, 11.04.2025 r.

OŚWIADCZENIE

Ja, niżej podpisana Karolina Krawczyk-Wołoszyn oświadczam, że przygotowana dysertacja pt. „Mikroskopia sił atomowych (AFM) jako innowacyjna metoda obrazowania i diagnostyki chorób włosów”, którą przedkładałam w przewodzie doktorskim procedowanym w Uniwersytecie Rzeszowskim została przygotowana i w pełni odpowiada założeniom projektu badawczego pt. Zastosowanie spektroskopii w podczerwieni (FTIR) i spektroskopii ramanowskiej w schorzeniach dermatologicznych”, który uzyskał pozytywną opinię Komisji Bioetycznej Uniwersytetu Rzeszowskiego (uchwała nr 9/10/2020 Wydana w dniu 22.10.2020r).

(promotor)

(składający oświadczenie)